nagra.

Arbeitsbericht NAB 16-12

FEBEX-DP on-site analyses report

August 2016

María Victoria Villar, Rubén Javier Iglesias,
Héctor Abós, Víctor Martínez,
Cristina de la Rosa, Miguel Ángel Manchón

National Cooperative
for the Disposal of
Radioactive Waste

Hardstrasse 73
P.O. Box 280
5430 Wettingen
Switzerland
Tel. +41 56 437 11 11

www.nagra.ch

nagra.

Arbeitsbericht NAB 16-12

FEBEX-DP on-site analyses report

August 2016

María Victoria Villar[1], Rubén Javier Iglesias[1],
Héctor Abós[2], Víctor Martínez[2],
Cristina de la Rosa[2], Miguel Ángel Manchón[2]

[1)] CIEMAT, Avd. Complutense 40, 28040 Madrid, Spain
[2)] AITEMIN, C/ Margarita Salas 14, 28918 Leganés (Madrid), Spain

KEYWORDS

Bentonite, large-scale test, geological disposal, engineered barrier, long term, thermo-hydraulic gradient

National Cooperative
for the Disposal of
Radioactive Waste

Hardstrasse 73
P.O. Box 280
5430 Wettingen
Switzerland
Tel. +41 56 437 11 11

www.nagra.ch

Nagra Arbeitsberichte ("Working Reports") present the results of work in progress that have not necessarily been subject to a comprehensive review. They are intended to provide rapid dissemination of current information.
This report was prepared on behalf of Nagra. The viewpoints presented and conclusions reached are those of the author(s) and do not necessarily represent those of Nagra.

Table of Contents

List of Tables

List of Figures

1 Introduction

The aim of FEBEX (Full-scale Engineered Barrier Experiment) was to study the behaviour of components in the near-field for a high-level radioactive waste (HLW) repository in crystalline rock. The project was based on the Spanish reference concept for disposal of radioactive waste in crystalline rock (AGP Granito): the waste canisters are placed horizontally in drifts and surrounded by a clay barrier constructed from highly-compacted bentonite blocks (ENRESA 1995). As part of this project, an "in-situ" test, under natural conditions and at full scale, was performed at the Grimsel Test Site (GTS, Switzerland), an underground laboratory managed by Nagra (ENRESA 2000, 2006). The thermal effect of the waste was simulated by means of heaters, whereas hydration was natural. The test was monitored, this allowed the evolution of the temperature, total pressure, water content, water pressure, displacements and other parameters to be obtained continuously in different parts of the barrier and the host rock. This information was used as a contrast to the predictions of the thermo-hydro-mechanical (THM) and thermo-hydro-geochemical (THG) models.

The basic components of the test (Fig. 1) were: the gallery, measuring 70 m in length and 2.3 m in diameter, excavated through the Aare granite (Fig. 2); the heating system, made up of two heaters placed inside a liner installed concentrically with the gallery and separated one from the other by a distance of 1.0 m, with dimensions and weights analogous to those of the real canisters; the clay barrier, formed by blocks of compacted bentonite; the instrumentation and the monitoring and control system for data acquisition and supervision and control of the test both autonomously and remotely from Madrid. The FEBEX test initially contained 632 sensors of very diverse types, installed to monitor the different thermo-hydro-mechanical processes that occurred in both the clay barrier and the surrounding rock throughout the entire life of the test. The gallery was closed by a concrete plug.

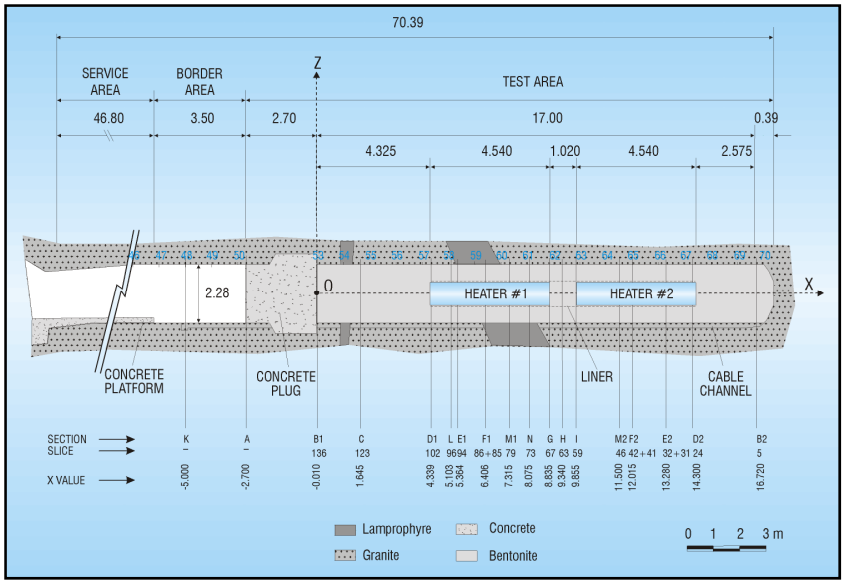

Fig. 1: General layout of the *in-situ* test during Phase I, including instrumented sections (ENRESA 2000).

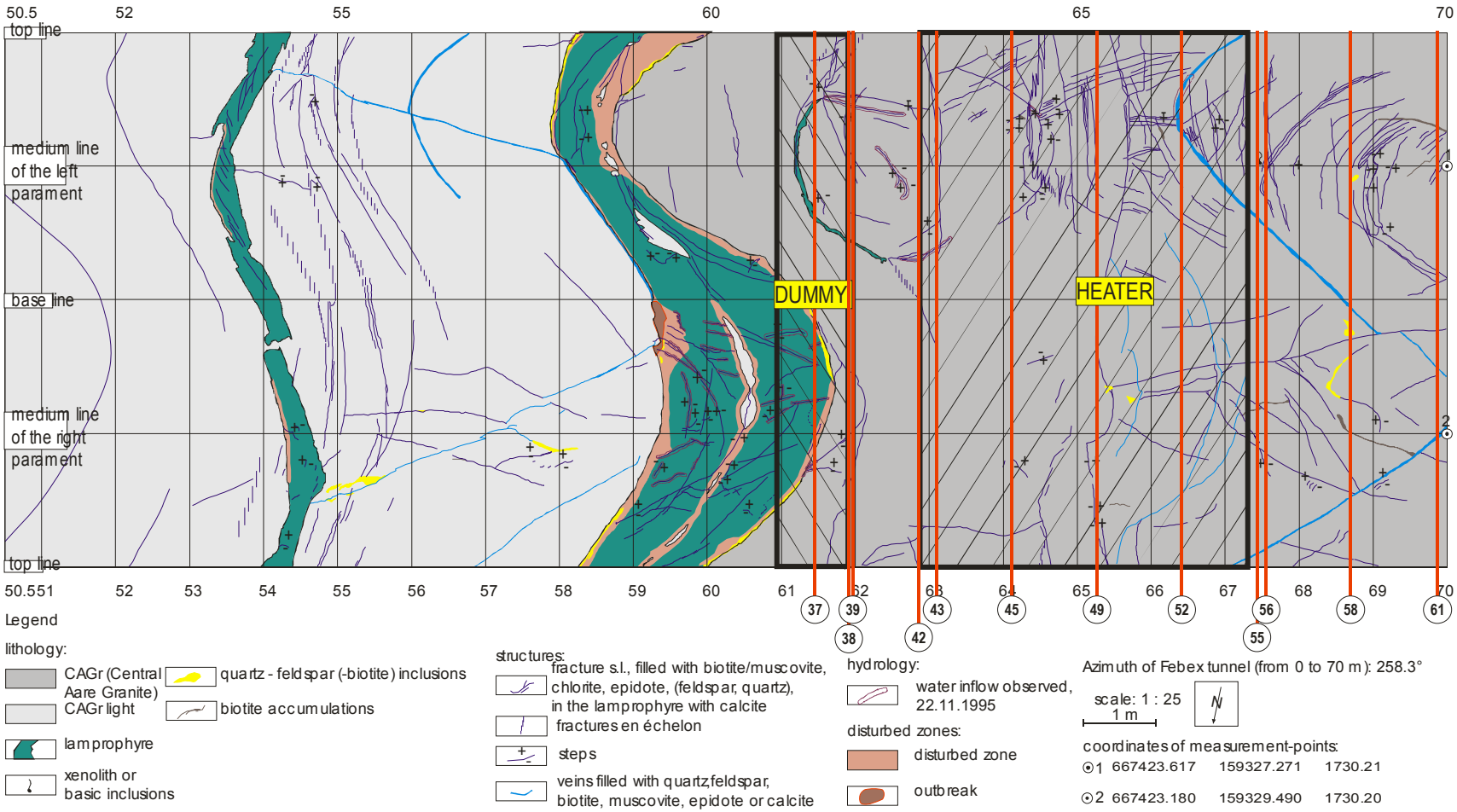

Fig. 2: Geological map of the gallery along the testing area (m. 50.5-70) (Pardillo et al. 1997).
The approximate location of dummy, Heater #2 and sampling sections is indicated.

The clay barrier was made of FEBEX bentonite, which was extracted from the Cortijo de Archidona deposit (Almería, Spain). The physico-chemical properties of the FEBEX bentonite, as well as its most relevant thermo-hydro-mechanical and geochemical characteristics obtained during the projects FEBEX I and II were summarised in the final reports of the project (ENRESA 2000, 2006). To build the clay barrier, various types of blocks were manufactured from the bentonite in the shape of 12-cm thick circular crown sectors. The blocks were arranged in vertical slices with three concentric rings. In the heater areas the interior ring was in contact with the steel liner, whereas in the non-heater areas a core of bentonite blocks replaced the heaters (Fig. 3). The geometry and dimensions of the blocks are shown in Fig. 4 and Tab. 1. The thickness of the bentonite barrier in the heater areas was 65 cm. The blocks were obtained by uniaxial compaction of the FEBEX clay at its hygroscopic water content using pressures of between 40 and 45 MPa. These blocks had dry densities of 1.69 – 1.70 g/cm^3, a density preselected by taking into account the probable volume of the construction gaps and the need to have a barrier with an average dry density of 1.60 g/cm^3 (ENRESA 2000).

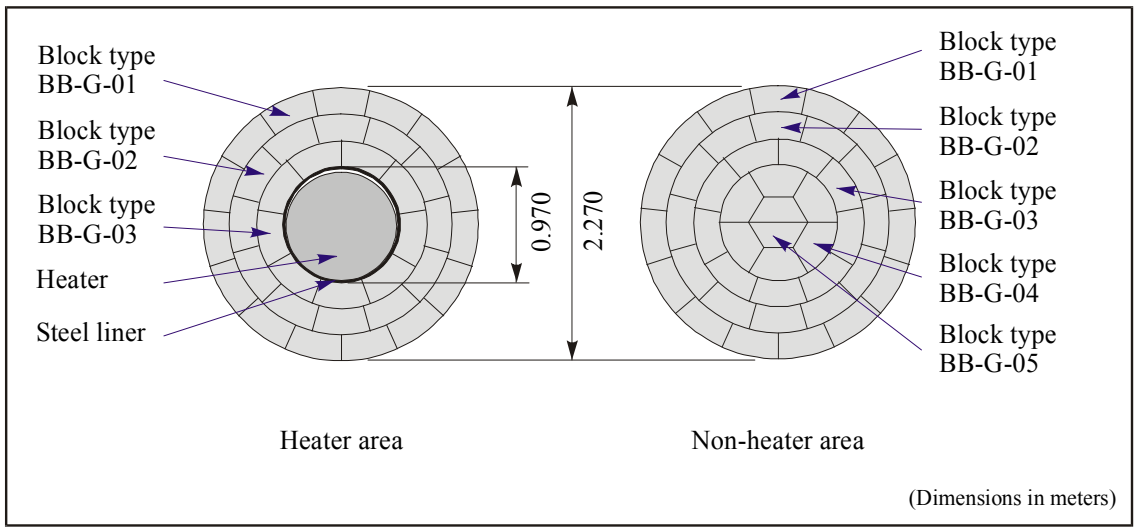

Fig. 3: Geometry of the clay barrier in the FEBEX *in situ* test at GTS (ENRESA 2000).

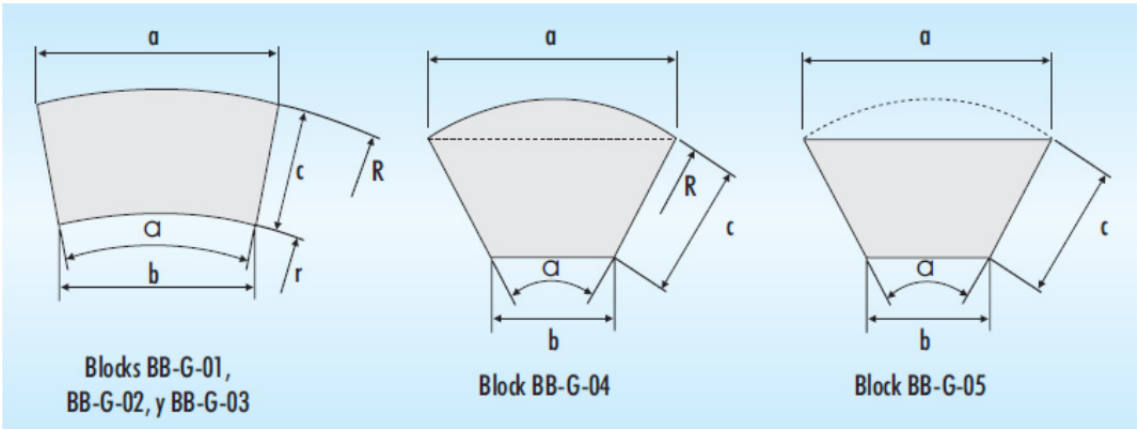

Fig. 4: Geometry of the different kinds of blocks (Fuentes-Cantillana & García-Siñeriz 1998).

Tab. 1: Dimensions of the blocks shown in Fig. 4 (Fuentes-Cantillana & García-Siñeriz 1998).

Block type	**External Radius R** (mm)	**Internal Radius r** (mm)	**R-r** (mm)	**Blocks per slice**	**Thickness** (mm)
BB-G-01	1'135.0	918.3	216.7	15	125.0
BB-G-02	918.3	701.7	216.7	12	125.0
BB-G-03	701.7	485.0	216.7	9	125.0
BB-G-04	485.0	242.5[a]	242.5	6	125.0
BB-G-05	242.5	0.0	242.5	2	125.0

[a] Radius of central hexagon

The heating stage of the in-situ test began on February 27th 1997. The power of the heaters was adjusted to keep the temperatures at their surfaces at 100 °C. After five years of uninterrupted heating at constant temperature, the heater closer to the gallery entrance (Heater #1) was switched off (February 2002). In the following months this heater and all the bentonite and instruments preceding and surrounding it were extracted (Bárcena et al. 2003). The gravimetric water content and dry density of numerous bentonite samples taken during dismantling were determined on site (Daucausse & Lloret 2003). A large number of bentonite samples were also taken for analysis in different laboratories (Villar et al. 2006). The remaining part of the experiment was used in the second operational phase (Fig. 5). As part of this second phase, new sensors were installed in the buffer, a non-heated generating partial canister (DUMMY) was installed in the remaining void where the heater was removed from and the system was sealed with a new sprayed concrete plug.

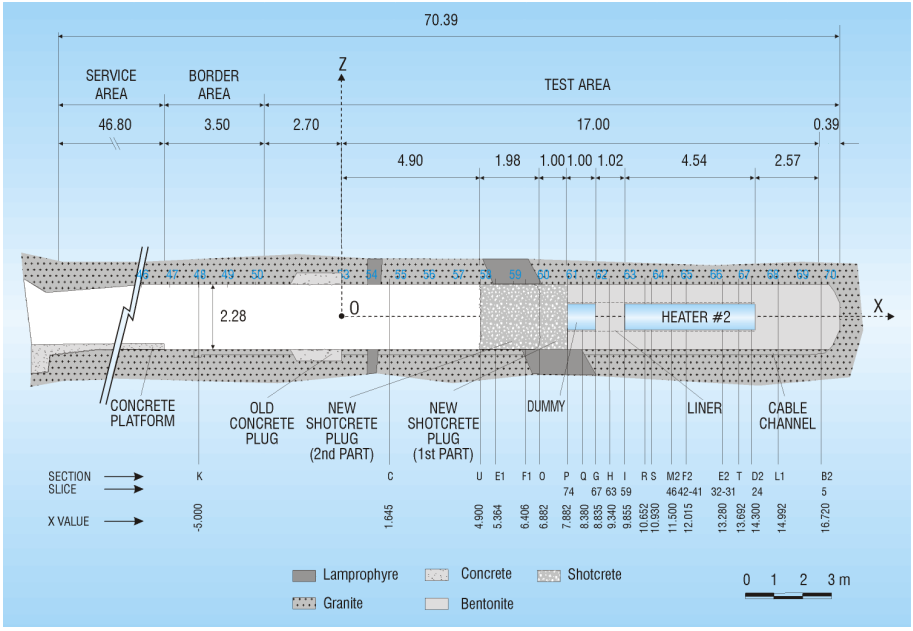

Fig. 5: General layout of the in-situ test during Phase II, including instrumented sections (ENRESA 2006).

The test continued running until April 2015, when Heater #2 was switched off. Demolition of the concrete plug – which was barely affected by the heater– started several days before turning off the heater, which was done with the shortest anticipation possible to allow cooling of the bentonite to temperatures compatible with human handling. The buffer removal and sampling took place between May 8th and August 5th (AITEMIN 2016a).

This report compiles and analyses the results of the on-site measurements performed by AITEMIN during the dismantling of the FEBEX in-situ test (FEBEX-DP project). In particular the water content and dry density determinations carried out in samples taken from selected sections evenly distributed along the gallery (Fig. 6) are provided. Additionally, their relationship with the blocks' measured dimensions, the x-coordinate changes and other field observations are assessed.

A summary of the methodology used for the on-site determinations, which is described in detail in AITEMIN (2016a), is presented in Chapter 2. In Chapter 3 the results obtained for every sampling section are presented. Finally, in Chapter 4 these results are discussed in an integrated way, taking into account the different observations and analyses.

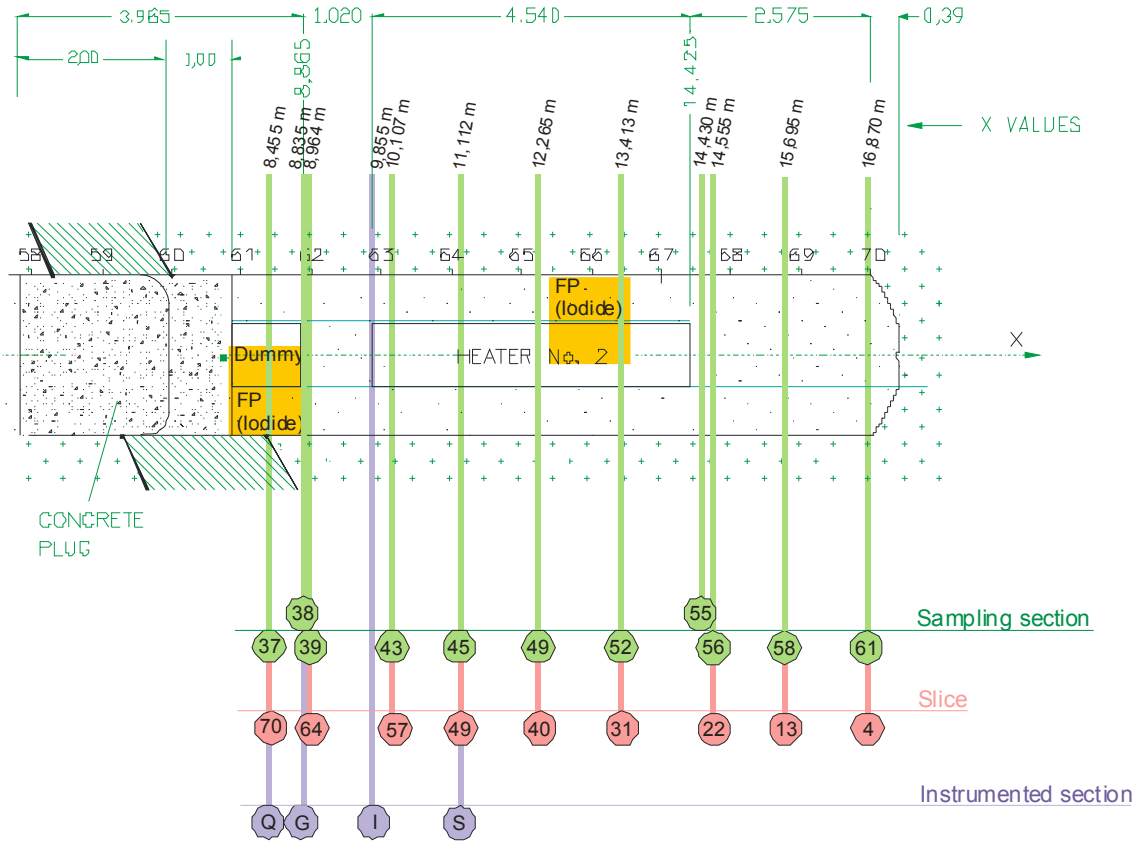

Fig. 6: Location along the gallery of the sampling sections used for bentonite water content and dry density on-site determinations.

2 Methodology of on-site determinations

The dismantling and sampling procedures are described in detail in AITEMIN (2016a), hence, only a summary of the relevant aspects is given here. Prior to sampling the x-coordinate of the section was measured using a laser distance-meter with an accuracy of ± 5 mm. These measurements were done at five different points on the surface of the section or at least at the locations P1 and P5 shown in Fig. 7. The length of the sampling radii as well as the dimensions of the blocks was measured in several sections before sampling. In each of the sampling sections (Fig. 6), samples were taken following 6 radii separated by 60° and named clockwise from A (the upper radius) to F. The bentonite blocks preceding the sampling radii were removed just before sampling, in order to prevent changes in the bentonite water content. Each section was usually sampled within a day, but in some cases different radii of the same section were sampled in consecutive days.

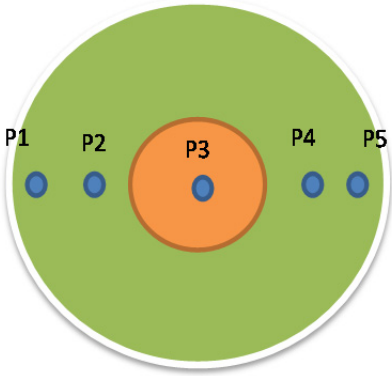

Fig. 7: Location of the points used for measurement of the *x*-coordinate.

The conditions in the service area of the FEBEX gallery (m. 44) during the bentonite dismantling period are shown in Fig. 8 (AITEMIN 2016b). The relative humidity was on average 86.4 ± 7.7 % and the temperature 15.8 ± 0.5 °C.

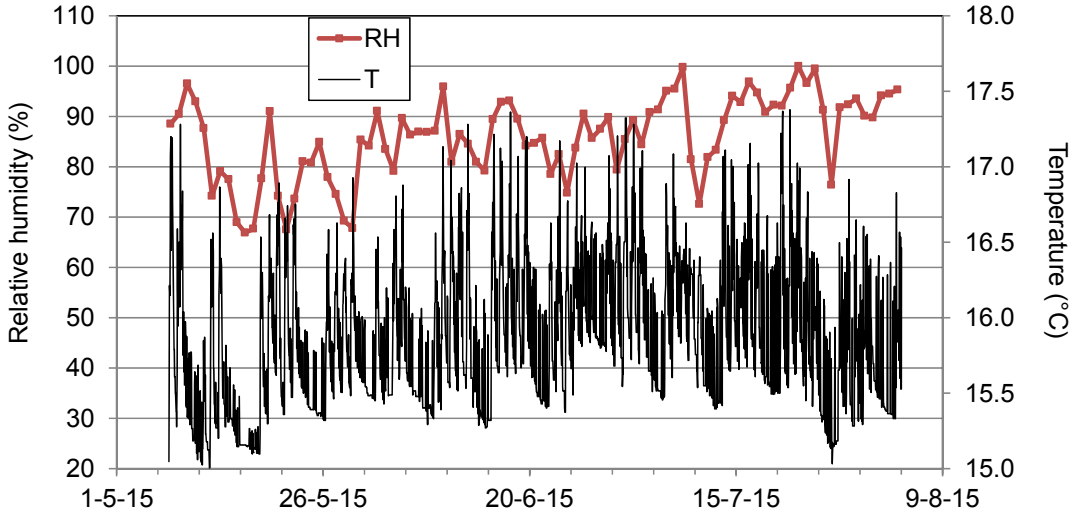

Fig. 8: Relative humidity and temperature in the service area of the FEBEX gallery (at location m. 44) during the bentonite dismantling period.

The samples were obtained by drilling the bentonite following a template (Fig. 9) with a crown drill bit (Fig. 10). In the sections around the liner, six samples were taken along each radius, and in those without liner, ten or eleven samples were taken along each radius. Additionally, in Sections 38 and 55 three samples were taken following a horizontal radius. The samples had a length of 6 cm and a diameter of 4.8 cm. They were immediately wrapped in plastic foil and taken to the on-site laboratory (Fig. 11), which was located at the start of the laboratory gallery at the northern end of the GTS (Fig. 12). Care was taken to cause as little disturbance as possible to the samples recovered, as the negative impact of bad practice on the results could be significant, as highlighted in the FEBEX-DP Round Robin test (Dixon & Kober 2015).

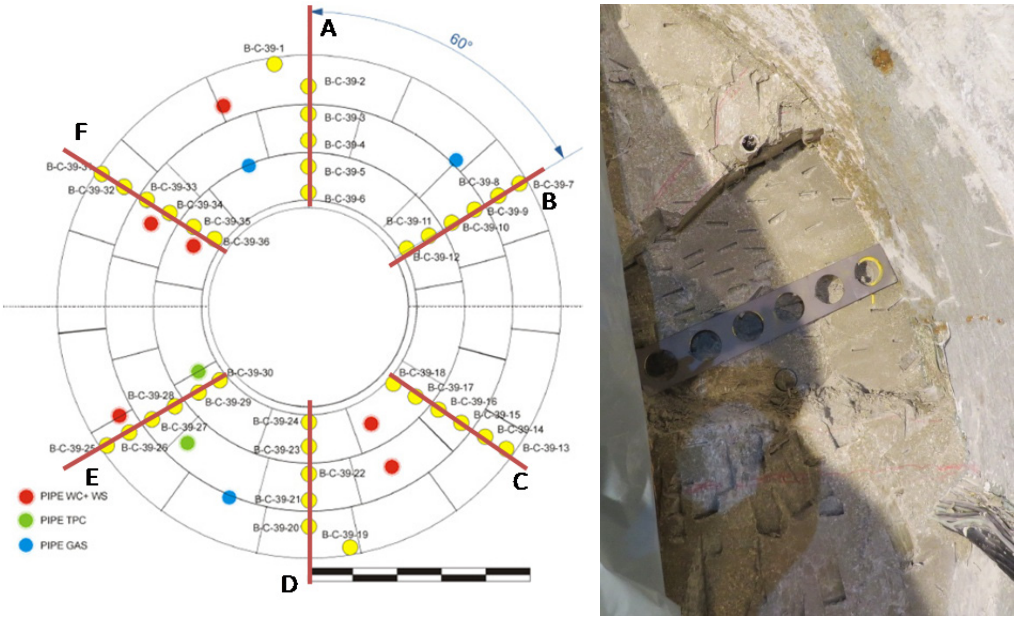

Fig. 9: Position of sampling radii in a section and template used to locate the drillings.

Fig. 10: Drilling of core samples for on-site determinations.

Fig. 11: On-site laboratory.

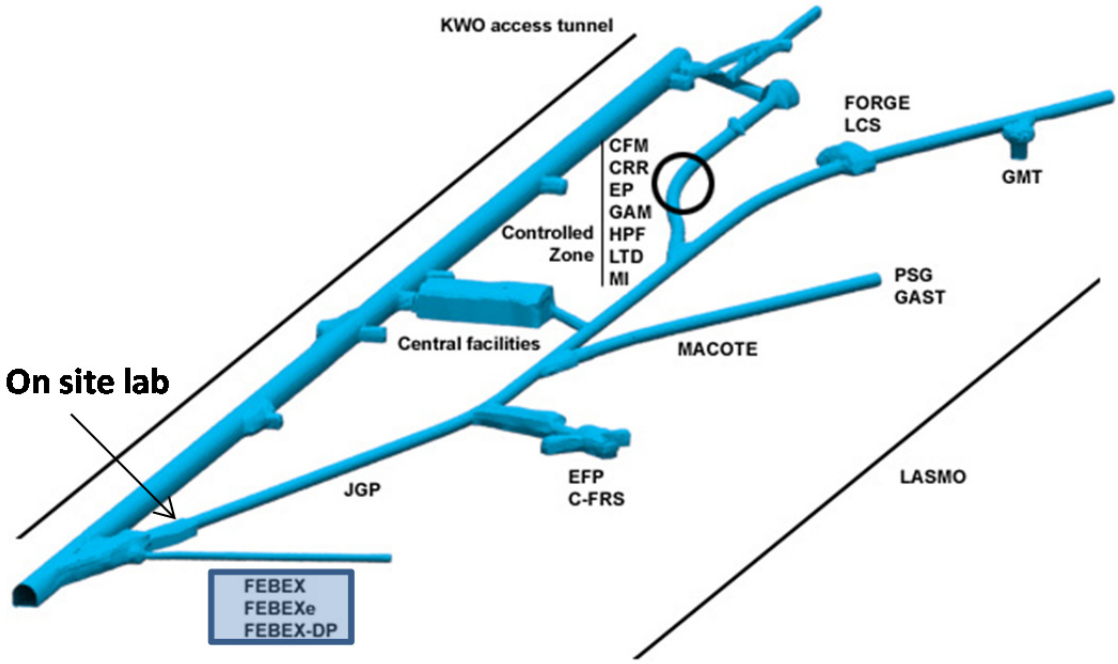

Fig. 12: Location of the laboratory for on-site determinations at the GTS (www.grimsel.com).

Once in the on-site lab each sample was cut and trimmed into two subsamples each of between 5 and 37 cm^3 volume (average volume 18 cm^3) and masses of between 10 and 75 g (average mass 35 g). The external part of the subsamples that had been in contact with the crown drill bit

was removed and the surfaces smoothed (Fig. 13). The one closer to the surface of the block towards the gallery entrance was referenced as subsample 1 and the more internal one as subsample 2. In each of these subsamples water content and dry density were determined.

Fig. 13: Removing of external surfaces of the subsamples and resulting subsample once smoothed.

The gravimetric water content (w) is defined as the ratio between the mass of water and the mass of dry solid expressed as a percentage. Consequently, all the values given in this report are weight percentages. The mass of water was determined as the difference between the mass of the sample and its mass after oven drying at 110 °C for 48 h (mass of dry solid). The precision of this measurement is about 0.2 %. Dry density (ρ_d) is defined as the ratio between the mass of the dry sample and the volume occupied by it prior to drying. The volume of the specimens was determined by immersing them in a vessel containing mercury and by weighing the mercury displaced (Fig. 14, Fig. 15), considering for the calculation of volume a mercury density of 13.6 g/cm^3. The precision of this measurement is between 0.01 and 0.02 g/cm^3. The same samples whose volumes had been determined were used for the water content determination (AITEMIN 2016a). The balance used was a Selecta GRAM FH-2000, with a range up to 2'000 g and a precision of 0.01 g.

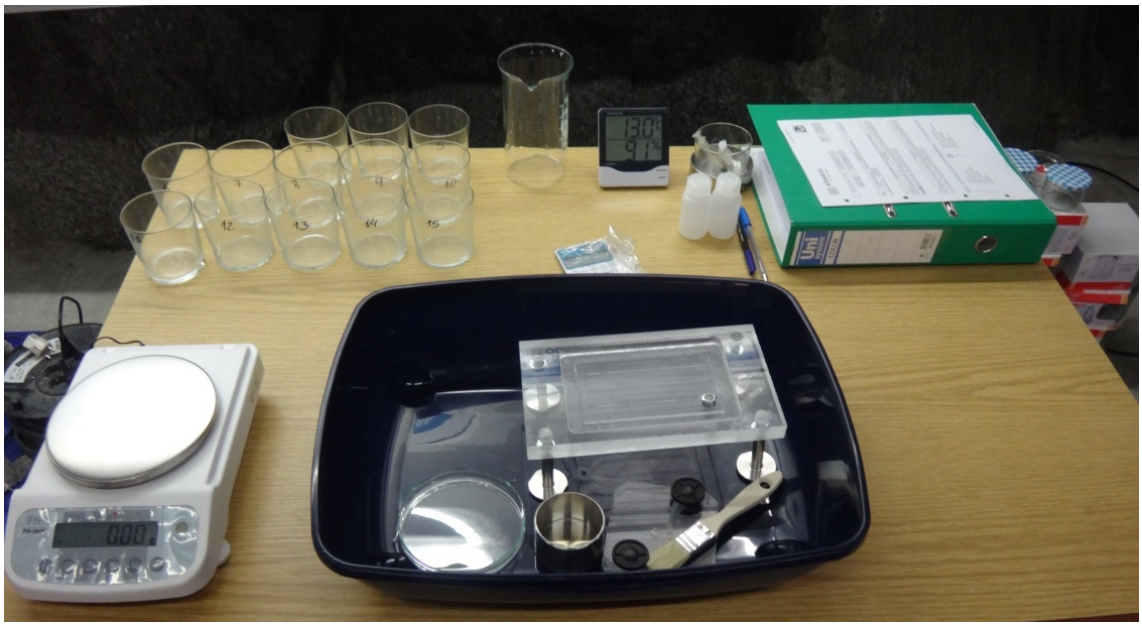

Fig. 14: Equipment for the on-site determination of dry density and water content.

Fig. 15: Different phases of the density and water content determinations: 1 and 2) immersion of the sample in mercury, 3) weighing of the mercury displaced, 4) weighing of the sample.

2.1 Assessment of the methodology: temperature and drying time

There is some debate about the time and temperature necessary to dehydrate bentonite, because the dehydration of bentonite is not only temperature-dependent but also time-dependent. It is known that the complete dehydration of the bentonites in divalent smectites takes place at temperatures as high as 170 °C (Ferrage et al. 2007). In fact, the FEBEX bentonite continues to dehydrate for temperatures as high as 175 °C. CIEMAT determined that the difference in water content computed using as dry mass that after two days drying at 110 °C and that at 175 °C is of almost 2 wt % for the FEBEX bentonite (Fig. 16). Upon drying at 200° the FEBEX bentonite continued to lose mass. This highlights the importance of using carefully controlled drying conditions when conducting moisture tests.

The temperature chosen for the on-site drying of the samples was 110 °C –which is frequently used in soil mechanics laboratories, as recommended by ASTM D2216– and the drying time 48 h. These values have been used at CIEMAT laboratories for several years. It should be noted that during the first dismantling the samples used for the on-site determinations were dried at 110 °C for 24 h (Villar et al. 2006). This means that care will need to be taken when comparing the results of these two dismantling operations.

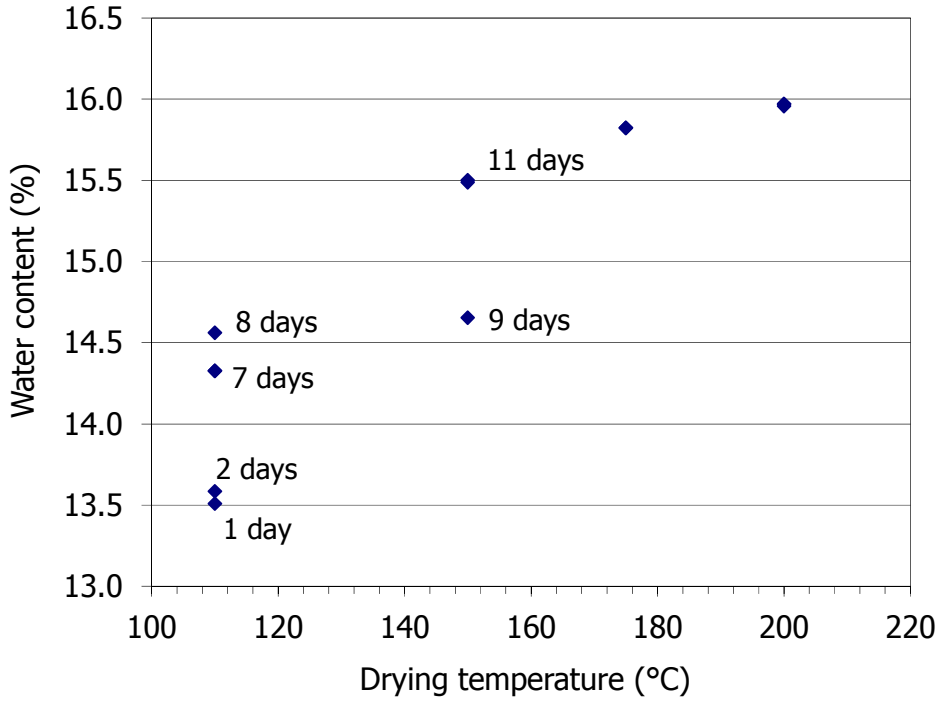

Fig. 16: Effect of drying time and temperature on FEBEX bentonite water content determined at CIEMAT laboratory.

For the purpose of evaluating the significance of drying time and temperature on the FEBEX samples, a few samples from S37 were kept in the on-site oven for several days. At 100 °C there was a mass loss from 48 h to 96 h corresponding to a water content increase of 0.2 – 0.4 %, and then the mass stabilized (Fig. 17). Since drying for 96 h would be impractical from an operational standpoint, the 48-h period was kept. However, it is important to be aware that some water loss can take place between 48 and 96 h of drying. The water content computed using the dry mass after drying for 48 h instead of 24 h can be 0.1 % higher in FEBEX samples with initial hygroscopic water content (Fig. 16).

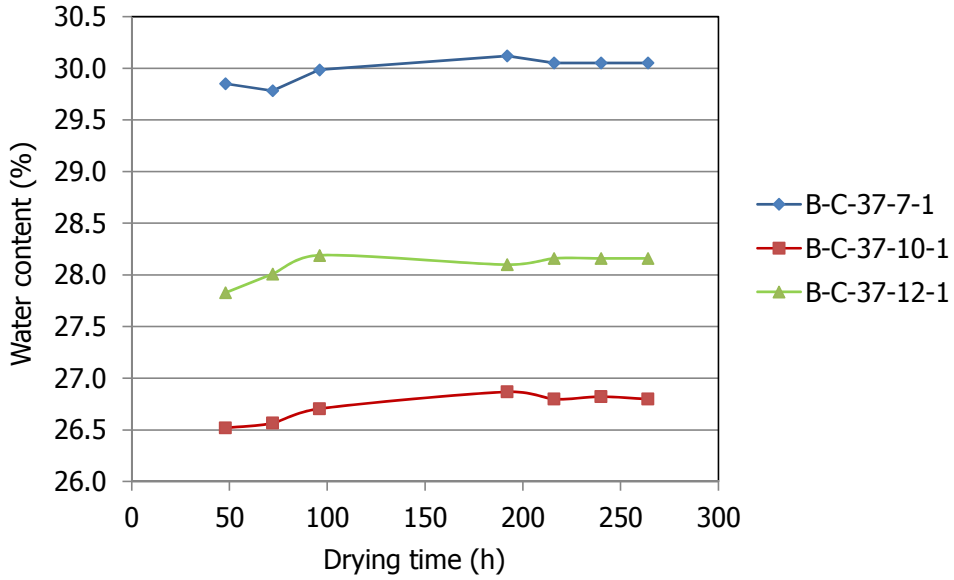

Fig. 17: Change in computed water content with drying time at 110 °C for 3 FEBEX samples.

2.2 Assessment of the methodology: different laboratories

In order to assess the methodology used on-site for the water content and dry density determinations, some subsamples in Sections 37 and 39 were vacuum-packed and sent to SKB laboratories, where these procedures were followed:

- For the determination of the water content, the specimens were dried for 24 hours at a temperature of 105 °C.
- The bulk density was calculated from the total mass of the specimen and the volume determined by weighing the specimen above and submerged into paraffin oil.

The results obtained on-site and at SKB for subsamples of the same cores are shown in Fig. 18 to Fig. 20 and summarised in terms of average values per set of samples in Tab. 2. These average values are very similar for the two laboratories, particularly with respect to water content, which indicates that the preservation conditions of the samples were good and that the differences in drying time did not affect the results noticeably. The dry density averages are the same for the two laboratories up to the second decimal, which is about the accuracy of the technique.

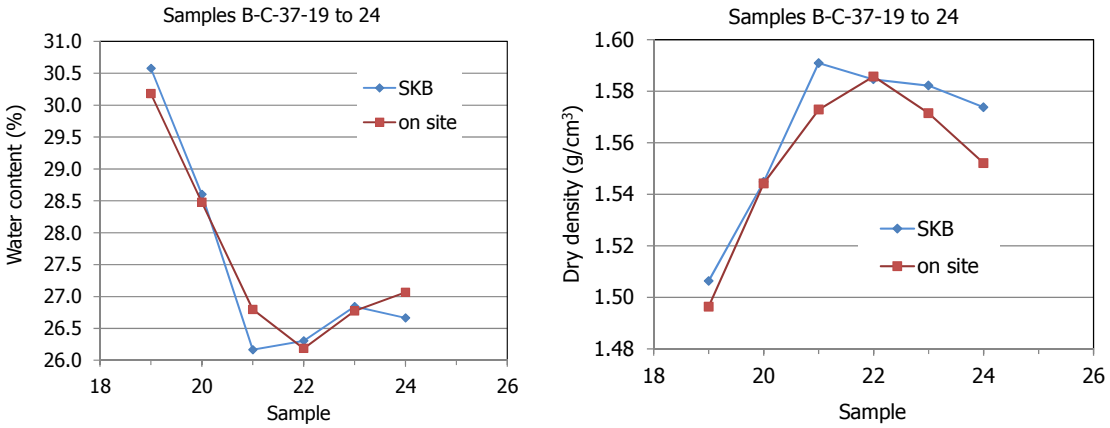

Fig. 18: Water content and dry density of samples from Section 37 (B-C-37-19 to 24, indicated in the *x*-axes of the figures) as obtained on-site and by SKB.

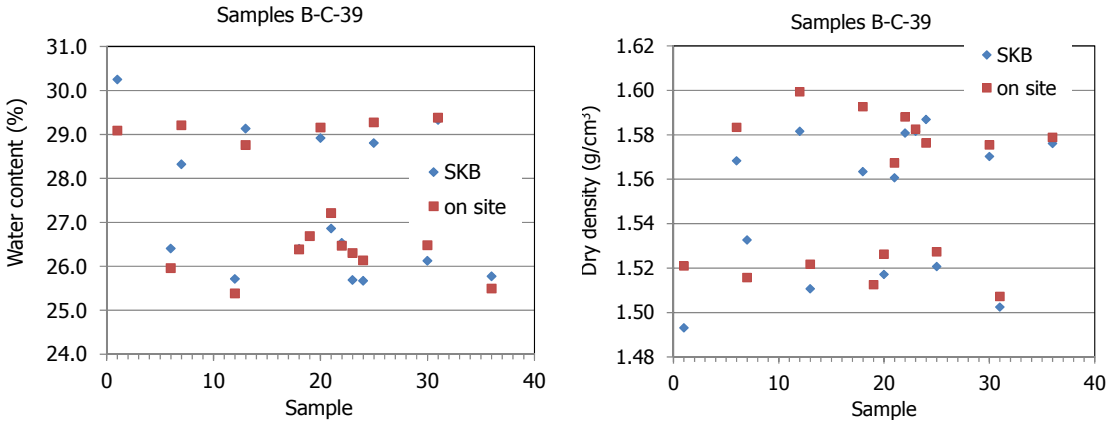

Fig. 19: Water content and dry density of samples from Section 39 (B-C-39-1 to 36, indicated in the *x*-axes of the figures) as obtained on-site and by SKB (samples outside the liner).

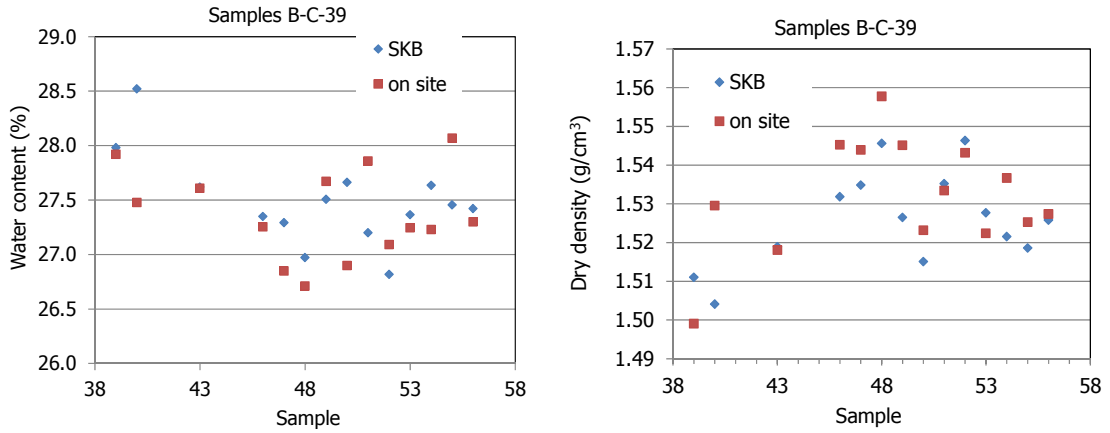

Fig. 20: Water content and dry density of samples from Section 39 (B-C-39-39 to 56, indicated in the *x*-axes of the figures) as obtained on-site and by SKB (samples inside the liner).

Tab. 2: Average values obtained on-site and by SKB for different sets of samples.

	S37		**S39 inside liner**		**S39 outside liner**	
	w (%)	ρ_d (g/cm^3)	*w* (%)	ρ_d (g/cm^3)	*w* (%)	ρ_d (g/cm^3)
On-site	27.6	1.55	27.3	1.55	27.4	1.53
SKB	27.5	1.56	27.3	1.55	27.5	1.53
Difference	0.05	-0.010	0.01	0.005	-0.12	0.006

3 Results

The location of the sections sampled on site is shown in Fig. 6. The slice to which these sections corresponded as well as the initial and final x-coordinates of the sections, as measured with the laser distance-meter and with the metric tape nailed down to the granite during installation, are given in Tab. 3. The coordinate origin is indicated in Fig. 5.

Tab. 3: Sections sampled for water content and dry density on-site determinations.

Section	**Slice**	**Instrumented**	**Original *x*-coordinate laser** (m)	**Final *x*-coordinate laser** (m)	**Final *x*-coordinate tape** (m)
37	70	Q	8.455	8.405	
38	67	G	8.835	8.815	
39	64		9.214	9.186	
42	59	I	9.855	9.831	
43	57		10.107	10.090	
45	49	S	11.112	11.100	11.100
49	40		12.265	12.253	
52	31		13.413	13.379	
55	23		14.430	14.410	
56	22		14.555	14.520	14.540
58	13		15.695	15.711	15.700
61	4		16.870	16.944	16.940

The following subchapters detail the results obtained for each sampling section in terms of water content and dry density determined on site. The corresponding degrees of saturation are also given, computed as detailed in the following subchapter.

Photographs of the sections after installation in 2002 and just before dismantling in 2015 are shown, as well as figures showing the location of the core samples according to the Sampling Book and the Dismantling Report (AITEMIN 2015, 2016a). The water content, dry density and degree of saturation have been plotted as a function of the distance to the gallery axis for each section. In these plots, the values obtained in the two subsamples per core are shown. The average values of these two subsamples are presented in Annex I and were used to obtain the 2-D plots for water content, dry density and degree of saturation of the sections. These plots have been obtained with the contour mapping software Surfer® using the Kriging gridding method. The same colour code has been used in all the sections to draw the contour plots for each parameter (water content, dry density, degree of saturation). In some of these plots (particularly those representing the degree of saturation) concentric isolines around a particular sampling point were drawn. In most cases those are plotting artefacts caused by the small range of values in the figures. The average values of each parameter have been computed by the mapping software for each section.

Taking into account the axial symmetry of the water content, dry density and degree of saturation distributions, the average values of these variables in a vertical section have been obtained by fitting polynomial functions to represent their variation with the distance to the gallery axis, as it was already done with the results of the first dismantling (Daucausse & Lloret 2003, Villar et al. 2005).

For each section a Table summarising the following information has been prepared:

- Temperature during operation, estimated based on the recordings of adjacent sections taken from Bárcena et al. (2006) for the 1st operational phase and from AITEMIN (2009, 2014, 2016b) for the 2nd operational phase
- Sampling date, days since switching off
- Thickness of the section, computed as the difference between the x-coordinate of the following slice and that of the section sampled. In a few cases the thickness of the blocks was also measured, as well as their radii. This information is presented in separate tables.
- Observations concerning the initial and final state of the section as well as sampling particularities
- Average values of water content, dry density and degree of saturation as computed by the mapping software and from the polynomial functions

3.1 Computating the degree of saturation

The degree of saturation (Sr), which is the ratio of volume of water to volume of voids, has been computed using the Equation:

$$S_r = \frac{w \times \rho_d}{n}$$

where w is the water content, ρ_d is the dry density, and n is the porosity, in turn computed using the dry density and the solid specific weight (G_s). This Equation assumes that the water has a density of 1 g/cm^3. To calculate the degrees of saturation shown in the following subchapters and in the Annex, the dry density and water content measured on-site for every sample have been used. The value obtained will depend thus on the solid specific weight (G_s) used. If a value lower than the actual one were used, the degrees of saturation would be fictitiously high and *vice versa*. For the FEBEX bentonite used to manufacture the blocks used at GTS, a solid specific weight of 2.70 ± 0.04 g/cm^3 (average of 20 measurements) was determined in pycnometers using water for soil suspension (Villar 2002, ENRESA 2000, 2006). In 25 samples taken from Grimsel during the 2015 dismantling, this parameter has been determined again and the same average value has been found. Given that the degrees of saturation computed for the samples analysed on-site are in some cases notably higher than 100 % –which makes no physical sense–, in addition to the average specific weight of 2.70 g/cm^3, the uppermost value of the range has also been used to compute the degrees of saturation shown in the Annex, and the two values appear in the Tables.

In addition to the uncertainties in the specific weight value determination, there is another reason for obtaining computed degrees of saturation incongruously high. This is the assumption in the calculation that the water density is 1 g/cm^3, although it is known to be higher in the water adsorbed in bentonites. There is increasing evidence from the fields of neutron diffraction, Monte Carlo computer simulations and quasi-elastic neutron scattering that the density of water attached to clay minerals may be greater than 1.0 g/cm^3 (Skipper et al. 1991, Monsalvo et al.

2006, Chávez-Paéz et al. 2001, Tambach et al. 2004, Huang et al. 1994), with values of water density in phyllosilicates of up to 1.38 g/cm^3, higher in smectites with divalent cations in the interlayer (such as FEBEX) than with monovalent ones (Jacinto et al. 2012). This fact becomes especially evident in highly compacted expansive clays close to water saturation, in which degrees of saturation much higher than 100 % can be computed if a water density value of 1.0 g/cm^3 is considered (Villar 2002, Marcial 2003, Lloret & Villar 2007). Thus, a computed degree of saturation of 115 % for a saturated sample would indicate that the average density of the water in it is 1.15 g/cm^3. Besides, the proportion of adsorbed water (with a density higher than 1 g/cm^3) over free water (with a density of 1 g/cm^3) increases as the dry density of the bentonite is higher.

Since there is no accurate knowledge on the values that the density of water can take (which would depend on the particular bentonite, its density and water content), the customary value of 1 g/cm^3 has been used in the calculations presented in the following subchapters and Annex, which would partially explain the degrees of saturation higher than 100 %.

3.2 Section 37, Slice 70

This sampling section corresponds to the installation Slice 70 and the instrumented Section Q, where relative humidity sensors were installed (it should be noted that these sensors had stopped working long before the dismantling operation). In Slice 74 (instrumented Section P), the total pressure sensors at the bentonite/concrete plug interface were recording values of around 6 MPa before dismantling. Section 37 was located around the dummy canister, which means that during the first five years of operation the bentonite had been subjected to a thermal gradient (Bárcena et al. 2006). After five years, Heater #1 was replaced by the dummy canister and 13 years of hydration under lower temperature followed. The closest thermocouples, located three slices closer to Heater #2, in Section 38 (Slice 67, instrumented Section G), recorded temperatures between 30 and 40 °C during the 2nd operational phase (AITEMIN 2014, 2016b). Following the heater's switching off and until Section 37 was dismantled, the temperatures in Slice 67 decreased to 24 °C (AITEMIN 2016b). Since Slice 70 was farther away from the heater than Slice 67, the temperatures at this location during operation and dismantling must have been slightly lower than 24 °C. The bottom right side of the section was affected by the lamprohyre dyke (Fig. 2).

Fig. 21 shows the initial and final appearance of this slice. The large gaps between blocks were completely sealed during operation, as well as the paths carved in the blocks for the passing of cables. The pipes sticking out of the bentonite that can be observed in the picture taken during dismantling were installed through the concrete plug after the first operational phase. Around the bottom surface of the liner, the bentonite was green-coloured, whereas in the upper part, the liner was deformed and bentonite had protruded between it and the liner (Extra Report No.13 in Kober [2015]) and was reddish in colour (Fig. 22). The lower right quarter of the gallery was covered with iodine-doped filter paper at this point. The area covered by the filter paper is shown in Fig. 23, where the location of the sampling points is indicated. The radial dimension of some blocks measured with a metric tape during dismantling is given in Tab. 4.

Fig. 21: Initial and final appearance of Slice 70 (Section 37).

Fig. 22: Green halo around the bottom part of the liner (left) and reddish-coloured bentonite protruded between liner and heater (right).

Tab. 4: Dimensions of the blocks along the radius in Slice 70, Section S37 (the kinds of block are indicated in Fig. 4, the original dimension for all was 216.7 mm).

Θ (°)	**BB-G-01** (mm)	**BB-G-02** (mm)	**BB-G-03** (mm)
45	225	221	180
80	220	220	215
90	218	225	215
280	220	215	
315	205	222	205
Average	218	221	204

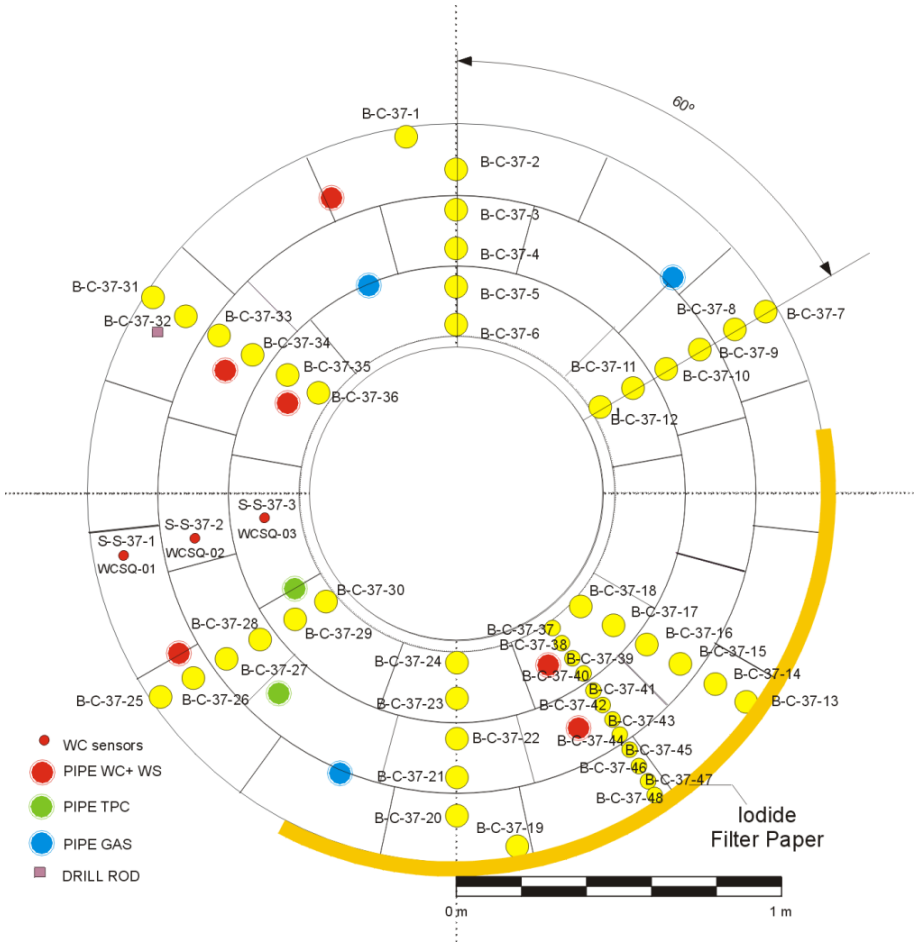

Fig. 23: Location of samples taken in Section 37.

Fig. 24 through Fig. 29 show the results for water content, dry density and computed degree of saturation, first as a function of the distance to the gallery axis and then as contour maps. The water content tended to decrease from the gallery wall towards the gallery axis in the outermost 35 cm of the barrier, whereas in more internal parts of it, the water content increased towards the axis of the gallery (Fig. 24, Fig. 25). The bentonite in this section could have taken up some of the water supplied at the time of concrete spraying at the beginning of the 2nd operational phase, but given the radial pattern of water distribution in the section, this must have not been a relevant input. The dry density followed reversed patterns to water content, i.e. it was lower towards the granite and towards the liner (Fig. 26, Fig. 27). The saturation of the section derived from the water content and dry density measurements are provided in Fig. 28 and Fig. 29. A summary of the characteristics of the section is given in Tab. 5.

The decrease of dry density towards the liner could be related to the intrusion of bentonite between the liner and the heater (Fig. 22). The blocks in the external ring (type BB-G-01) and those in the medium ring (type BB-G-02) were longer in the radial direction than those in the inner ring (Tab. 4). Taking into account that the initial radial dimension of the blocks was 217 mm (Tab. 1), the internal ring was considerably compressed, while the two others expanded. Upon compression, the bentonite in the internal ring protruded inside the liner, and this would mean that the dry density of the inner part of the barrier would decrease and its water content increase. This would also ease the expansion of the blocks in the middle ring.

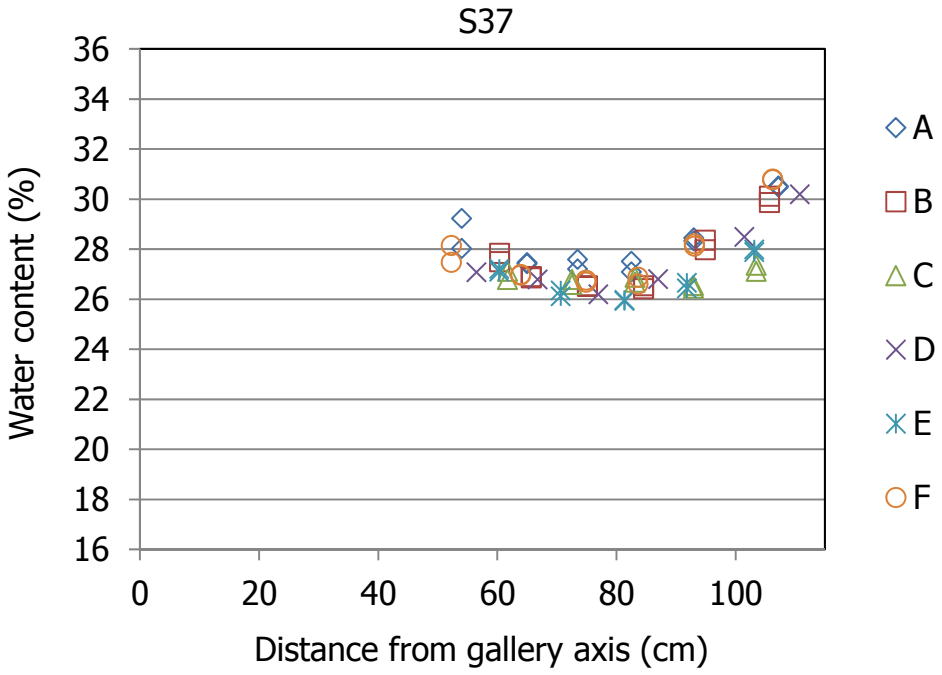

Fig. 24: Water content measured in subsamples along the six sampling radii in Section 37.

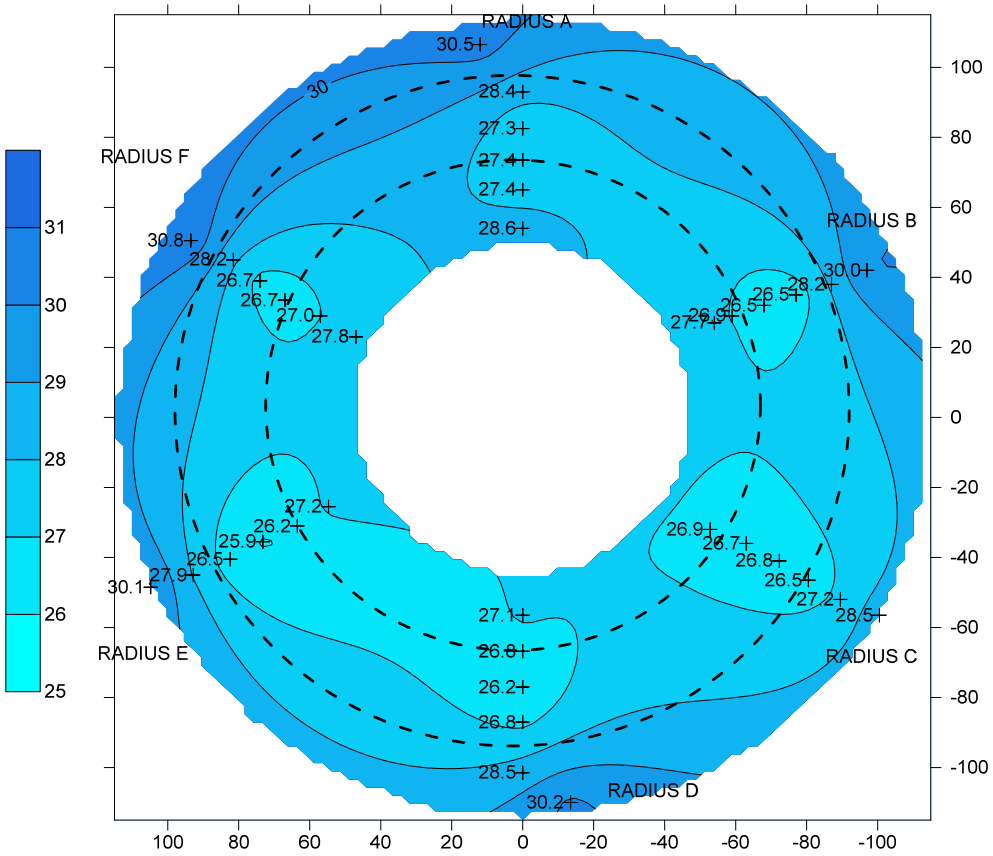

Fig. 25: Contour map for water content in Section 37.

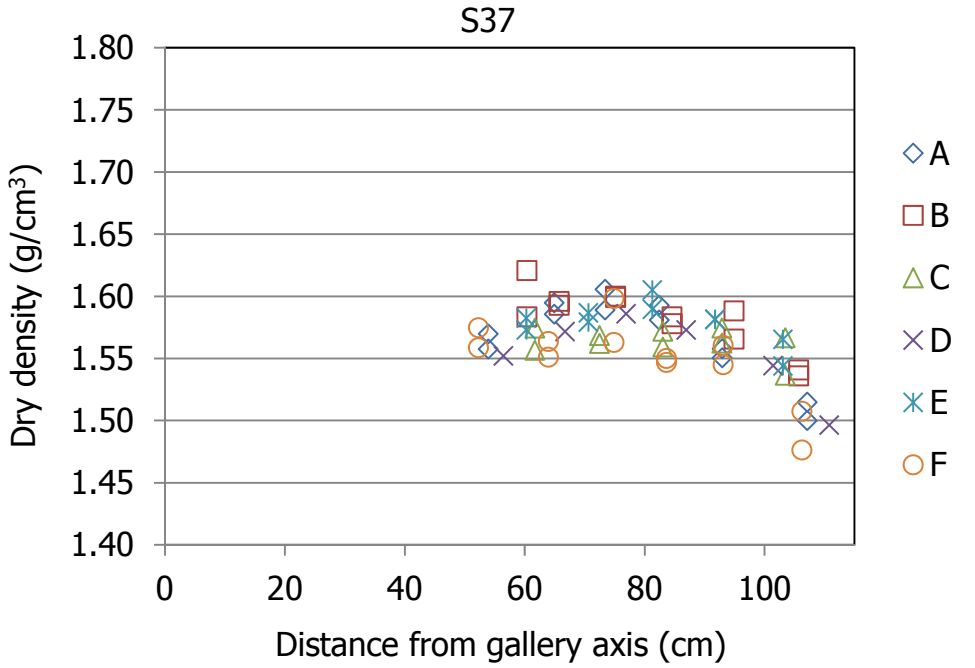

Fig. 26: Dry density measured in subsamples along the six sampling radii in Section 37.

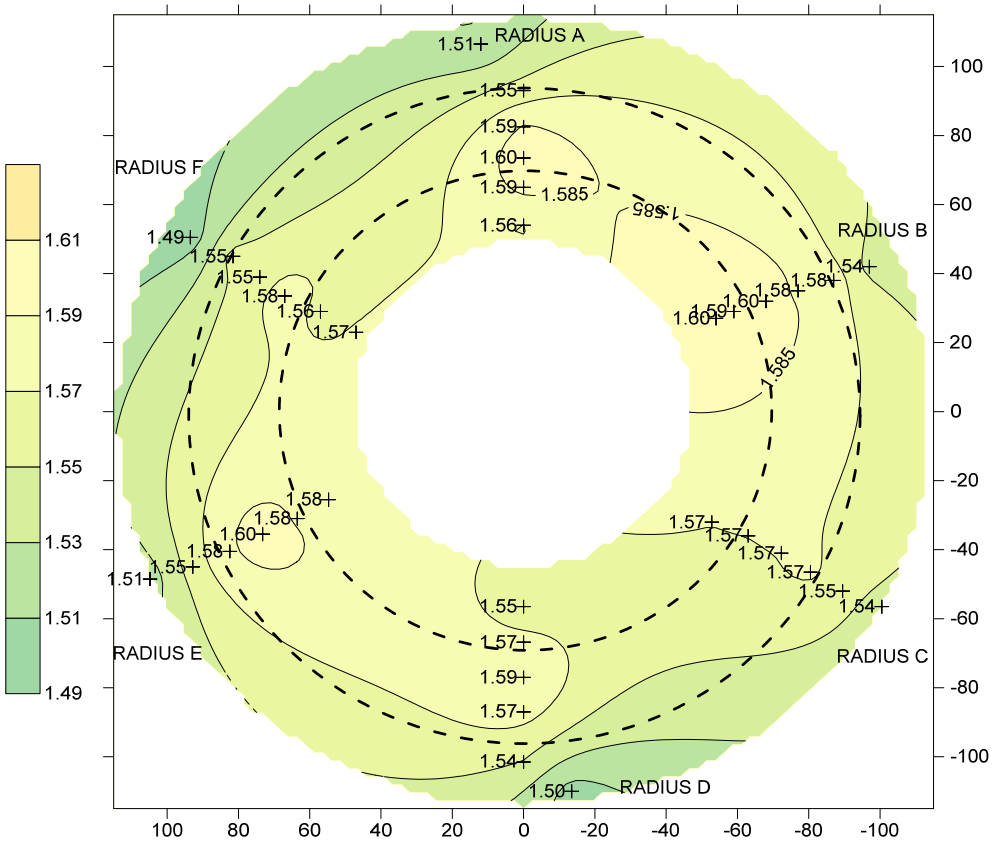

Fig. 27: Contour map for dry density in Section 37.

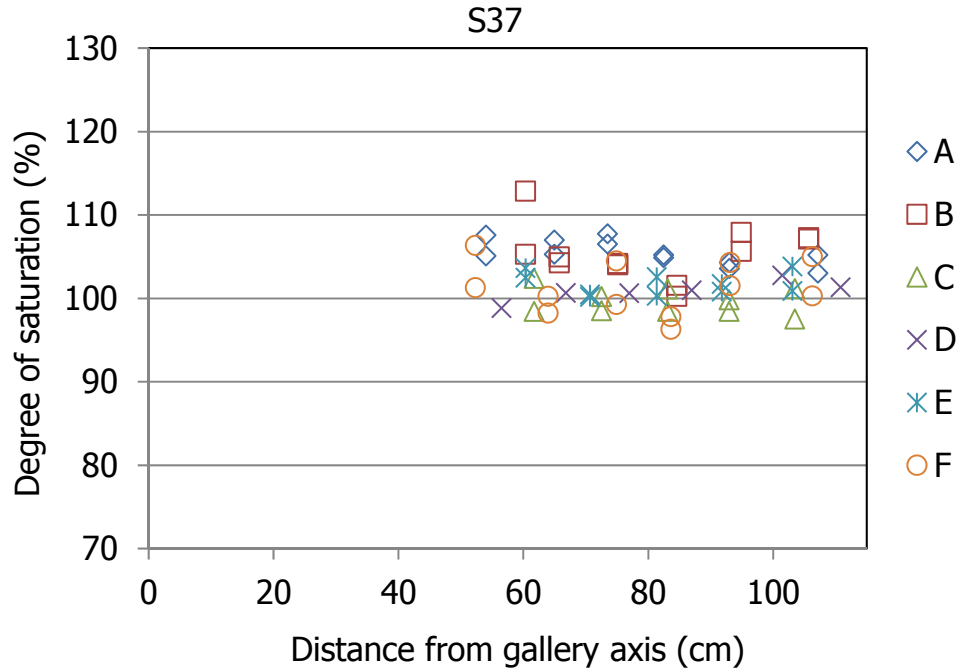

Fig. 28: Degree of saturation of subsamples along the six sampling radii in Section 37 (inexact values because of solid specific weight and water density uncertainties).

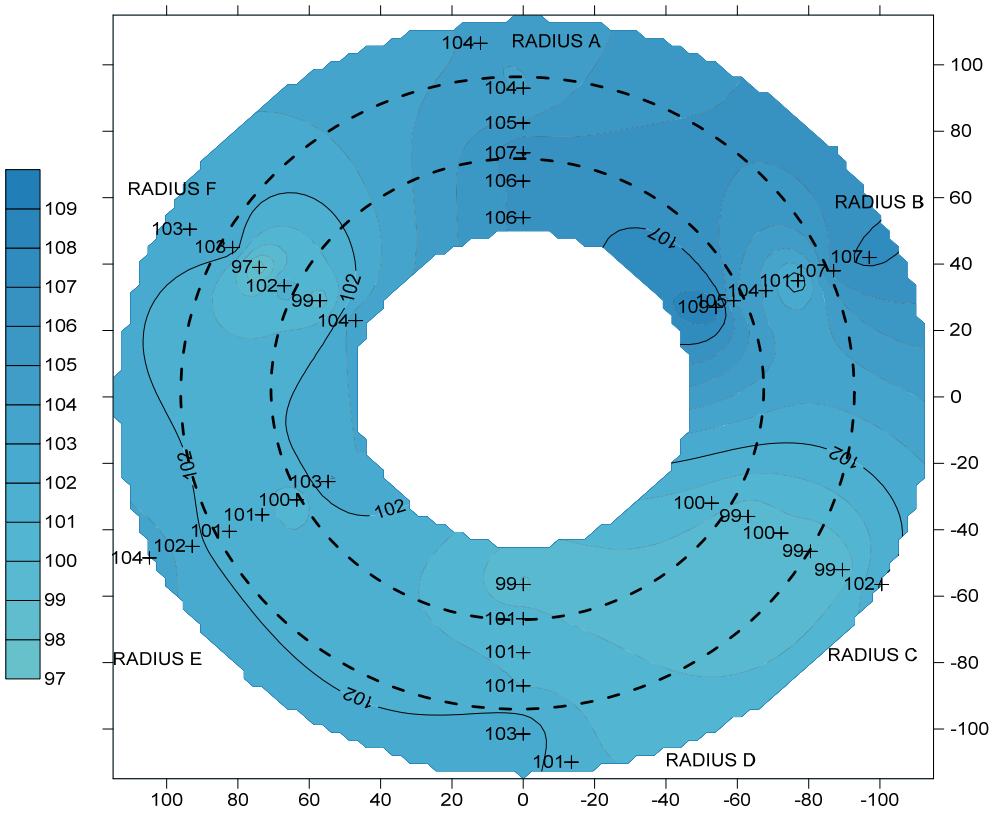

Fig. 29: Contour map for degree of saturation in Section 37 (inexact values because of solid specific weight and water density uncertainties).

The water content and dry density spatial changes probably reflect the superposition of the two operation phases: a first one under thermal gradient and a second one under a more homogeneous temperature. The fact that the water content was higher in the internal part of the barrier could be related to the higher water retention capacity of the bentonite subjected to higher temperatures and desiccation during the 1st operational phase, because owing to hysteresis, the water retention capacity of a material is higher if it has experienced previous drying. The degree of saturation was homogeneous all through the section and in most samples higher than 100 % (as it has been explained above these inconsistent values are a consequence of the uncertainties in the water density and solid specific weight values used in the computations), as reported in Fig. 28 and Fig. 29.

Radii C and E had in the external part water contents slightly lower than the other radii. Otherwise no significant differences among the radii were observed, and the lamprophyre crossing the bottom right part of the gallery (Fig. 2) does not seem to have had an influence on the water distribution inside the barrier.

Tab. 5: Summary Section 37.

Slice/instrumented section	70/Q (relative humidity)	
Estimated T during operation	< 44 – 104 °C 1st operational phase; 28 – 40 °C 2nd operational phase (based on G instrumented section)	
Sampling date/time since switching-off	May 18 – 20th 2015/24 – 26 days	
As built/final x-coordinate (m)	8.455/8.405	
Observations	• Lamprophyre dyke at the right hand bottom • I-doped filter paper lower-right quarter • Green halo around bottom of liner • Bentonite protruded between heater and deformed liner	
Initial/final thickness (mm)	125/133	
	Mean output grid values	Polynomial function
w (%)	28.3	27.9
ρd (g/cm3)	1.55	1.56
Sr (%)	103	103

3.3 Section 39, Slice 64

This section should have been sampled according to the Sampling Book (AITEMIN 2015) in installation Slice 66, but it was moved to Slice 64. The bottom left side of the gallery at this level (61.964 m) was affected by a lamprophyre dyke (Fig. 2). It is one slice apart from the back of the dummy canister. This means it was never in direct contact with the heater, although during the 1st operational phase the temperatures in it could have been quite high. In fact, in Slice 67 (corresponding to instrumented Section G) the temperatures were between 44 and 104 °C in the 1st Phase (Bárcena et al. 2006). When Heater #1 was replaced by the dummy canister for the 2nd Phase of testing, the temperatures in Slice 64 were probably higher than 30 – 40 °C (based on the temperatures recorded in instrumented Sections G and I). Based on the recordings of the nearest instrumented sections (G and I), the temperatures in this section by the

time it was dismantled had decreased to less than 24 °C (AITEMIN 2016b). In the neighbouring Slice 63 (instrumented Section H) the psychrometers installed in the two external rings of the barrier indicated suctions of 0 kPa at the end of the 1st operational phase, and were not functioning in the 2nd phase. The capacitive sensors installed during the 2nd operational phase in Sections G and I recorded RH of ~100 % in the three external rings of the barrier before they stopped working (AITEMIN 2009), and the total pressure cell in the middle of instrumented Section G was recording 5.7 MPa just before dismantling.

Fig. 30 shows the initial and final appearance of Slice 64. The pipes sticking out of the bentonite were installed through the concrete plug after the 1st operational phase. The location of the sampling points is indicated in Fig. 31. The cores inside the liner were taken later on the same day as the others. According to the installation records (Fuentes-Cantillana & García-Siñeriz 1998) the blocks inside the liner in the area between the two heaters had to be machined during installation to adjust them to the internal diameter of the liner, and this made the average dry density inside the liner decrease to 1.55 g/cm^3 and the water content to 8 %. A summary of the characteristics of the section is given in Tab. 6.

Fig. 32 through Fig. 37 show the results for water content, dry density and computed degree of saturation for Section 39, first as a function of the distance to the gallery axis and then as contour maps. There are differences between the samples taken inside and outside the liner. Despite the fact that the range of water content and dry density in the entire section is not large, the samples taken inside the liner had slightly higher water content and lower dry density than the others. Moreover, the samples outside the liner showed a trend of water content decrease and dry density increase from the gallery wall towards the axis of the gallery. The lower dry density inside the liner is a consequence of the installation differences commented above. The average dry density in the part of the barrier outside the liner was higher than that inside the liner, and this could not change during operation because the liner did not allow any significant solid mass transfer. The differences in water content distribution are probably a result of the superposition of the two operation phases: a first one under a high thermal gradient and a second one under a more homogeneous temperature. The degree of saturation was ~100 % in most samples but decreased to about 95 % in the central block.

Fig. 30: Initial appearance of Slice 66 and final appearance of Slice 64 (sampling S39).

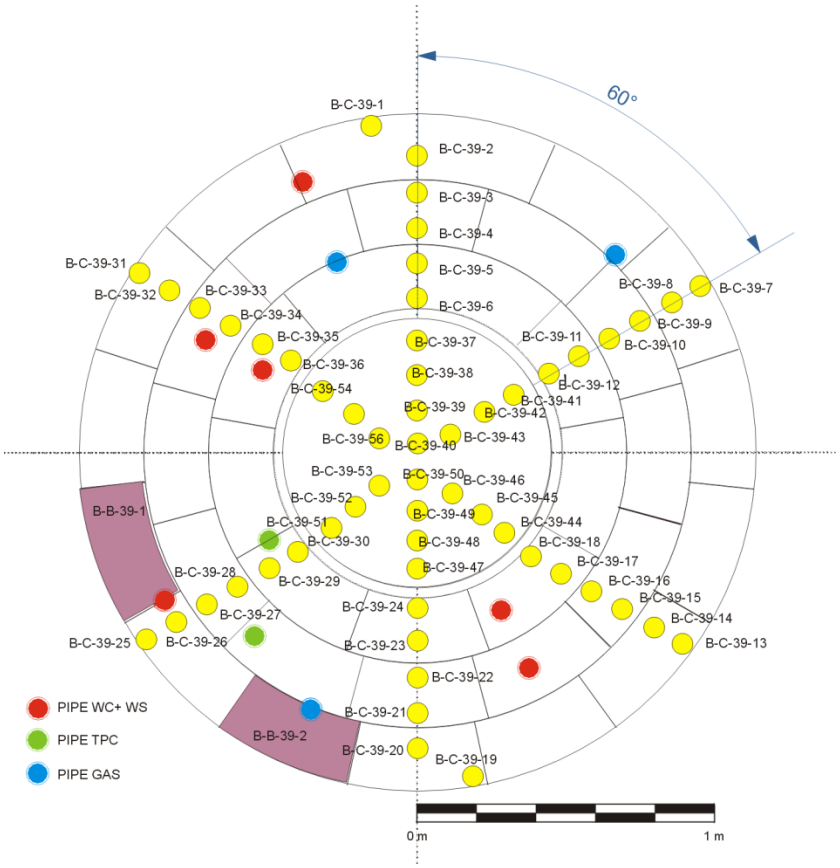

Fig. 31: Location of samples taken in Section 39 (sample B-C-39-19 was finally taken alligned with the others in Radius D).

Tab. 6: Summary Section 39.

Slice/instrumented section	64	
Estimated T during operation	< 44 – 104 °C 1st operational phase; 28 – 40 °C 2nd operational phase (based on G instrumented section)	
Sampling date/time since switching-off	May 26 – 27th 2015/32 – 33 days	
As built/final x-coordinate (m)	9.214/9.186	
Observations	• Initial dry density of the barrier inside the liner 1.55 g/cm^3 and water content 8 % (due to mechanization during installation) • Bottom left side of the gallery affected by lamprophyre dyke • Samples inside the liner taken later the same day	
Initial/final thickness (mm)	126/127	
	Mean output grid values	Polynomial function
w (%)	27.7	27.3
ρd (g/cm^3)	1.54	1.56
Sr (%)	100	100

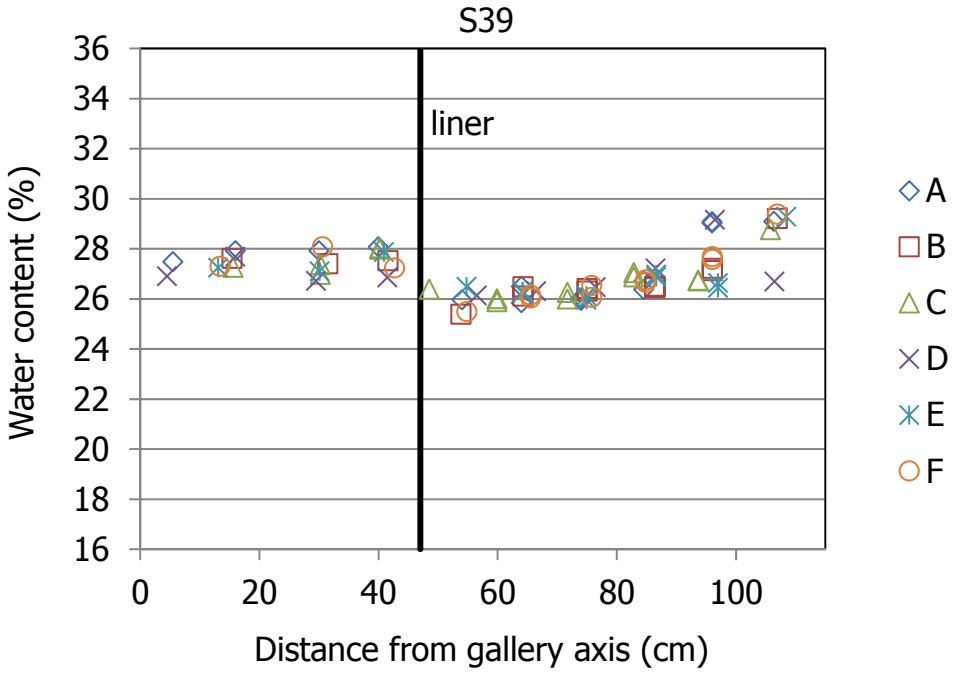

Fig. 32: Water content measured in subsamples along the six sampling radii in Section 39.

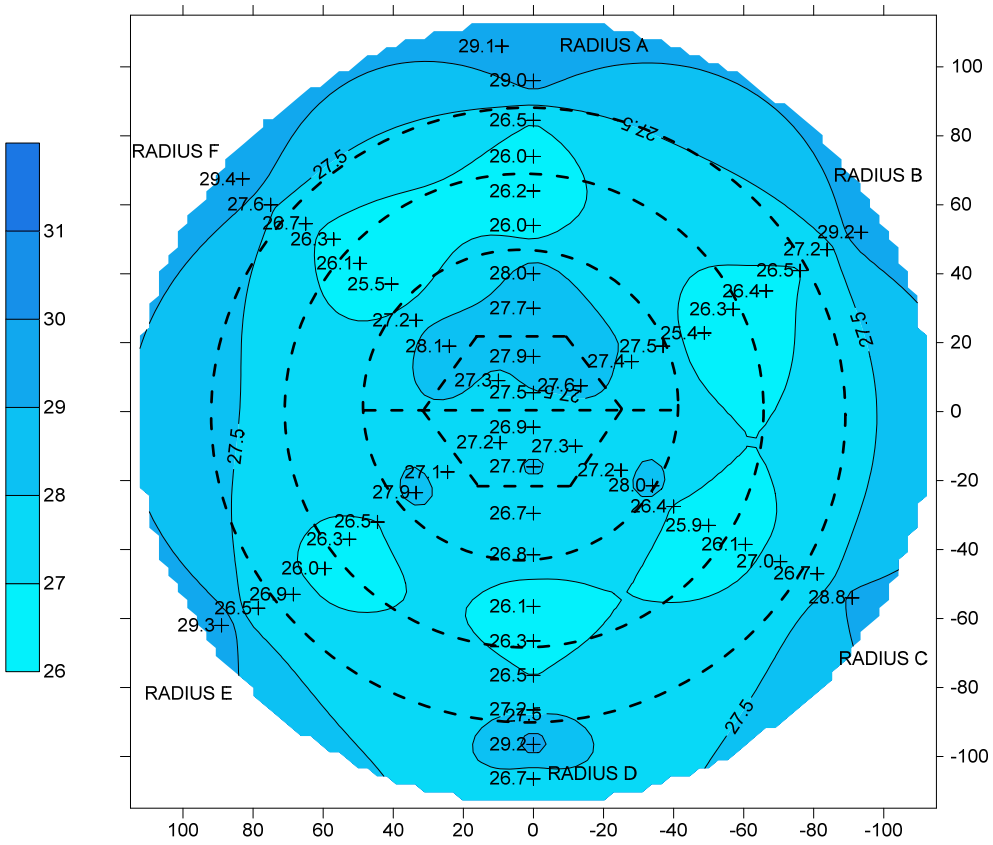

Fig. 33: Contour map for water content in Section 39.

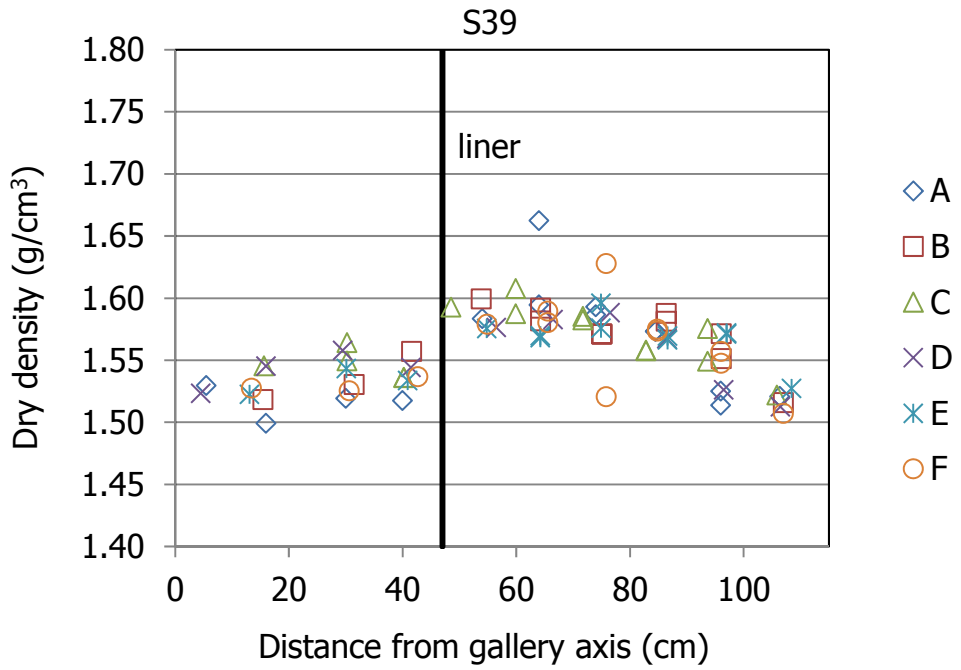

Fig. 34: Dry density measured in subsamples along the six sampling radii in Section 39.

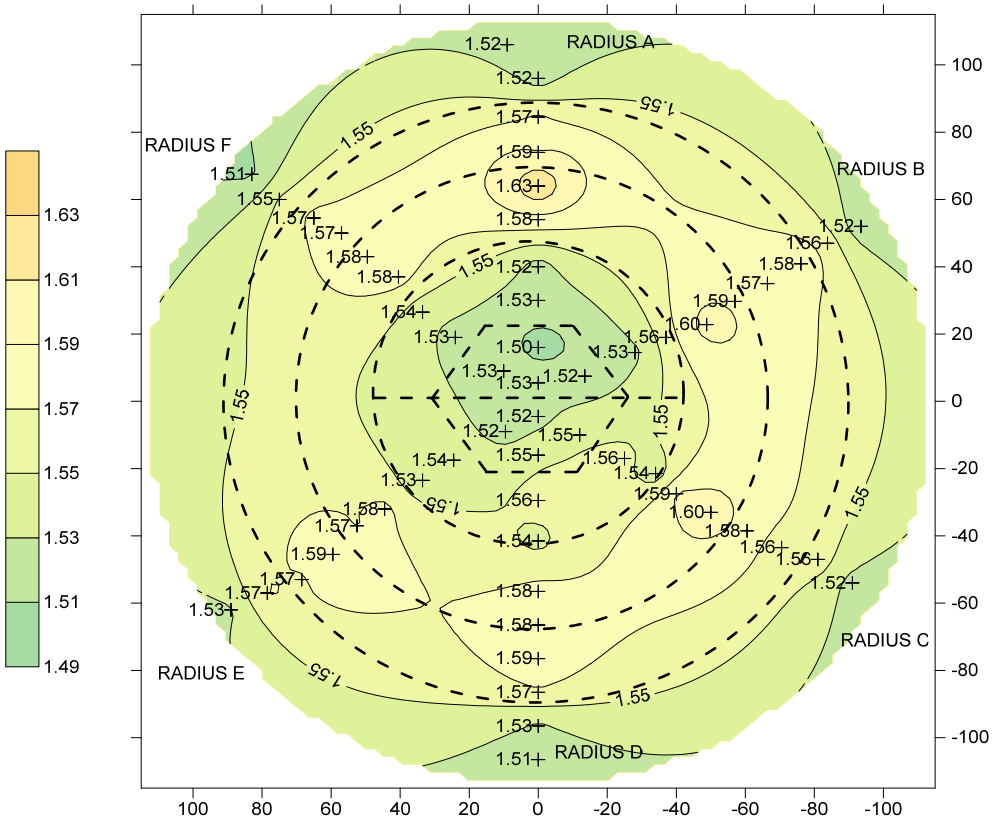

Fig. 35: Contour map for dry density in Section 39.

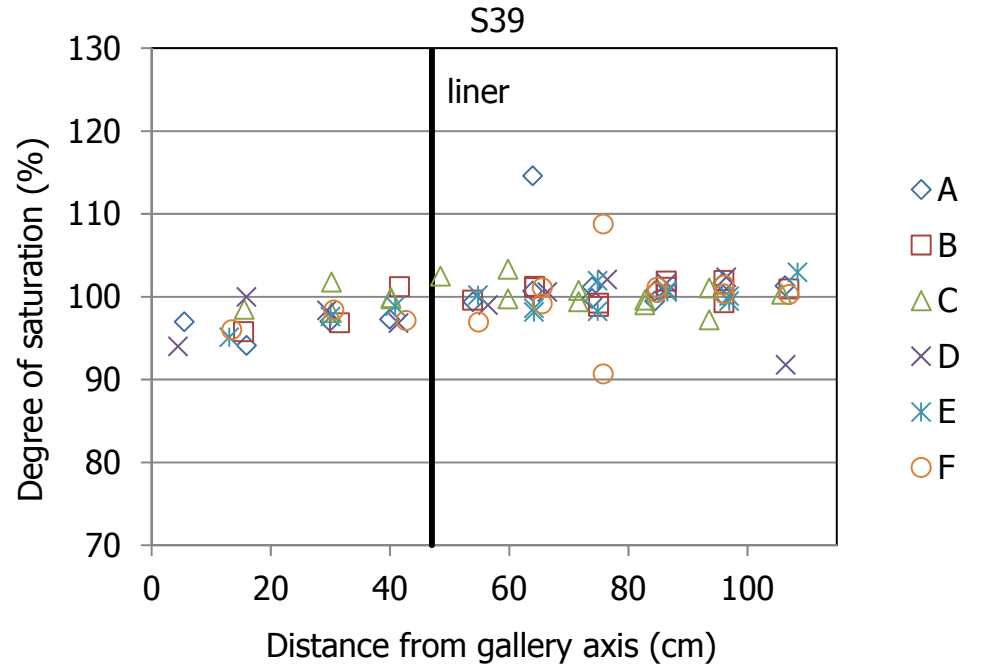

Fig. 36: Degree of saturation of subsamples along the six sampling radii in Section 39 (inexact values because of solid specific weight and water density uncertainties).

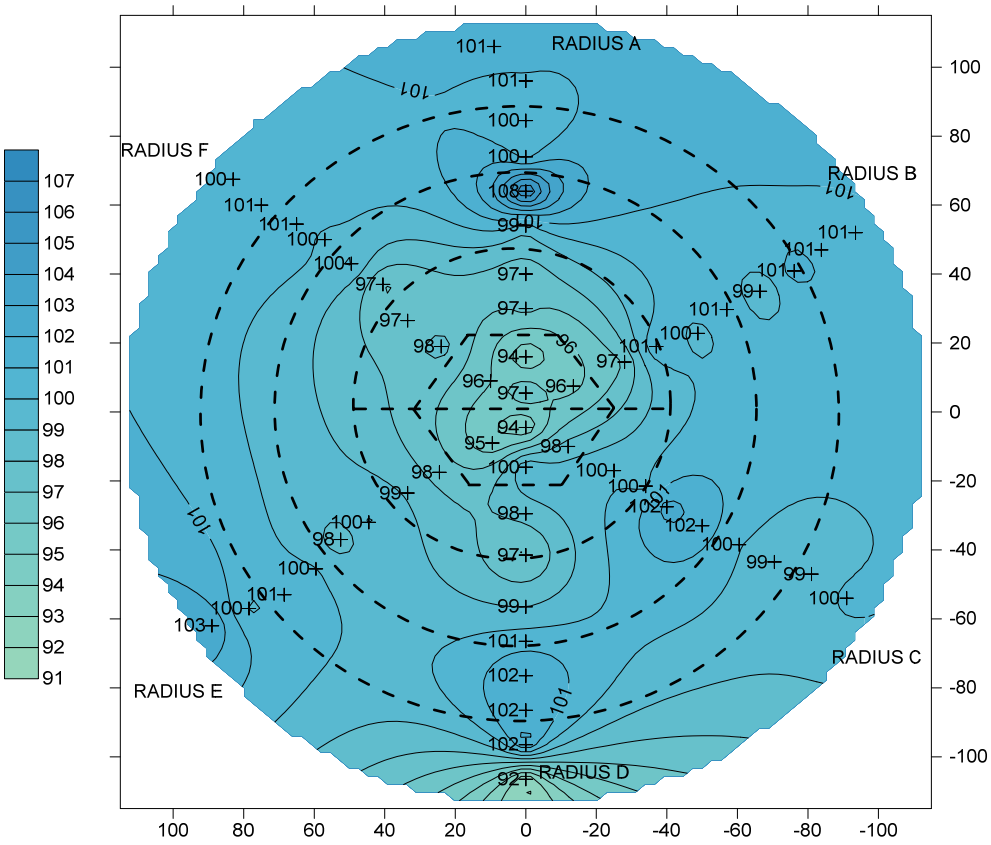

Fig. 37: Contour map for degree of saturation in Section 39 (inexact values because of solid specific weight and water density uncertainties).

3.4 Section 43, Slice 57

This section was in front of Heater #1. Before switching off the heater, the temperatures in it could have been between 40 and 88 °C (slightly higher during the 1st operational phase, according to the measurements taken in Slice 59 [instrumented Section I]). When the section was dismantled the temperatures in it had decreased below 20 °C. This significant temperature decrease could have caused certain water redistribution in the internal part of the barrier. In instrumented Section I a capacitive sensor placed in the inner ring was recording a RH of 74 % in 2009 and of 56 % just before the final dismantling, while the sensors placed in the two external rings had been flooded for many years. A total pressure sensor installed in the middle bentonite ring (70AIT-P-SI-03) was measuring 2.1 MPa just before dismantling (AITEMIN 2016b). The bottom left side of the gallery at this level (63.107 m) was affected by several fractures (Fig. 2).

Fig. 38 shows the initial and final appearance of this slice. The pipes sticking out of the bentonite that can be observed in the picture taken during dismantling were installed through the concrete plug after the first operational phase. Close to one of them, a drill bit was abandoned (probably during the installation of these pipes), and a corrosion halo could be seen around it (Fig. 39, left). A peculiarity of this section is that a plastic sheet was placed between the granite and the lower right part of the bentonite barrier during installation (Fig. 39, right), most likely to prevent early damage of the blocks due to a water leak through a particularly conductive feature of the granite. This was possibly inadvertently left behind. Between the liner and the heater bentonite had intruded, which became clear upon extraction of the heater on June 4th 2015 (Fig. 40, Extra Report No. 6 in Kober [2015]). Two samples of bentonite intruded inside the liner in Section S42 (just at the front of the heater) were taken for on-site analyses just before heater extraction, and the results obtained are shown in Tab. 7. The dry densities were very low, which is logical, since the material was extruded, and the water contents higher than those measured in the blocks in contact with the liner, which suggests that the bentonite inside the liner was affected by the high RH of the gallery during dismantling.

The location of the sampling points is indicated in Fig. 41.

Fig. 38: Initial and final appearance of Slice 57 (Section 43).
The highlighted cores were taken on June 10th, the others on June 11th 2015.

Fig. 39: Upper left part of the barrier showing the pipes and the corrosion halo around an abandoned drill bit (left) and lower right part of the barrier with the plastic sheet between granite and bentonite (right).

Fig. 40: Appearance of the bentonite intruded between the liner and the heater after extraction of the heater.

Tab. 7: Results of on-site measurements on samples taken between the liner and the heater in Section S42 before heater extraction (June 3rd 2015).

Sample	***W*** (%)	ρ_d (g/cm^3)	S_r (%)
B-S-42-4.1	32.1	1.31	81
B-S-42-4.2	34.6	1.16	70

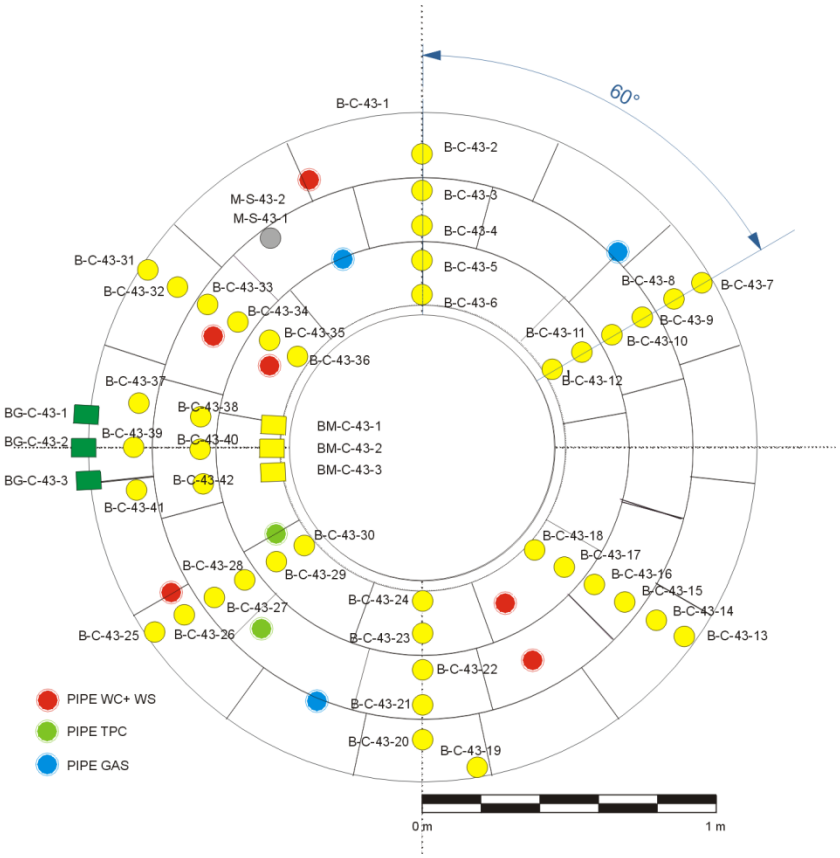

Fig. 41: Location of samples taken in Section 43 (sample B-C-43-19 was finally taken alligned with the others in Radius D).

Fig. 42 through Fig. 47 show the results for water content, dry density and computed degree of saturation, first as a function of the distance to the gallery axis and then as contour maps. The information about the section is summarised in Tab. 8. The water content decreased from the gallery wall towards the liner, while the dry density increased, more steeply in the external part of the barrier. At the contact with the liner the dry density of radii A and F was lower than at other locations. This was possibly caused by bentonite intrusion between the liner and the heater in the upper part of the installation (Fig. 40), which would result in a decreasing density of the internal ring of the buffer. In contrast, the calculated degree of saturation did not show any particular trend and was higher than 100 % in most of the samples. Radius C, which was in the middle of the lower right quarter of the barrier, had lower water content and higher dry density than the others in the external part of the barrier. This could have been caused by the plastic sheet that was placed between the granite and the bentonite in this part of the barrier, which hindered the direct water entrance to this area. However, Radius D, at the bottom of the section, had the highest water contents and degrees of saturation, possibly because it received the water accumulated under the plastic sheet above. The filled fracture in the granite at the bottom left side of the gallery could have also contributed to the higher water content of the external part of Radius D. Towards the inner part of the barrier, the differences among radii faded. This effect is clearly seen in the contour plots shown in Fig. 43 and Fig. 47.

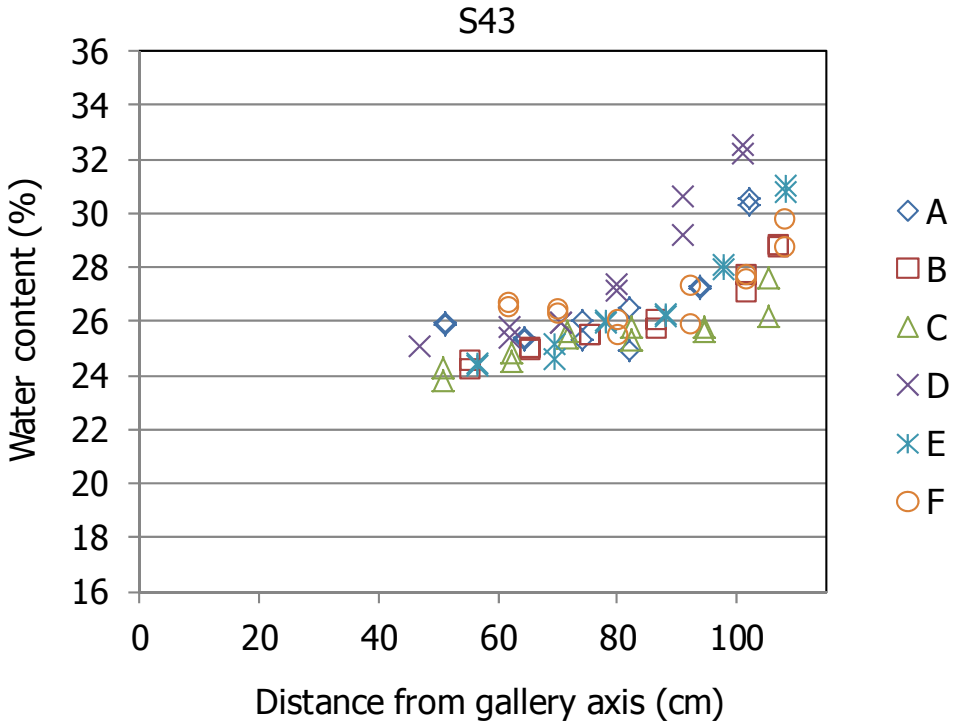

Fig. 42: Water content measured in subsamples along the six sampling radii in Section 43.

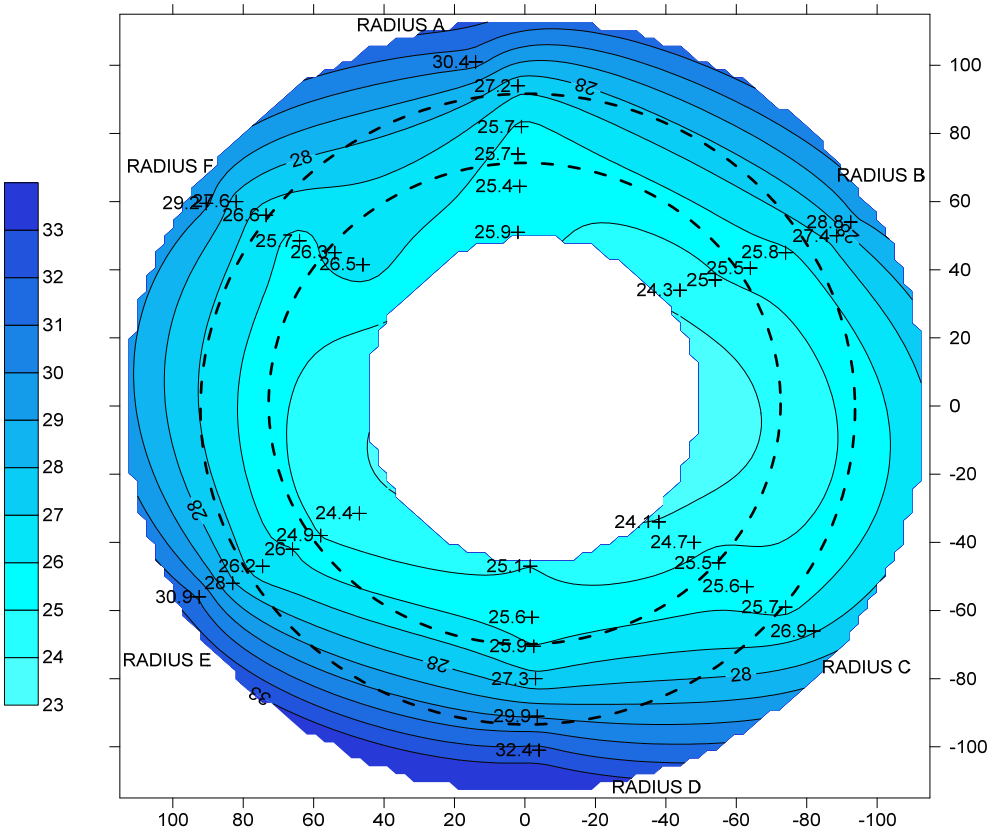

Fig. 43: Contour map for water content in Section 43.

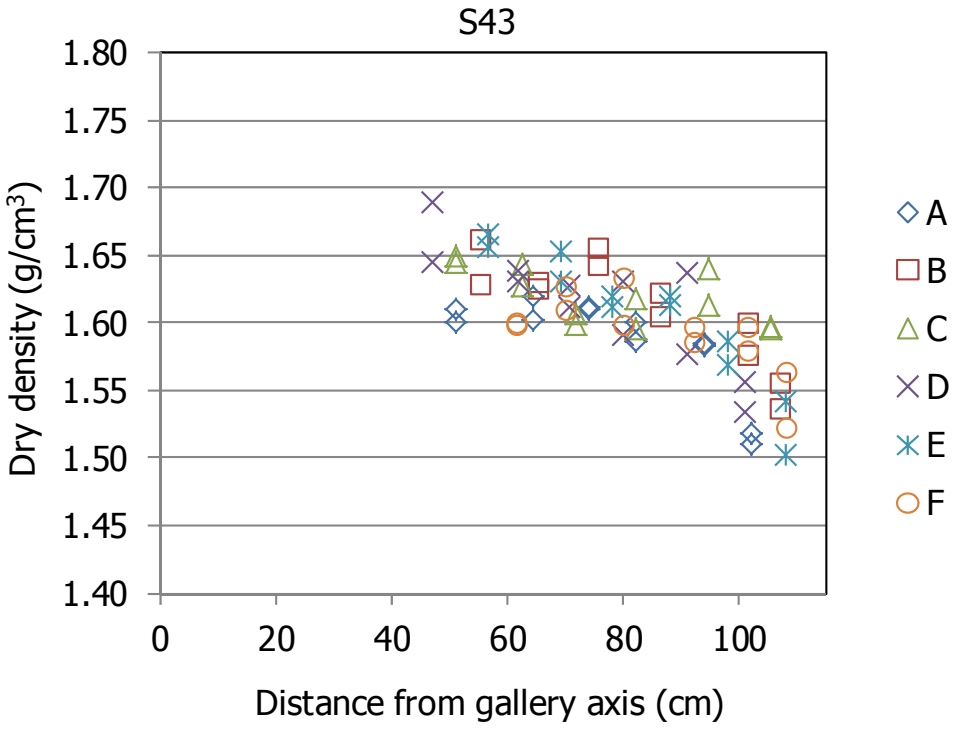

Fig. 44: Dry density measured in subsamples along the six sampling radii in Section 43.

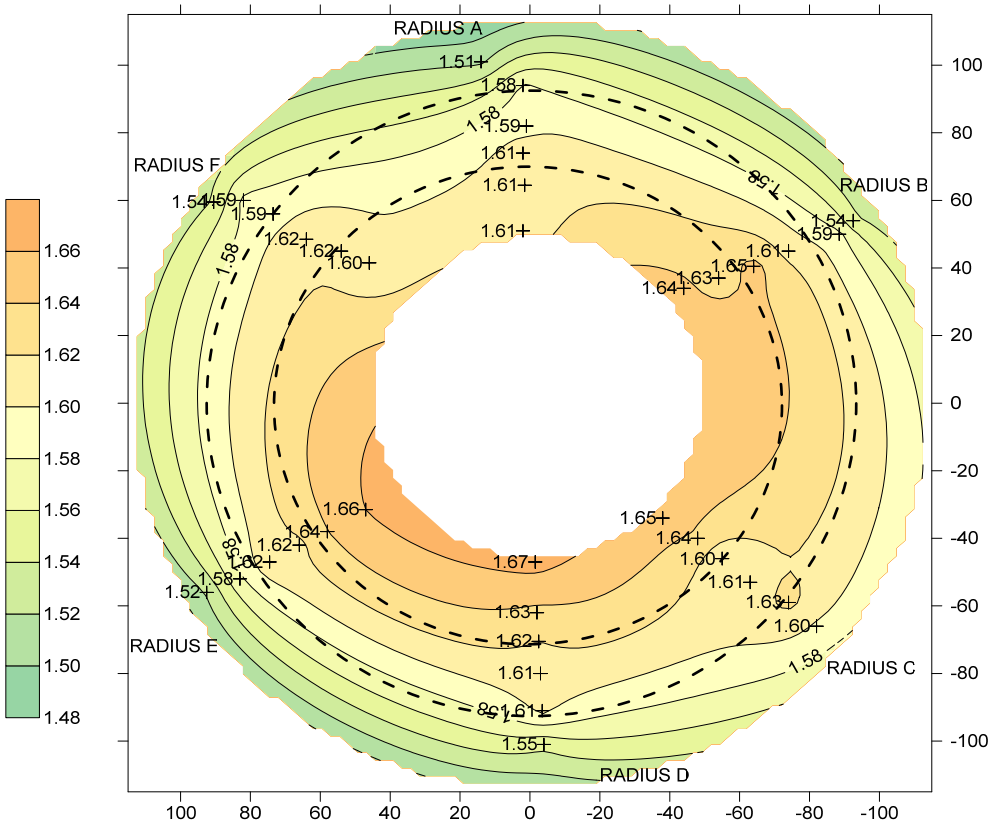

Fig. 45: Contour map for dry density in Section 43.

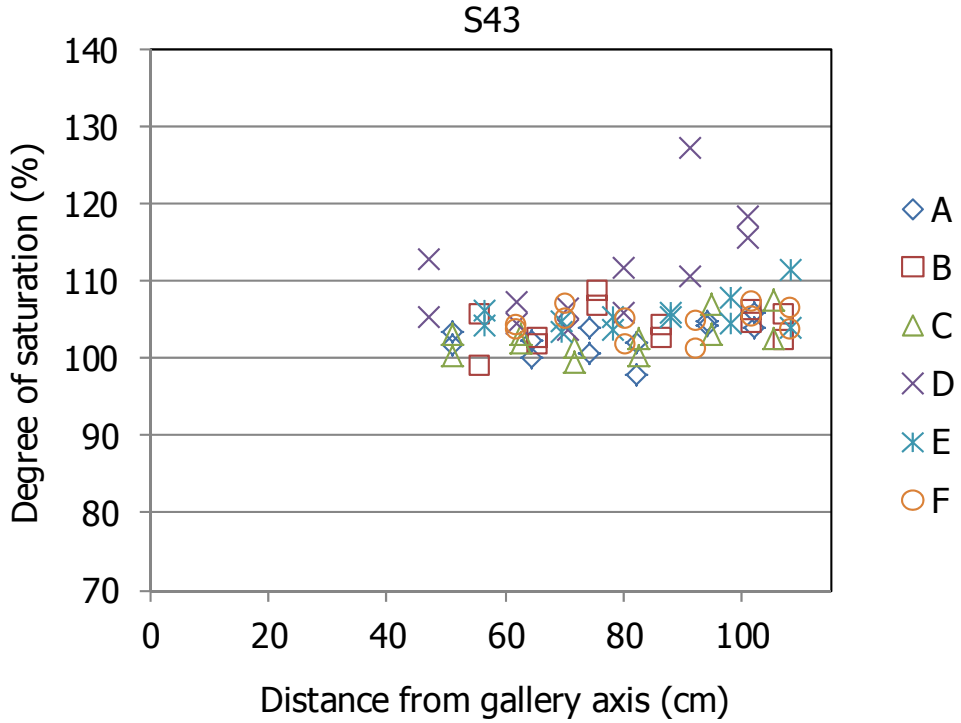

Fig. 46: Degree of saturation of subsamples along the six sampling radii in Section 43 (inexact values because of solid specific weight and water density uncertainties).

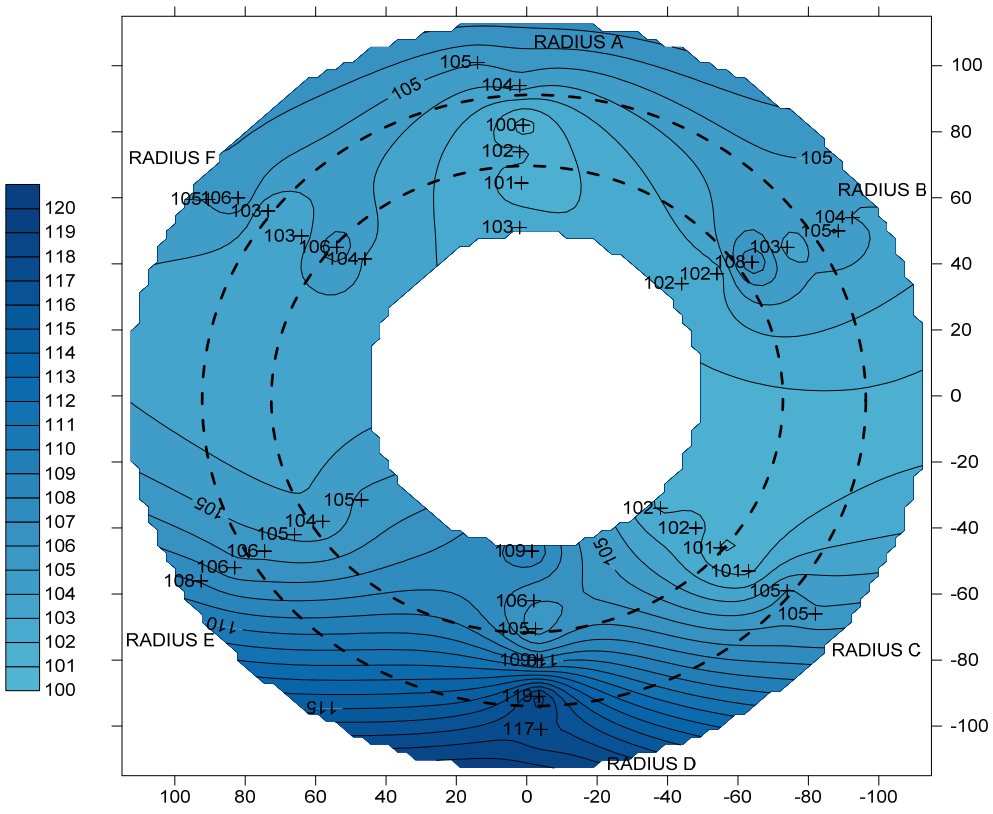

Fig. 47: Contour map for degree of saturation in Section 43 (inexact values because of solid specific weight and water density uncertainties).

Tab. 8: Summary Section 43.

Slice/instrumented section	57	
Estimated *T* during operation	> 44 – 88 °C 1st operational phase; 40 – 88 °C 2nd operational phase (based on I instrumented section)	
Sampling date/time since switching-off	June 10 – 11th 2015/47 – 48 days	
As built/final *x*-coordinate (m)	10.107/10.090	
Observations	• Filled fractures at the bottom left side of the gallery • Drilling bit left-behind in the upper left part of the barrier • Plastic sheet between granite and bentonite in lower right part • Bentonite intruded between liner and top of heater	
Initial/final thickness (mm)	128/128	
	Mean output grid values	Polynomial functions
w (%)	27.3	27.0
ρ_d (g/cm^3)	1.59	1.59
S_r (%)	106	105

3.5 Section 45, Slice 49

This section was placed around the heater, and the two thermocouples inserted in this section in the 2nd operational phase, recorded 68 and 92 °C in the two internal rings of the barrier (instrumented Section S). By the time the section was dismantled, the temperatures in it had decreased below 20 °C at all locations (AITEMIN 2016b). This means that the temperature change in the proximity to the heater was of more than 70 °C, and this could have caused some water redistribution before dismantling. The closest section with information about suction or RH was the instrumented Section F2 (sampling Section 48, Slice 42), in which by 2009 all the sensors indicated full saturation, except for the two located in the internal ring, which recorded values about 60 % RH before they failed.

Fig. 48 shows the initial and final appearance of this slice. The pipes sticking out of the bentonite that can be observed in the picture taken during dismantling were installed through the concrete plug after the first operational phase. A detail of the bottom part of the barrier can be seen in Fig. 49, in which the blocks limits can be clearly seen. Fig. 50 shows the location of the sampling cores. The radial dimension of some blocks measured with a metric tape during dismantling is given in Tab. 9.

Fig. 48: Initial and final appearance of Section 45 (Slice 49).

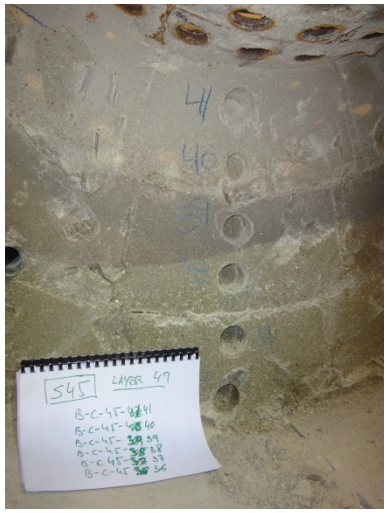

Fig. 49: Location of samples taken in Radius D

Tab. 9: Dimensions of the blocks along the radius in Slice 49, Section S45 (the kinds of block are indicated in Fig. 4, the original dimension for all was 216.7 mm)

Θ (°)	**BB-G-01** (mm)	**BB-G-02** (mm)	**BB-G-03** (mm)
0	227	218	204
60	226	220	208
120	226	218	210
180	228	221	209
270	229	219	211
Average	227	219	208

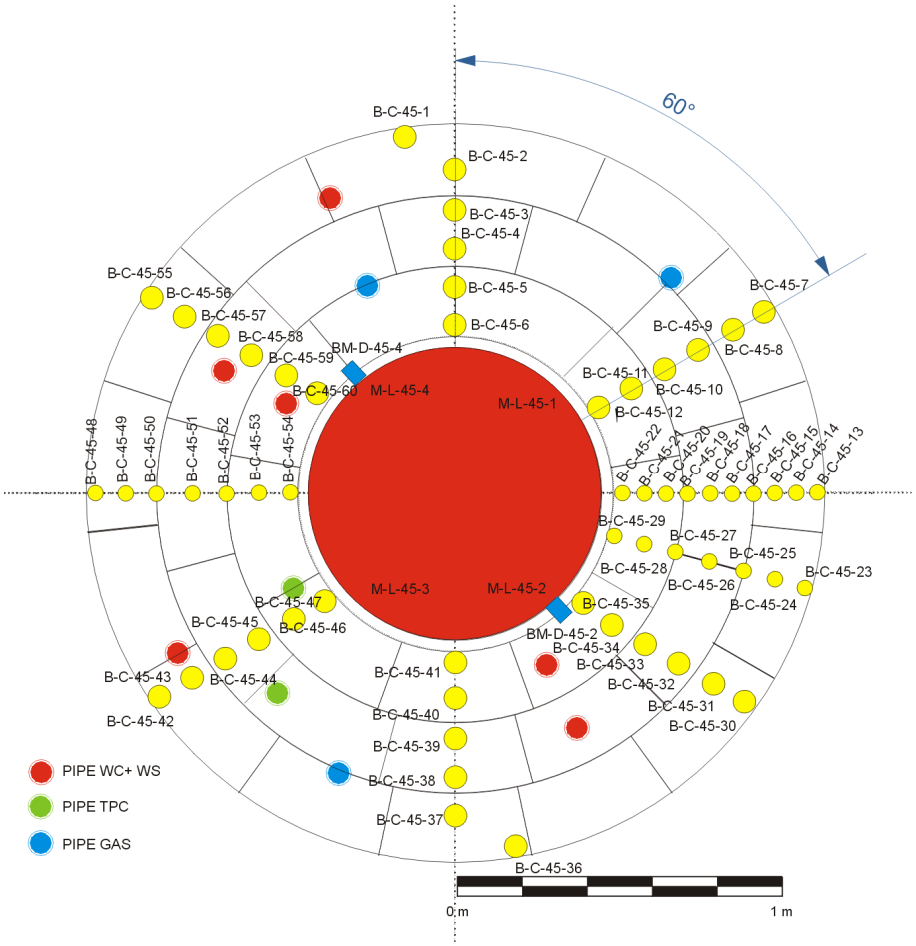

Fig. 50: Location of samples taken in Section 45 (sample B-C-45-36 was finally taken alligned with the others in Radius D).

Fig. 51 through Fig. 56 show the results for water content, dry density and computed degree of saturation, first as a function of the distance to the gallery axis and then as contour maps. The information about the section is summarised in Tab. 10. The water content decreased from the gallery wall towards the liner almost linearly (Fig. 51), while the dry density increased (Fig. 53). The six sampled radii gave very similar values, particularly for water content. Only the radius under the heater (Radius D) had lower water contents than the others in the proximity to the heater. The degree of saturation was close to 100 % in the 35 cm closest to the gallery wall, and then decreased towards the heater (Fig. 55). The change of dry density along the radii is well correlated with the radial dimensions of the blocks shown in Tab. 9. The external ring of the barrier expanded, its radial dimension increasing from the initial 217 mm (Tab. 1) to an average of 227 mm. The middle ring experienced also certain expansion and the inner ring was clearly compressed, this giving rise to the higher dry densities.

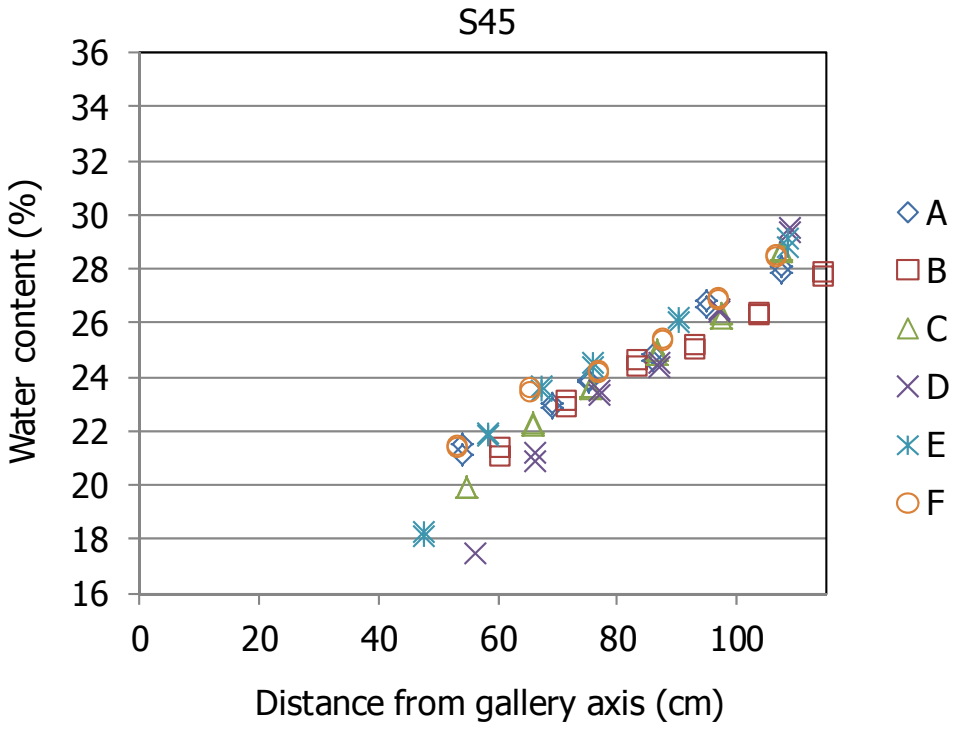

Fig. 51: Water content measured in subsamples along the six sampling radii in Section 45.

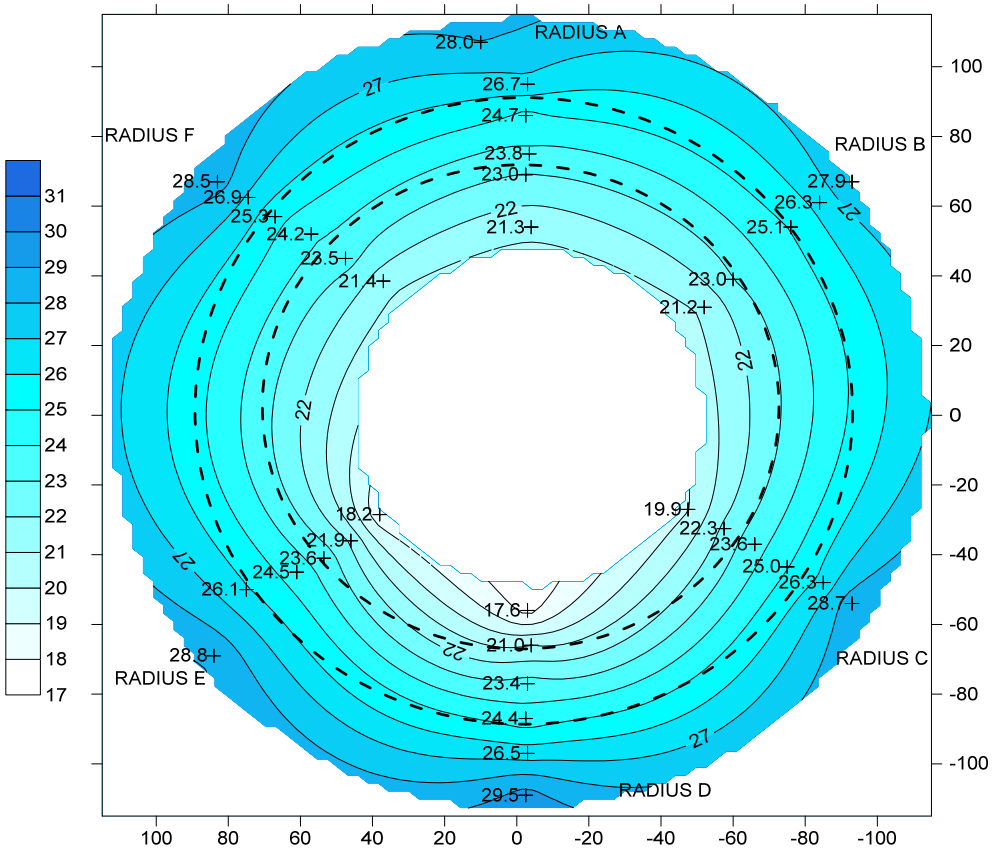

Fig. 52: Contour map for water content in Section 45.

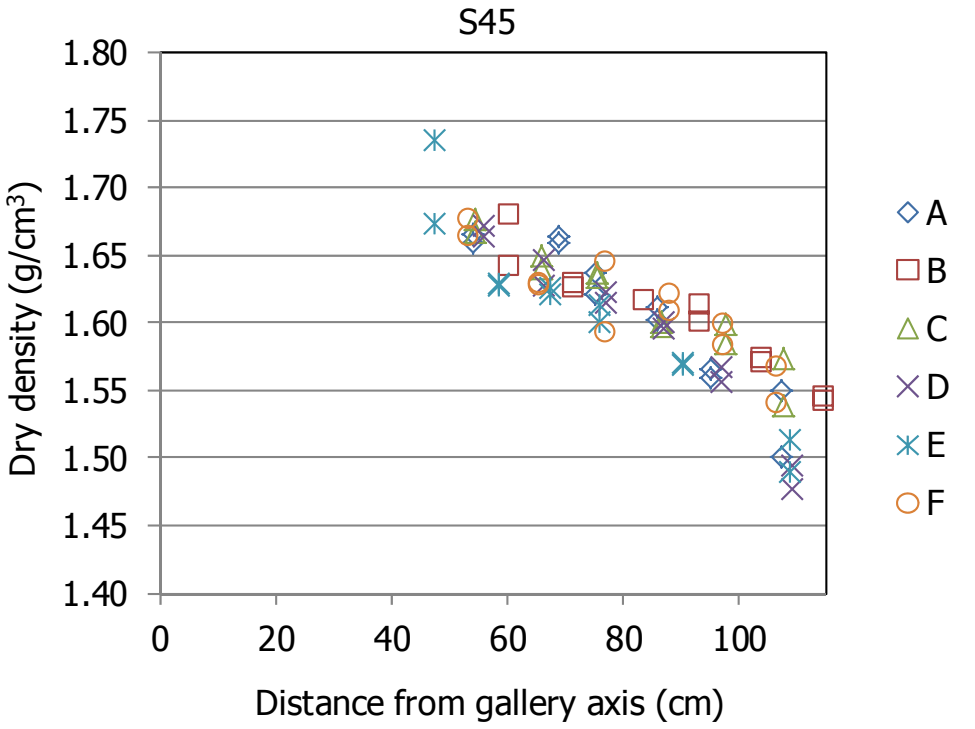

Fig. 53: Dry density measured in subsamples along the six sampling radii in Section 45.

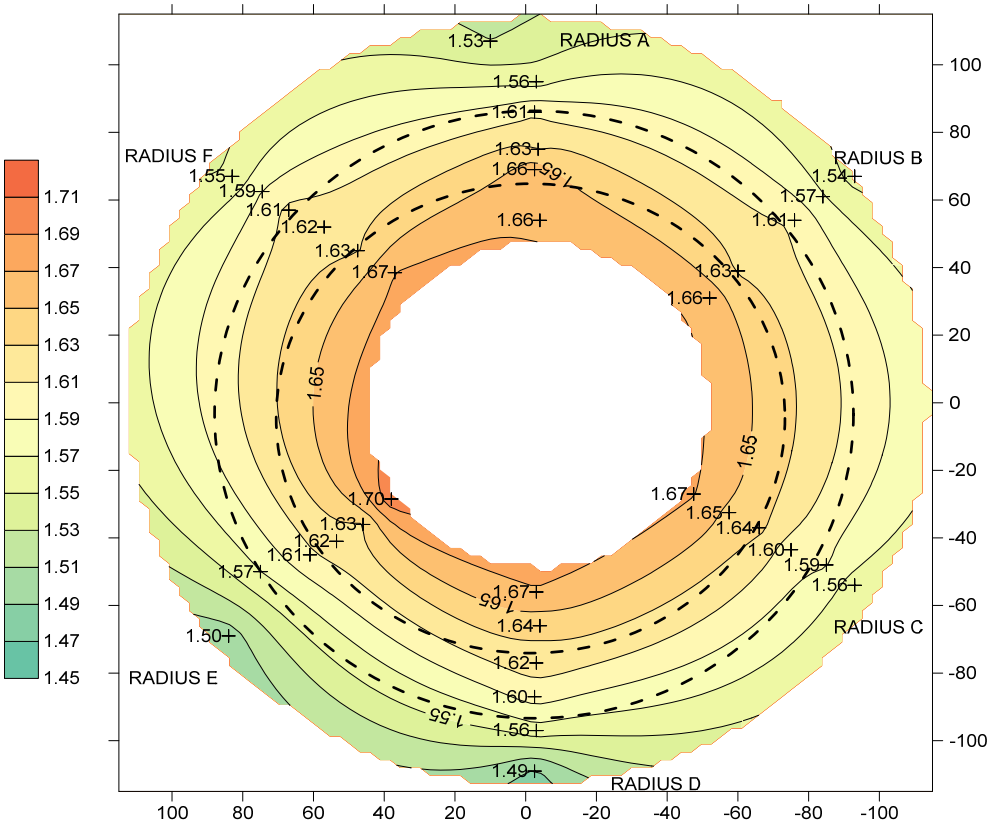

Fig. 54: Contour map for dry density in Section 45.

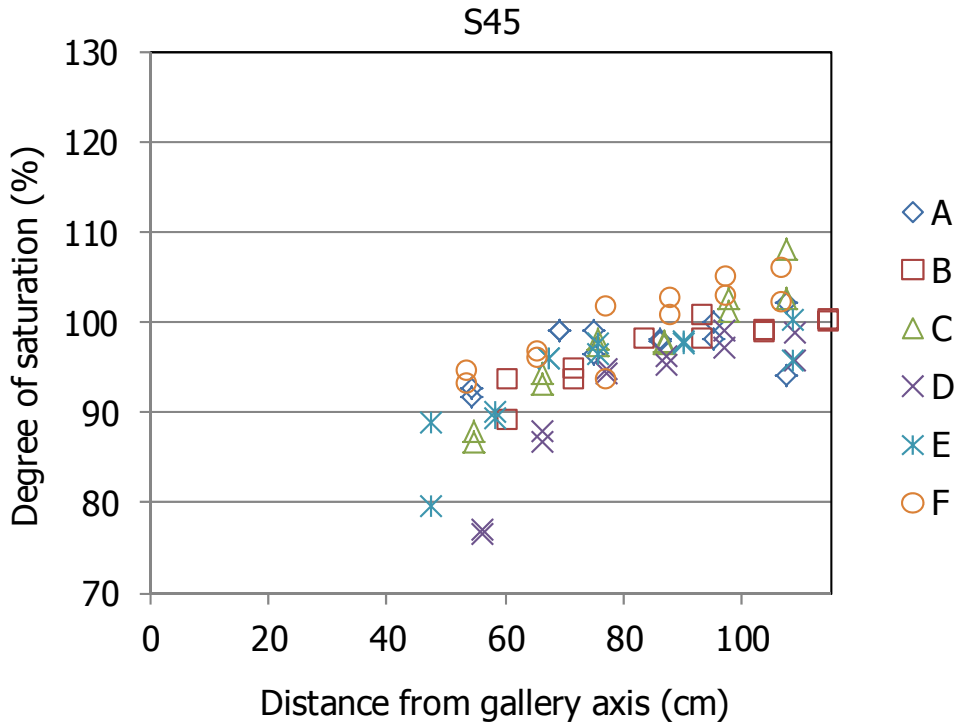

Fig. 55: Degree of saturation of subsamples along the six sampling radii in Section 45 (inexact values because of solid specific weight and water density uncertainties).

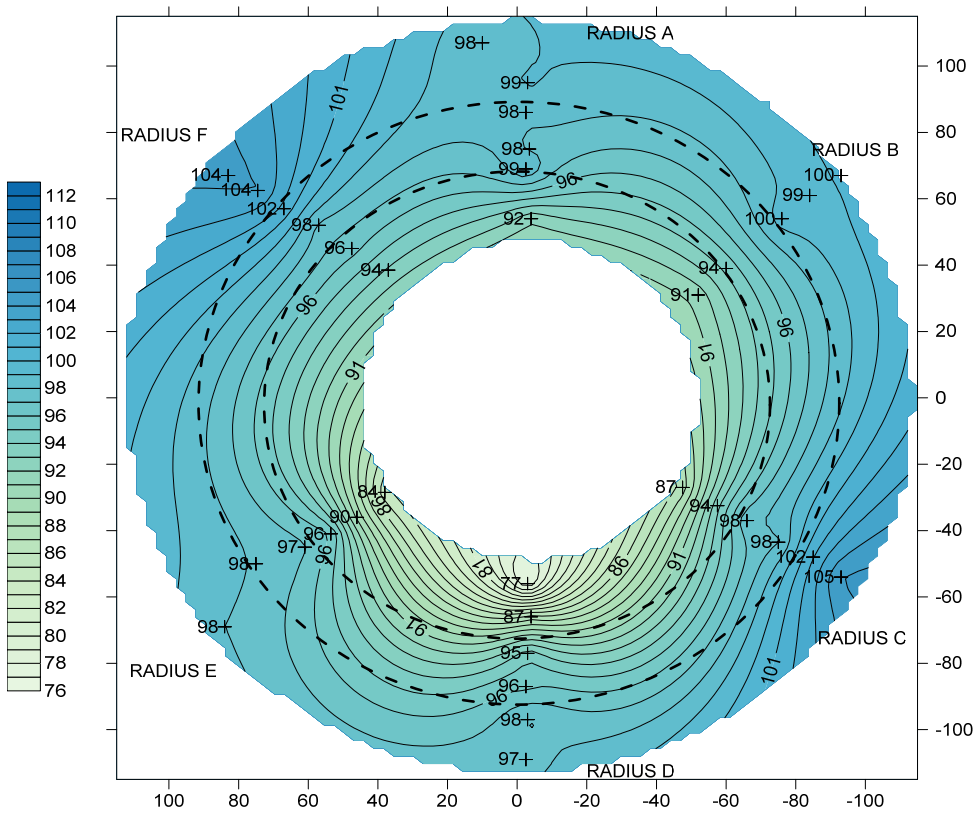

Fig. 56: Contour map for degree of saturation in Section 45 (inexact values because of solid specific weight and water density uncertainties).

Tab. 10: Summary Section 45.

Slice/instrumented section	49/S	
Estimated *T* during operation	Up to 92 °C during 2nd operational phase	
Sampling date/time since switching-off	June 22nd 2015/59 days	
As built/final *x*-coordinate (m)	11.112/11.100	
Observations		
Initial/final thickness (mm)	128/138	
	Mean output grid values	Polynomial functions
w (%)	25.0	24.9
ρ_d (g/cm^3)	1.59	1.60
S_r (%)	97	97

3.6 Section 49, Slice 40

This section was located around the middle part of the heater, close to the instrumented Section F2 (Slice 42). The thermocouples inserted in this section in the two internal rings of the barrier, recorded 72 and 100 °C at the time of heater shutdown. After switching off the heater the temperatures dropped sharply and when the section was dismantled, 70 days later, the temperature at all locations was around 20 °C. As it has been commented above, the cooling of the internal rings of the barrier could have resulted in some water redistribution between switching off and dismantling. By 2009 all the capacitive sensors indicated full saturation, except for the two located in the internal ring, which recorded values about 60 % RH before they failed. The total pressure sensor located at the bottom of the barrier in the contact with the granite (70AIT-PSF2-01), recorded a pressure of 6.6 MPa, and a sensor located in the bentonite middle ring (70AIT-PSF2-06), a pressure of 2 MPa when they stopped working in 2013 (AITEMIN 2014).

Fig. 57 shows the initial and final appearance of this slice. In the photograph corresponding to the final state, the previous slice, Slice 41, had not been removed yet in some parts. This is because Section 49 was dismantled stepwise: the parts of the Slice 41 which were covering the areas of the barrier in which radii A, B, C and F had to be sampled were removed first, and four days later (July 7th 2015) the rest of Slice 41 was removed, to allow the sampling of radii D and E. The pipes sticking out of the bentonite that can be observed in the picture taken during dismantling were installed through the concrete plug after the first operational phase. Fig. 58 shows the location of the sampling cores.

Tab. 11 shows the measurement taken on the surface of the blocks. The information about the section is summarised in Tab. 12 and Fig. 59 through Fig. 64 show the results for water content, dry density and computed degree of saturation, first as a function of the distance to the gallery axis and then as contour maps. The water content decreased linearly from the gallery wall towards the heater (Fig. 59), while the dry density increased (Fig. 61). The increase of dry density towards the heater is well correlated to the changes in the radial dimension of the blocks shown in Tab. 11, which decreased from the external to the internal ring of the barrier. In particular, the two external rings had radial dimensions longer than the initial one (which was

217 mm) and the inner ring had a considerable shorter radius. This indicates that expansion took place in the external part of the barrier while the internal ring was compressed. The sampling radii had similar values among them, except radii D and E, which had lower water content than the others (23.5 vs. 25.2 on average) and particularly higher dry density (1.66 vs. 1.59 on average). These two radii were sampled four days later than the others, and although the previous bentonite slice was kept on site during this time, the bentonite could have dried and shrunk, causing the density increase. Nevertheless, in other sections in which a similar sampling procedure was followed, no higher dry density was observed in the samples taken later (see Chapter 2.4 in Discussion). As a consequence of the distinct density increase, the degrees of saturation along radii D and E were higher than in the rest of the section (Fig. 63, Fig. 64). Overall, the degree of saturation was close to or higher than 100 % in the 35 cm closest to the gallery wall, and then decreased towards the heater.

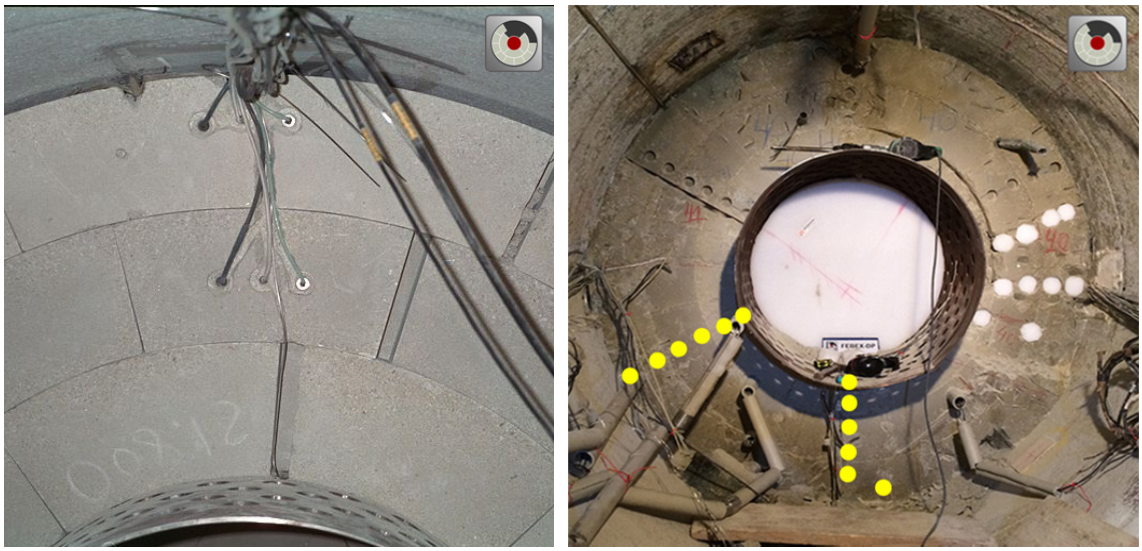

Fig. 57: Initial and final appearance of Section 49 (Slice 40).
The highlighted cores were taken on July 6th, the others on July 3rd 2015.

Tab. 11: Dimensions of the blocks along the radius in Slice 40, Section S49 (the kinds of block are indicated in Fig. 4, the original dimension for all was 216.7 mm)

Θ (°)	**BB-G-01** (mm)	**BB-G-02** (mm)	**BB-G-03** (mm)
225	228	220	205

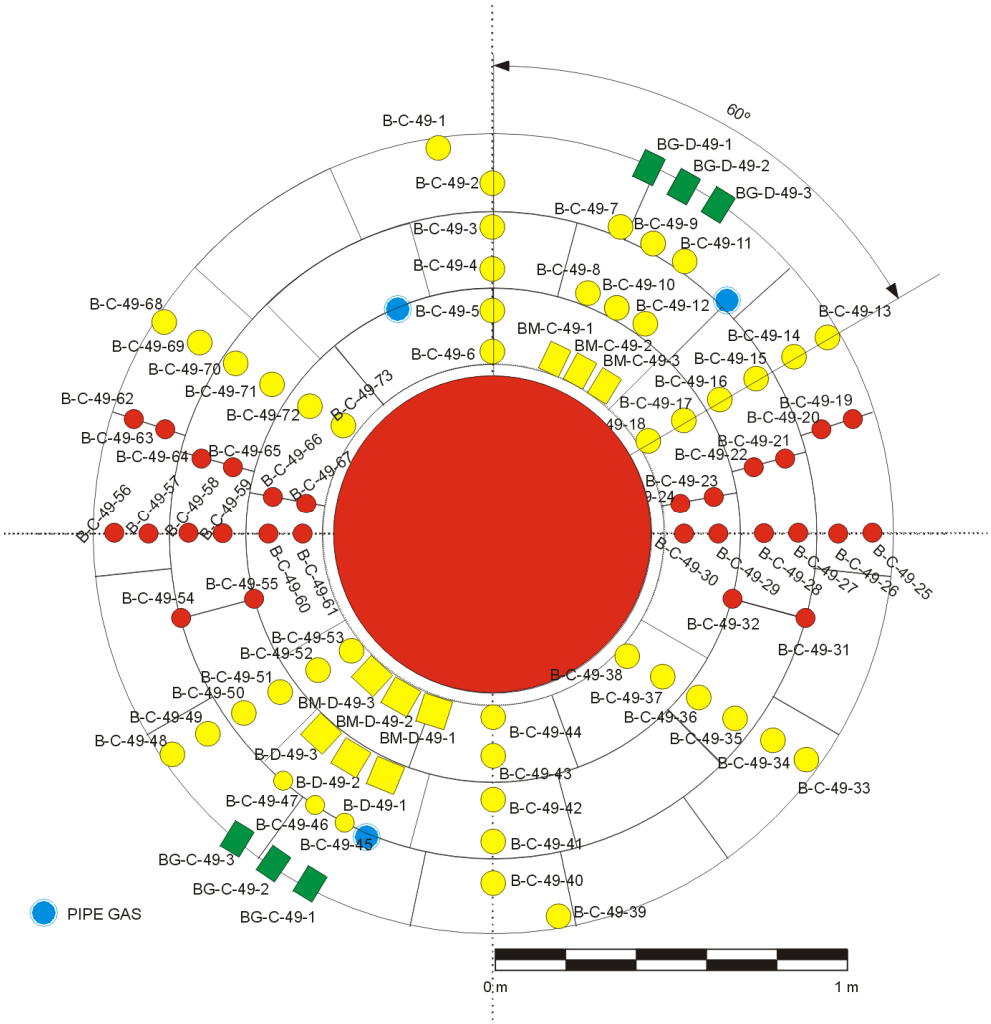

Fig. 58: Location of samples taken in Section 49.

Tab. 12: Summary Section 49.

Slice/instrumented section	40	
Estimated *T* during operation	Up to 100 °C (Section F2)	
Sampling date/time since switching-off	July 3 – 7th 2015/70 – 74 days	
As built/final *x*-coordinate (m)	12.265/12.253	
Observations	• Radii D and E were sampled 4 days later	
Initial/final thickness (mm)	128/117	
	Mean output grid values	Polynomial functions
w (%)	25.0	25.0
ρ_d (g/cm^3)	1.60	1.60
S_r (%)	98	98

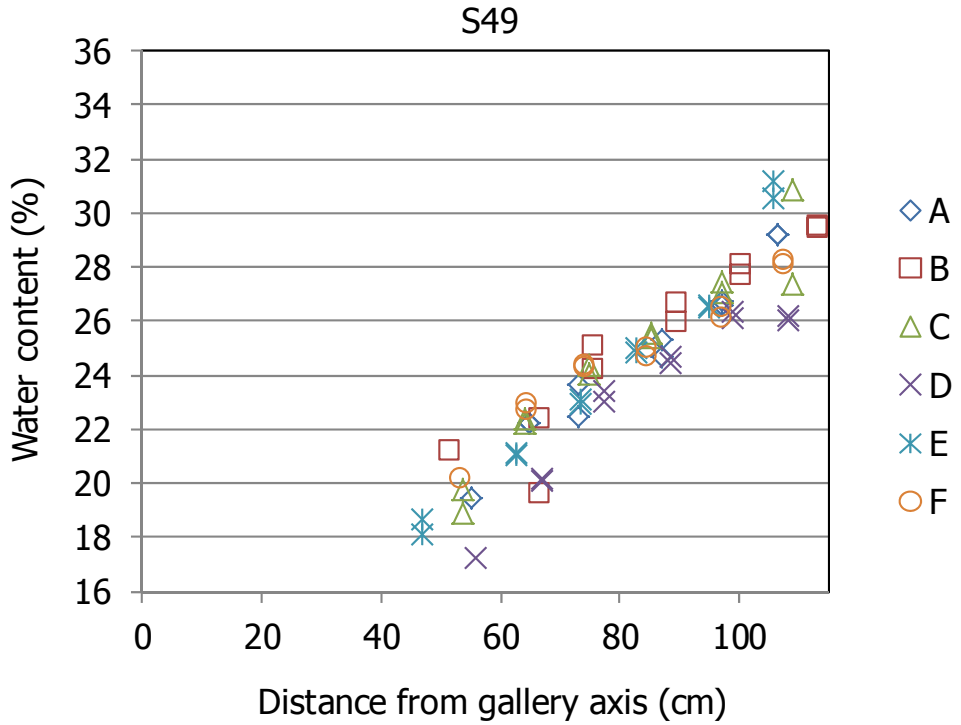

Fig. 59: Water content measured in subsamples along the six sampling radii in Section 49.

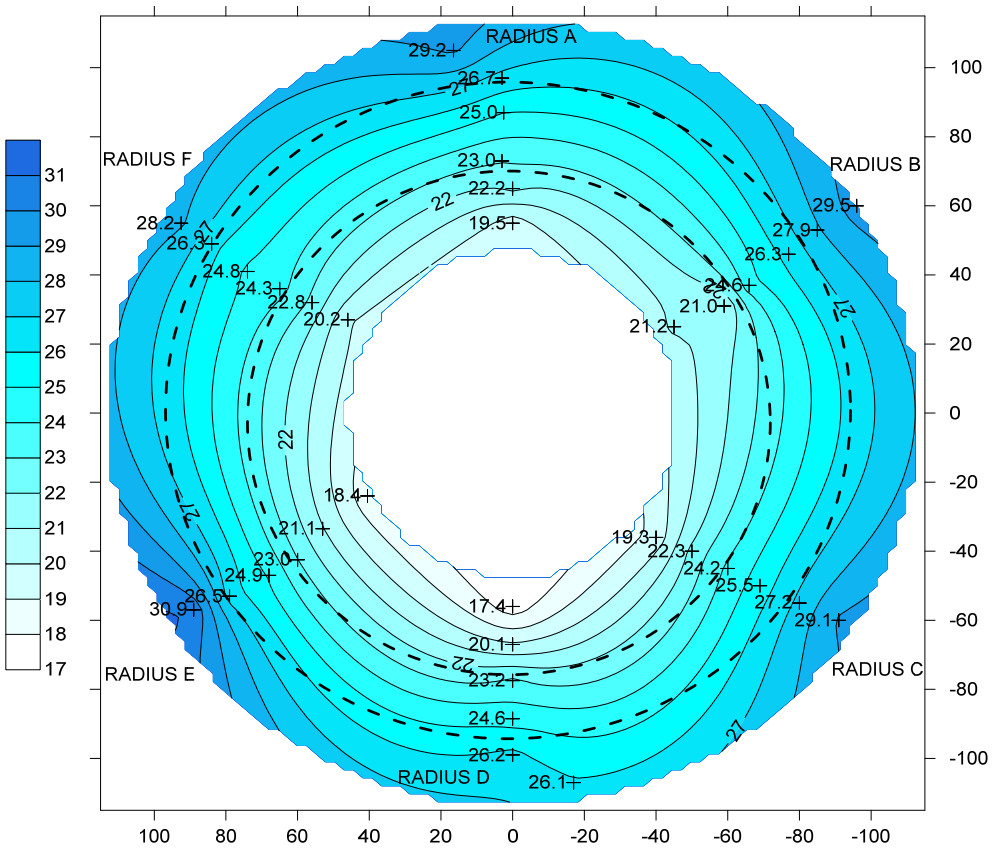

Fig. 60: Contour map for water content in Section 49.

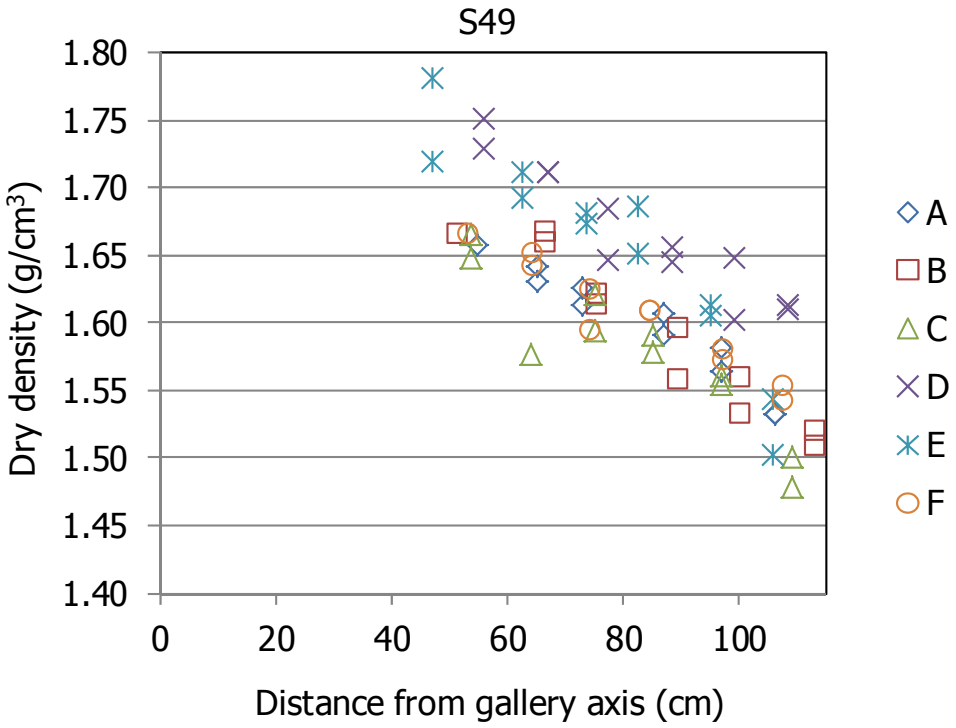

Fig. 61: Dry density measured in subsamples along the six sampling radii in Section 49.

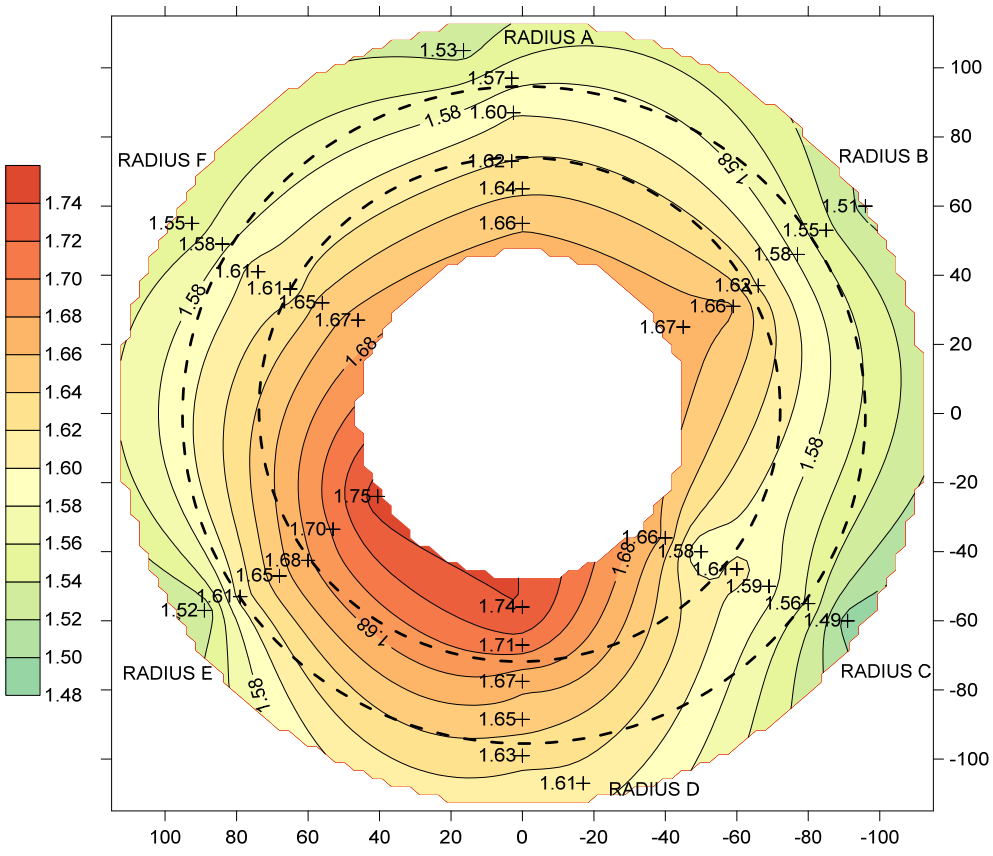

Fig. 62: Contour map for dry density in Section 49.

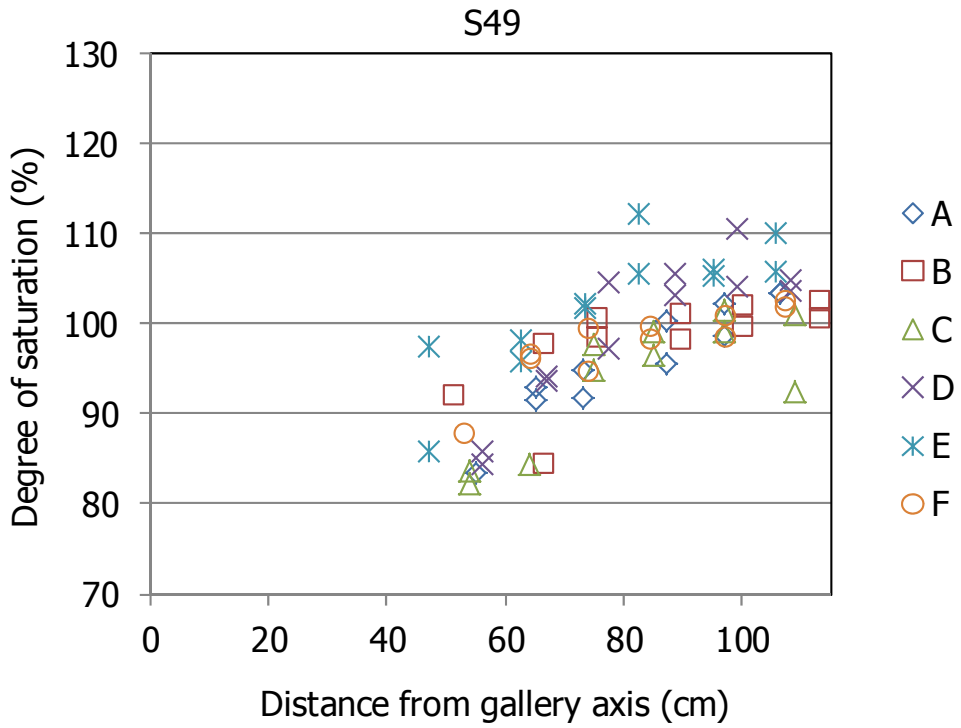

Fig. 63: Degree of saturation of subsamples along the six sampling radii in Section 49 (inexact values because of solid specific weight and water density uncertainties).

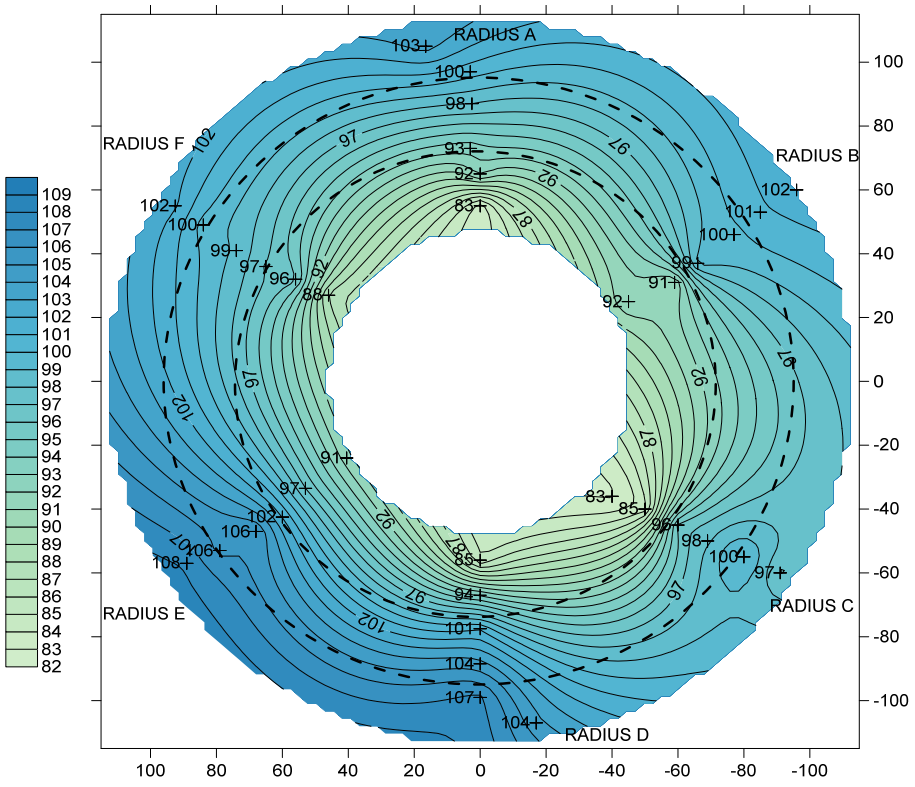

Fig. 64: Contour map for degree of saturation in Section 49 (inexact values because of solid specific weight and water density uncertainties).

3.7 Section 52, Slice 31

This section was located at the inner end of the heater cavity, very close to the instrumented Section E2 (Slice 32). In this section a thermocouple placed at the base of the liner was measuring 96 °C during the 2nd operational phase. The section was dismantled 76 days after switching off, and by this time the temperature at all locations dropped to 20 °C. No sensors giving information about saturation were operational during the 2nd operational phase, but before 2009 the total pressure sensor placed between the bentonite and the granite on the right middle part of the barrier (sensor 70AIT-P-SE2-03) was measuring 5 MPa, which is about the swelling pressure corresponding to the saturated FEBEX bentonite compacted to 1.58 g/cm^3. Also, a pore pressure sensor at the same location (sensor 70AIT-QSE2-05) was measuring 0.4 MPa shortly before dismantling (AITEMIN 2016b). For pore pressure to be positive the region around it would have needed to be saturated. The upper left side of the gallery was crossed at this area by a thick vein filled by different minerals (Fig. 2).

Fig. 65 shows the initial appearance of this slice and its appearance at the end of the first sampling day, with radii A (four samples), B and C sampled. The two bentonite slices covering the part of the barrier where the other radii were located had not yet been removed, because this section was dismantled stepwise. Radius F was sampled the following day (Fig. 66, right) and radii D and E four days later. In the upper left part of the barrier, filter paper doped with iodine was placed during installation between the granite and the bentonite (Fig. 66, left). The location of the cores drilled for on-site determinations is shown in Fig. 67.

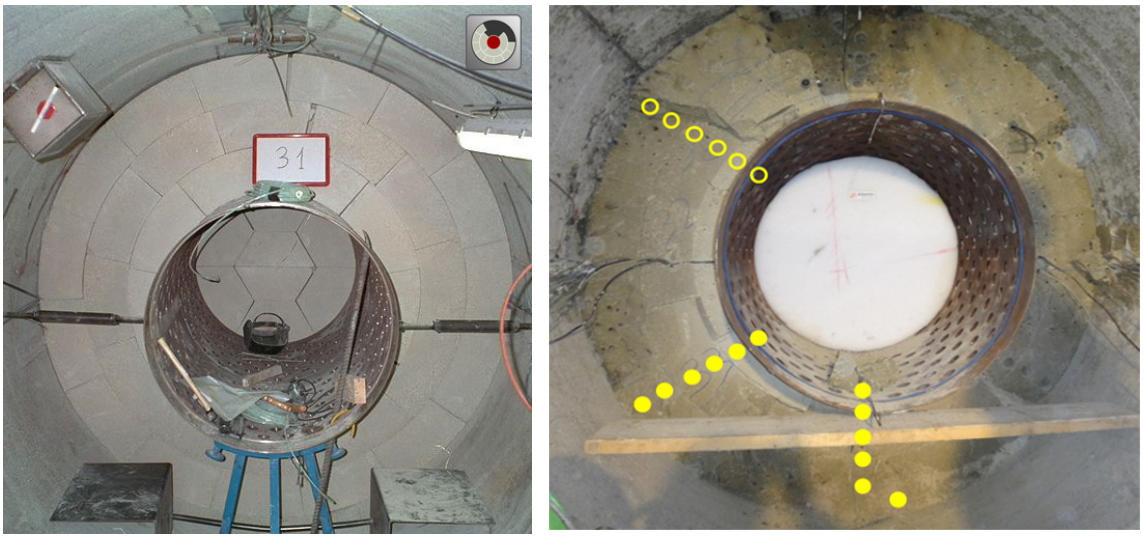

Fig. 65: Initial appearance of Section 52 (Slice 31) and after the first sampling day (July 9th 2015), with only radii B, C and half A uncovered and sampled.

The circled cores (Radius F) were sampled on July 10th and the highlighted cores (radii D and E) on July 13th 2015.

Fig. 66: Radius F of Section 52 on the second sampling day and appearance of the filter paper between the granite and the bentonite in the upper left part of the barrier.

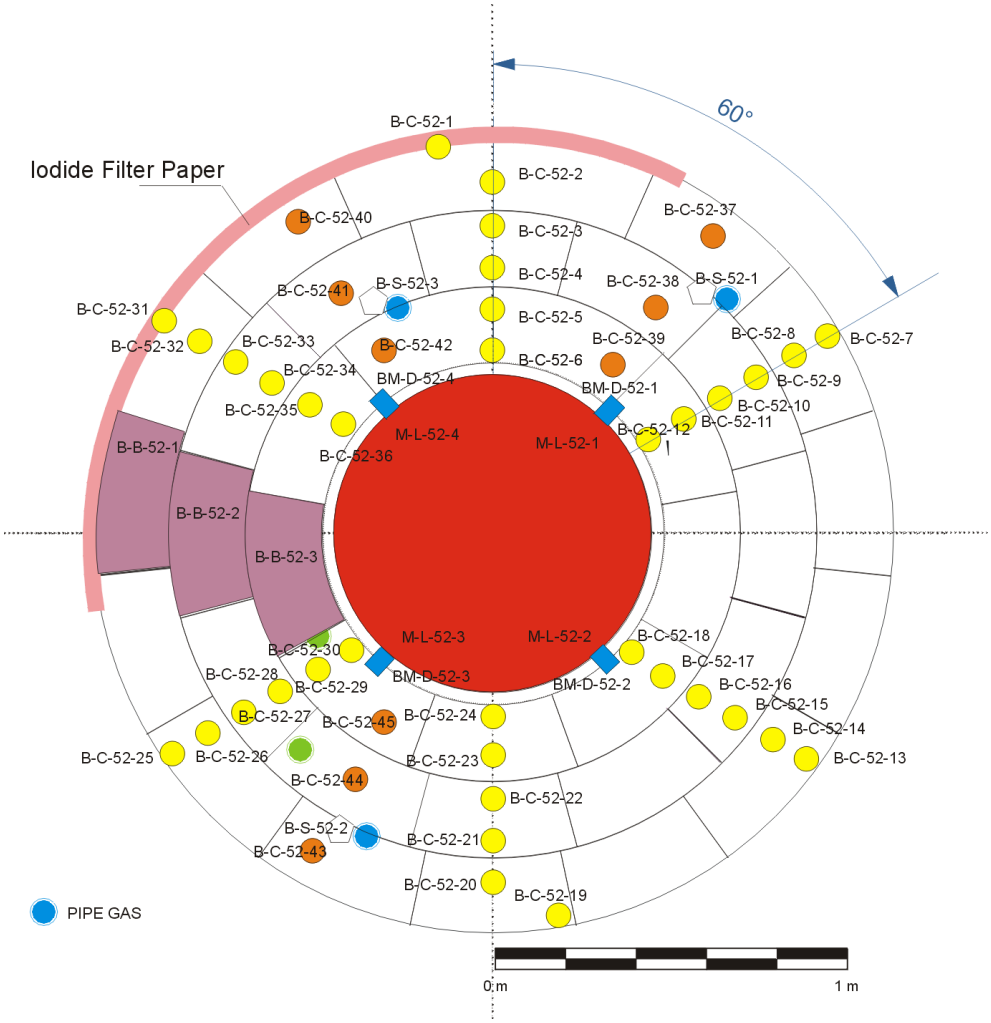

Fig. 67: Location of samples taken in Section 52.

The information about the section is summarised in Tab. 13 and Fig. 68 through Fig. 73 show the results for water content, dry density and computed degree of saturation, first as a function of the distance to the gallery axis and then as contour maps. The water content decreased linearly from the gallery wall towards the heater (Fig. 68), while the dry density increased (Fig. 70). Although the trend of the dry density to decrease towards the heater is clear, a large dispersion among radii is noticeable, which was not found in other sections. As it happened in Section 49, radii D and E, sampled four days later than the others, had slightly lower water contents (23.5 vs. 25.2 on average), but only Radius D had a significantly higher dry density than the others (1.67 vs. 1.58 on average). The lower dry density and degree of saturation of the samples from Radius F, which were taken a day later than radii A, B and C is also remarkable (Fig. 72). Overall, the degree of saturation was close to or higher than 100 % in the 35 cm closest to the gallery wall (except in Radius F), and then decreased towards the heater.

Tab. 13: Summary Section 52.

Slice/instrumented section	31	
Estimated *T* during operation	Up to 96 °C (instrumented Section E2, Slice 32)	
Sampling date/time since switching-off	July 9 – 13th 2015/76 – 80 days	
As built/final *x*-coordinate (m)	13.413/13.379	
Observations	• Radius F sampled 1 day later and radii D and E sampled 4 days later • Filter paper and a thick filled vein on the upper left part of the gallery	
Initial/final thickness (mm)	127/134	
	Mean output grid values	Polynomial functions
w (%)	24.8	25.0
ρ_d (g/cm^3)	1.59	1.59
S_r (%)	95	97

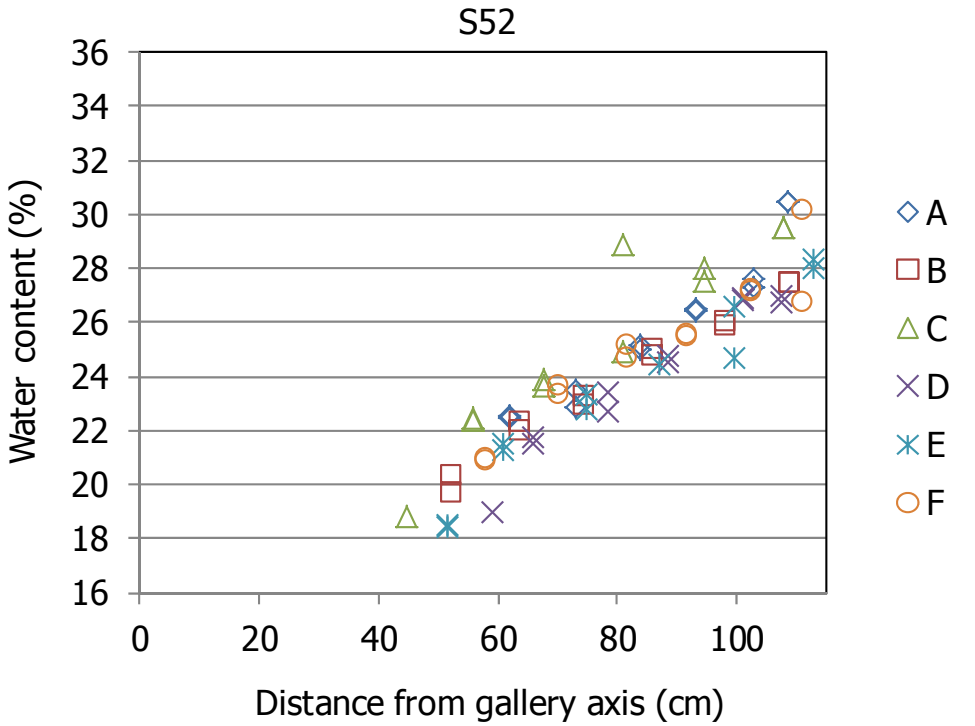

Fig. 68: Water content measured in subsamples along the six sampling radii in Section 52.

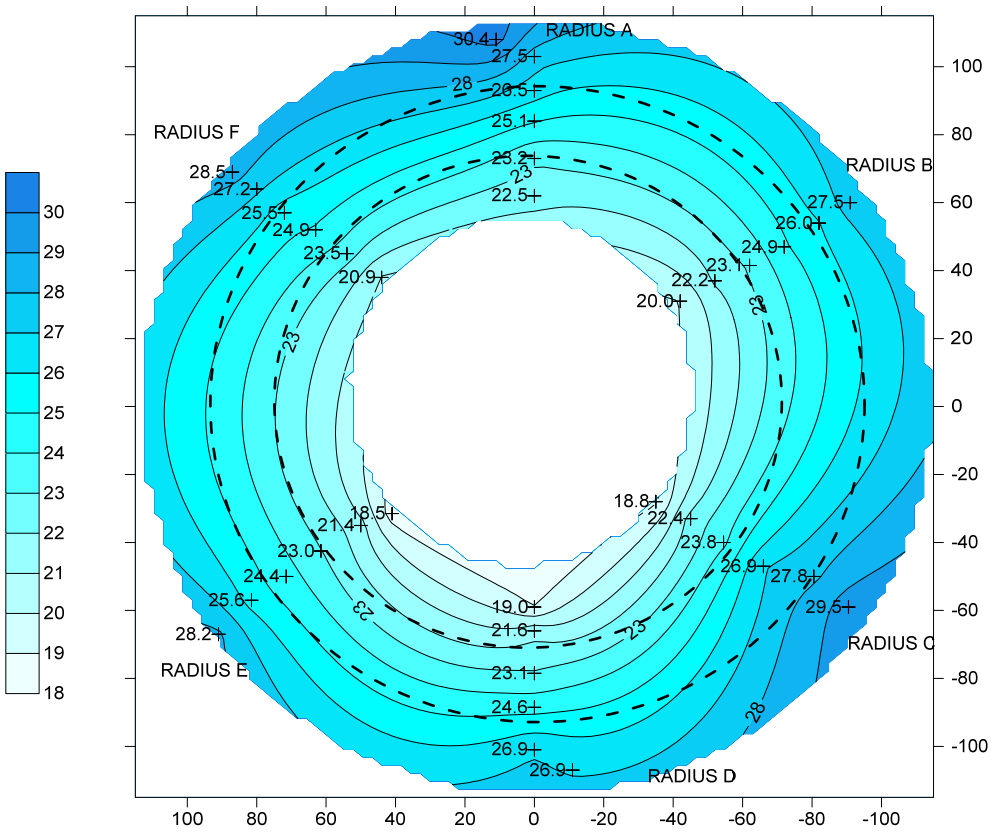

Fig. 69: Contour map for water content in Section 52.

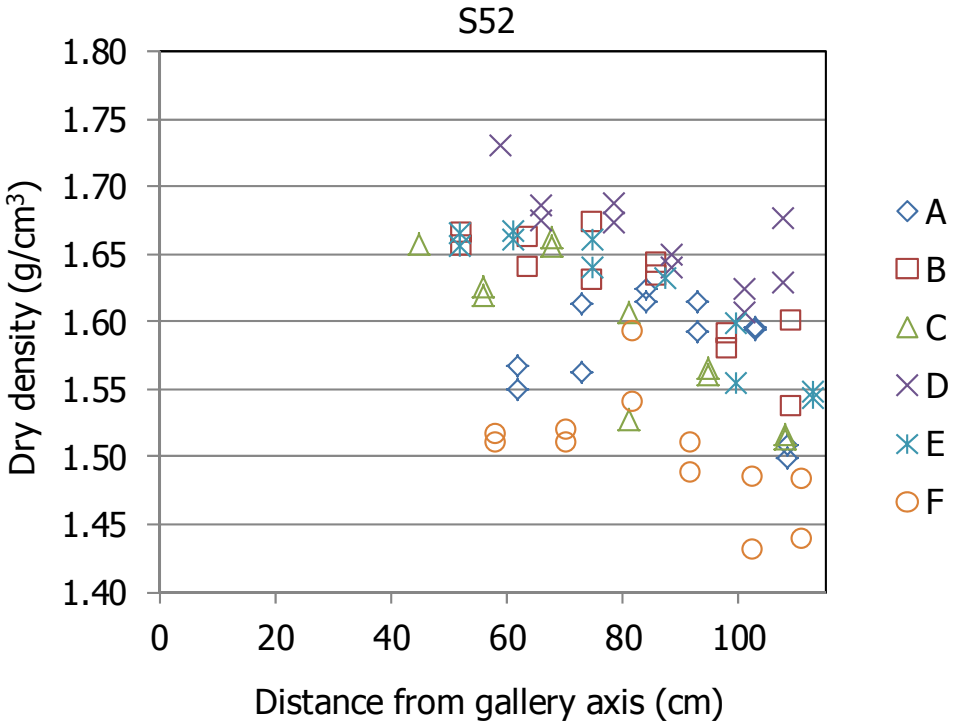

Fig. 70: Dry density measured in subsamples along the six sampling radii in Section 52.

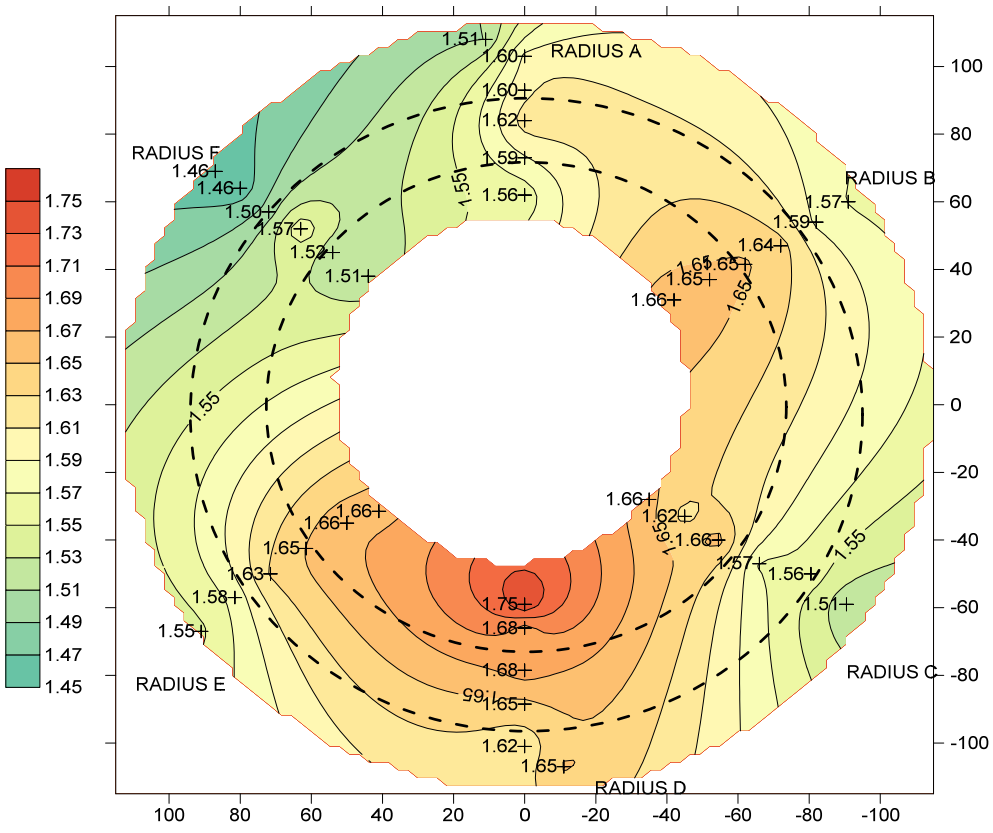

Fig. 71: Contour map for dry density in Section 52.

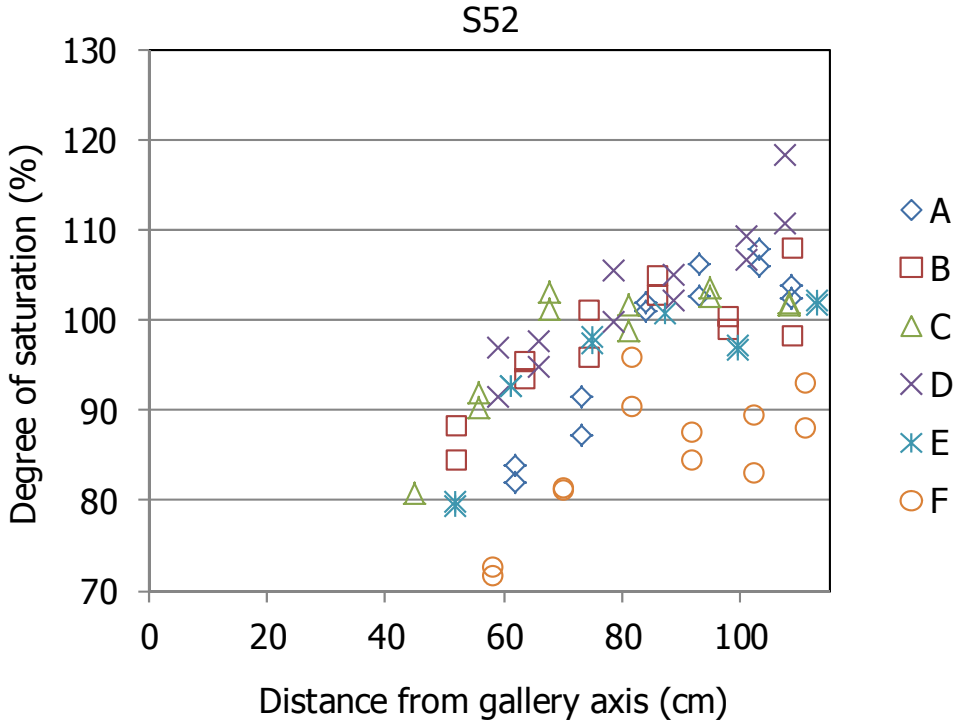

Fig. 72: Degree of saturation of subsamples along the six sampling radii in Section 52 (inexact values because of solid specific weight and water density uncertainties).

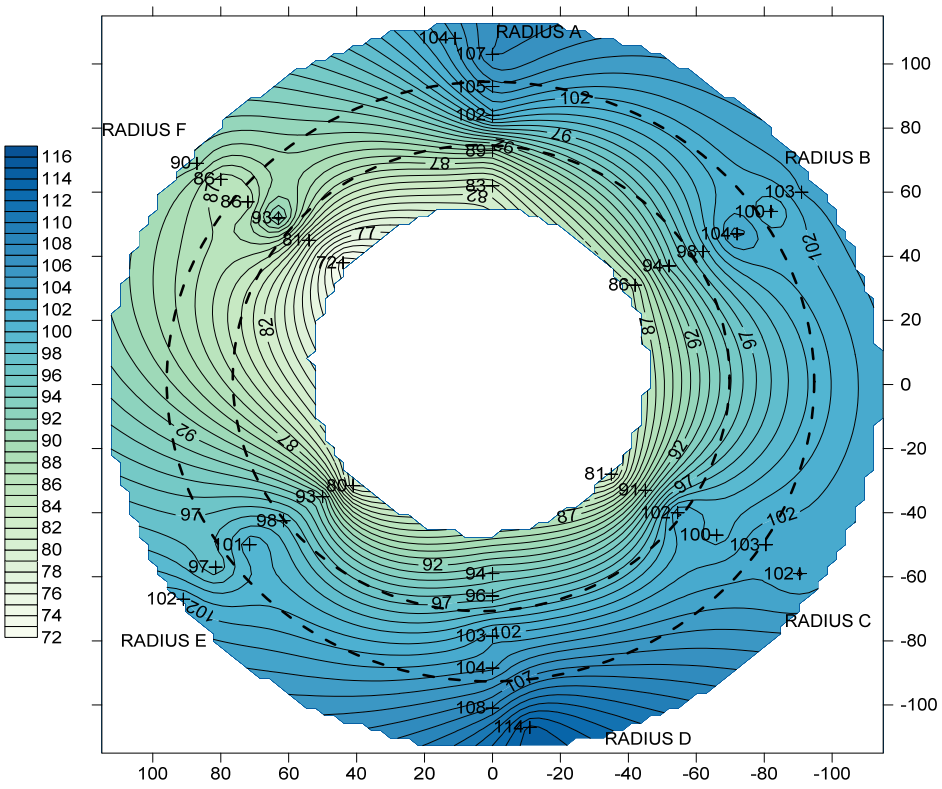

Fig. 73: Contour map for degree of saturation in Section 52 (inexact values because of solid specific weight and water density uncertainties).

3.8 Section 56, Slice 22

This section was one slice beyond the back of the heater. The closest instrumented section was Section D2 (Slice 24), in which temperatures between 36 (at the bentonite/granite contact) and 88 °C (at the bentonite/liner contact) were measured during operation (AITEMIN 2014). The bottom left side of the gallery was crossed at this area by a thick vein filled by different minerals (Fig. 2).

Fig. 74 shows the initial and final appearance of this slice. It was sampled in two days: the first day only the samples highlighted in the Figure were taken, and the following day all the other ones. Slice 23 was kept in place until the cores for on-site determinations were drilled. The lighter colour in the central part of the section is an indication of its lower water content. The radial dimensions of the blocks measured on their surface before extractions are shown in Tab. 14. The location of the cores drilled for on-site determinations is shown in Fig. 75.

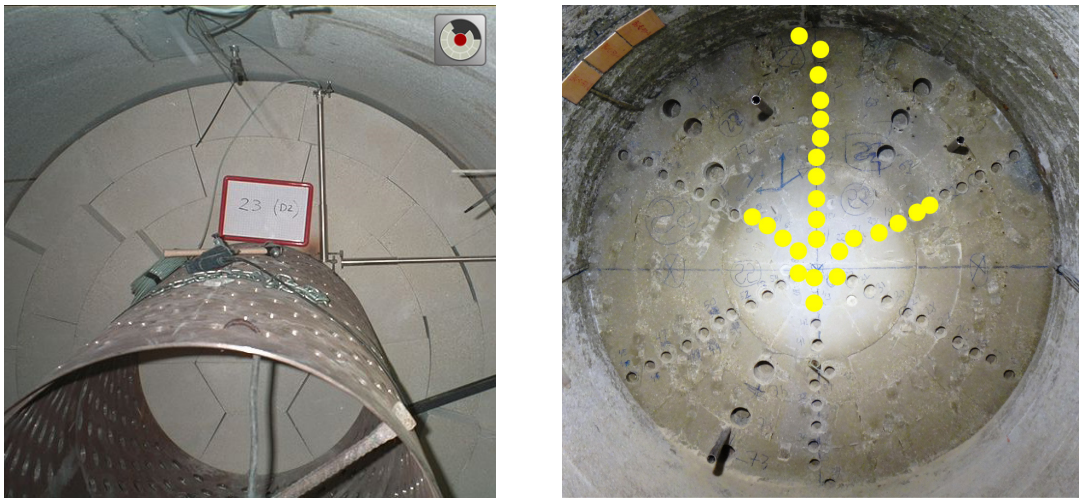

Fig. 74: Initial and final appearance of Section 56 (Slice 22).
The highlighted cores were taken on July 20th, the others on July 21st 2015.

Tab. 14: Dimensions of the blocks along the radius in Slice 22, Section S56 (the kinds of block are indicated in Fig. 4, the original dimension for all was 216.7 mm).

Θ (°)	**BB-G-01** (mm)	**BB-G-02** (mm)	**BB-G-03** (mm)
0	225	228	214
60	225	217	210
120	226	220	215
180	229	220	215
225	225	220	220
315	224	220	218
Average	226	221	215

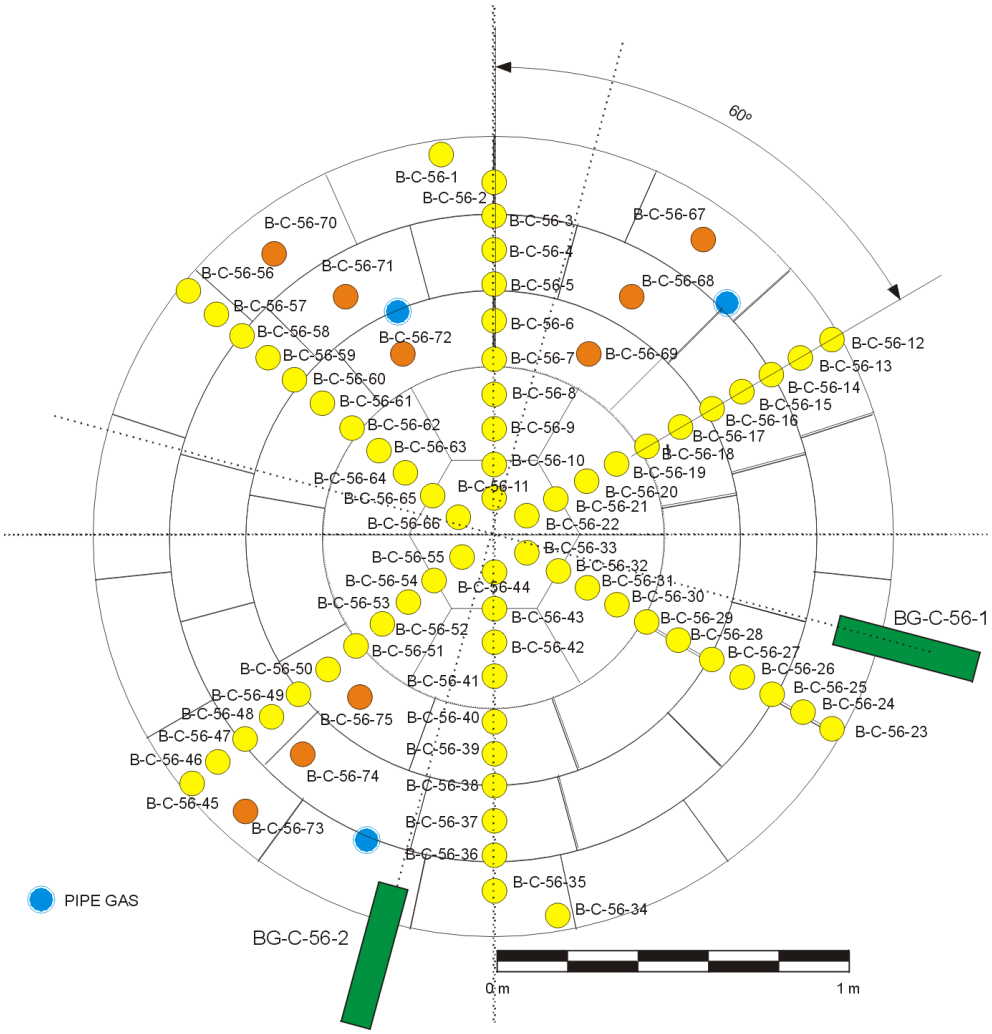

Fig. 75: Location of samples taken in Section 56.

Fig. 76 through Fig. 81 show the results for water content, dry density and computed degree of saturation, first as a function of the distance to the gallery axis and then as contour maps. The information about the section is summarised in Tab. 15. The water content decreased from the gallery wall towards the axis of the barrier, more steeply in the 35 cm closest to the gallery wall (Fig. 76). Even in the core centre of the barrier, the water content was above the initial one (which was about 14 %). The dry density in the core of the barrier and the inner ring was below the initial density of the blocks (1.70 g/cm^3) and then decreased further towards the gallery wall as the water content increased (Fig. 78, Fig. 79). The radial dimension of the blocks increased from the inner ring –where it was below the initial value of 217 mm– towards the granite (Tab. 14). This indicates that the two external rings expanded during operation whereas the inner one was compressed, which relates well to the density variations. Besides, the thickness of the slice increased during operation (Tab. 15), which would contribute to the overall density decrease with respect to the installation one. The degree of saturation in the 20 cm closest to the granite was close to 100 % and then decreased towards the axis of the gallery. The values measured were similar in all the radii, except for Radius A which had higher water content and lower dry density than the others (Fig. 80).

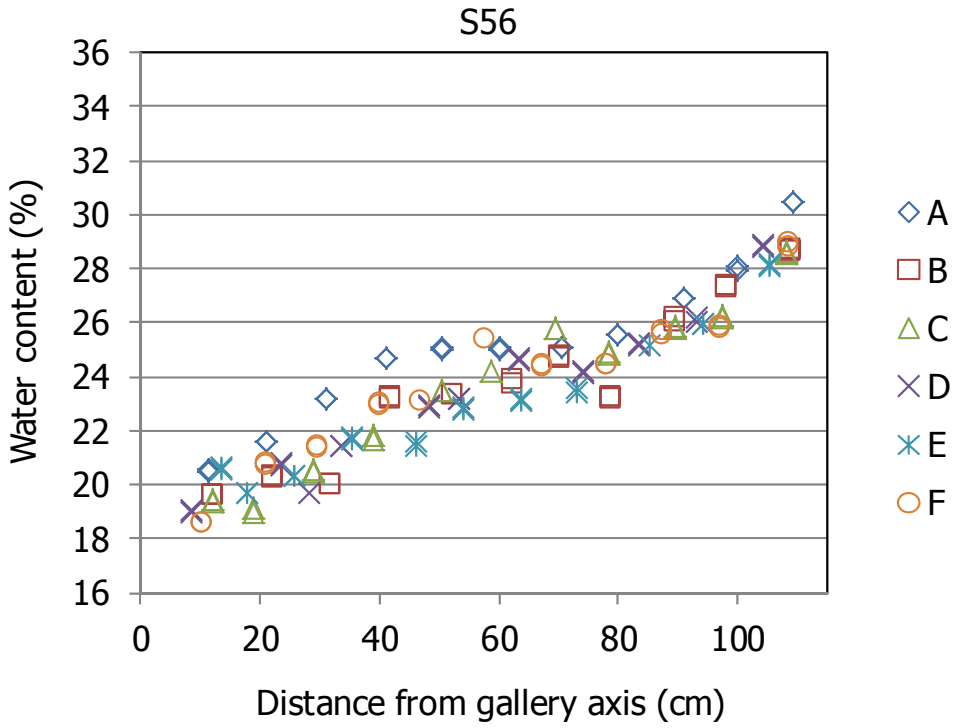

Fig. 76: Water content measured in subsamples along the six sampling radii in Section 56.

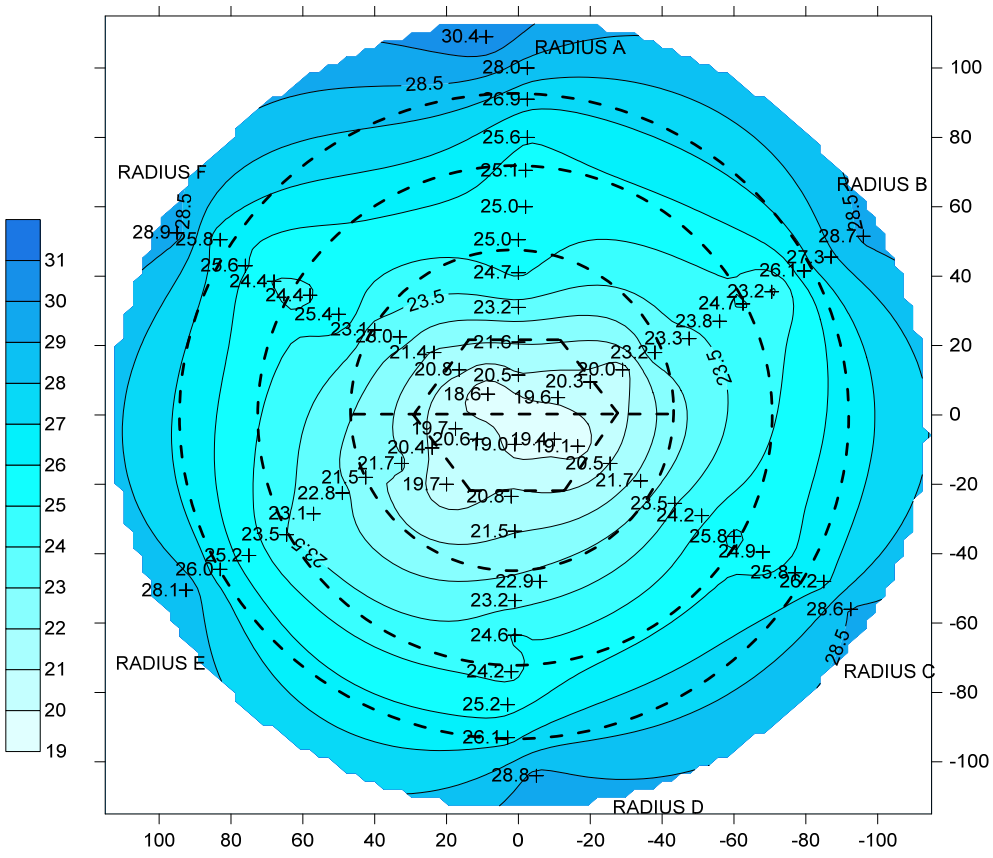

Fig. 77: Contour map for water content in Section 56.

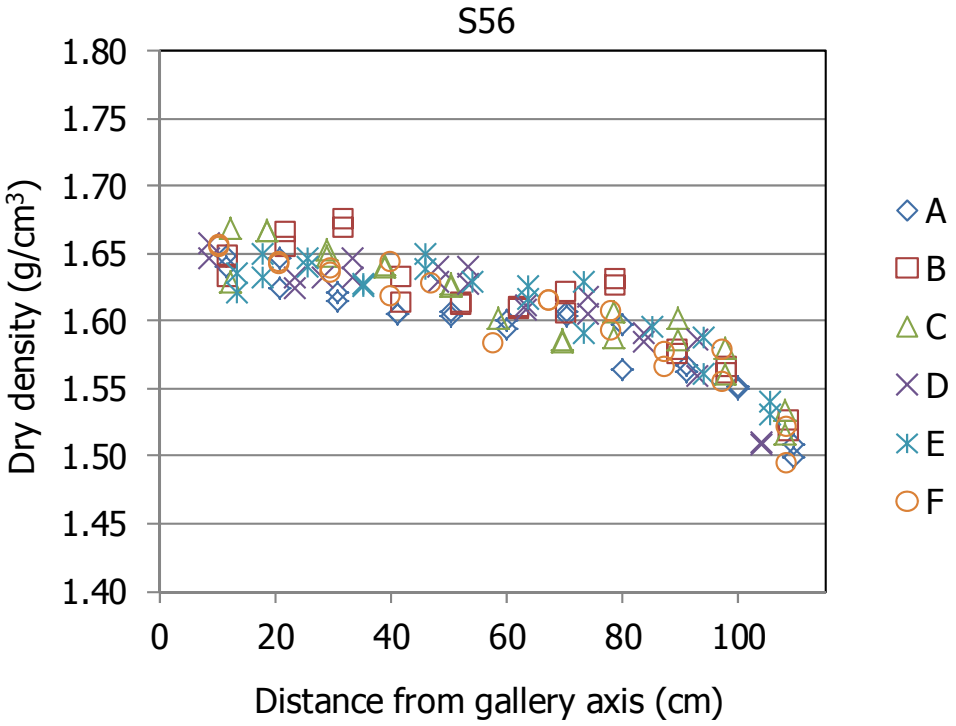

Fig. 78: Dry density measured in subsamples along the six sampling radii in Section 56.

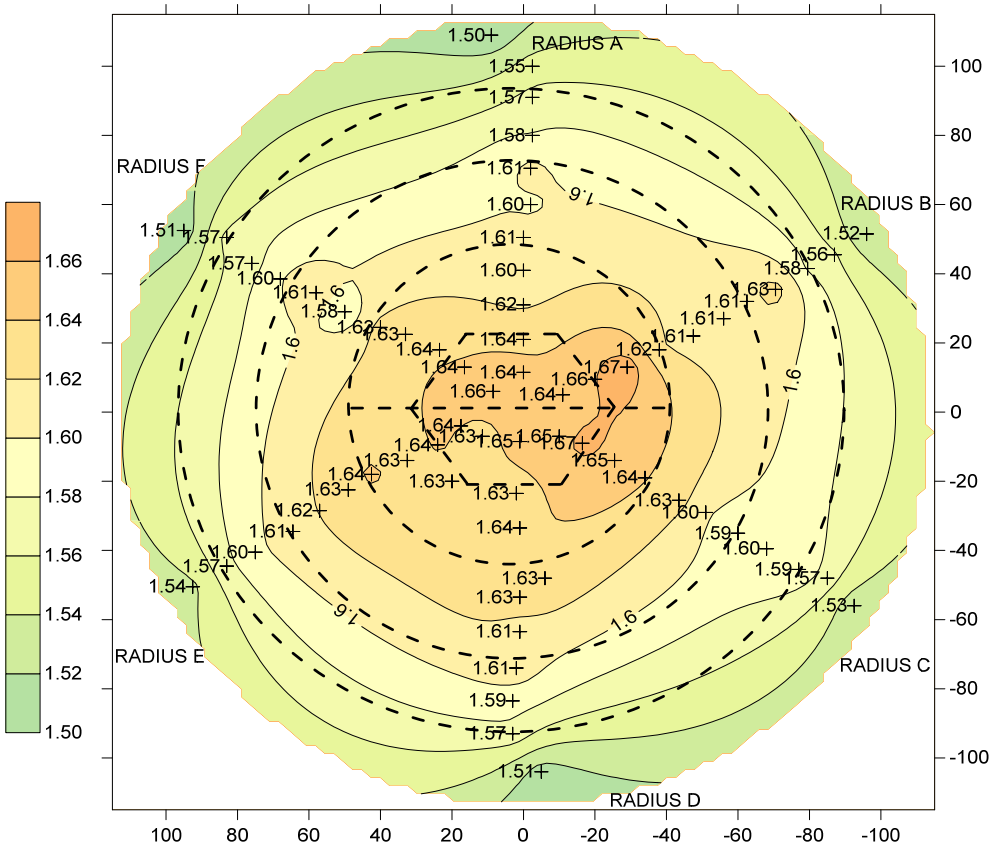

Fig. 79: Contour map for dry density in Section 56.

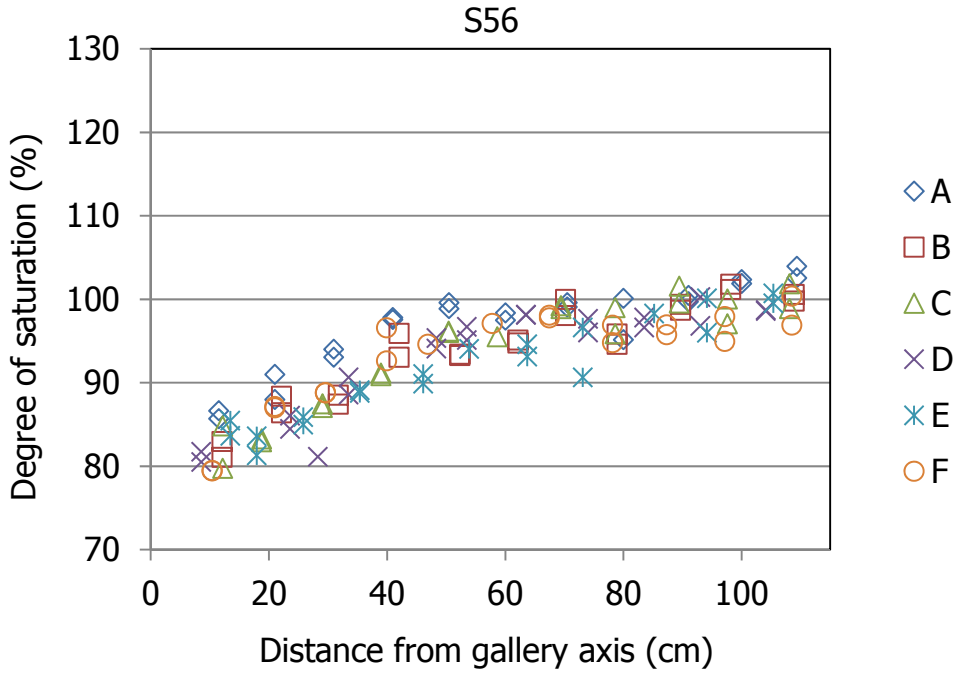

Fig. 80: Degree of saturation of subsamples along the six sampling radii in Section 56 (inexact values because of solid specific weight and water density uncertainties).

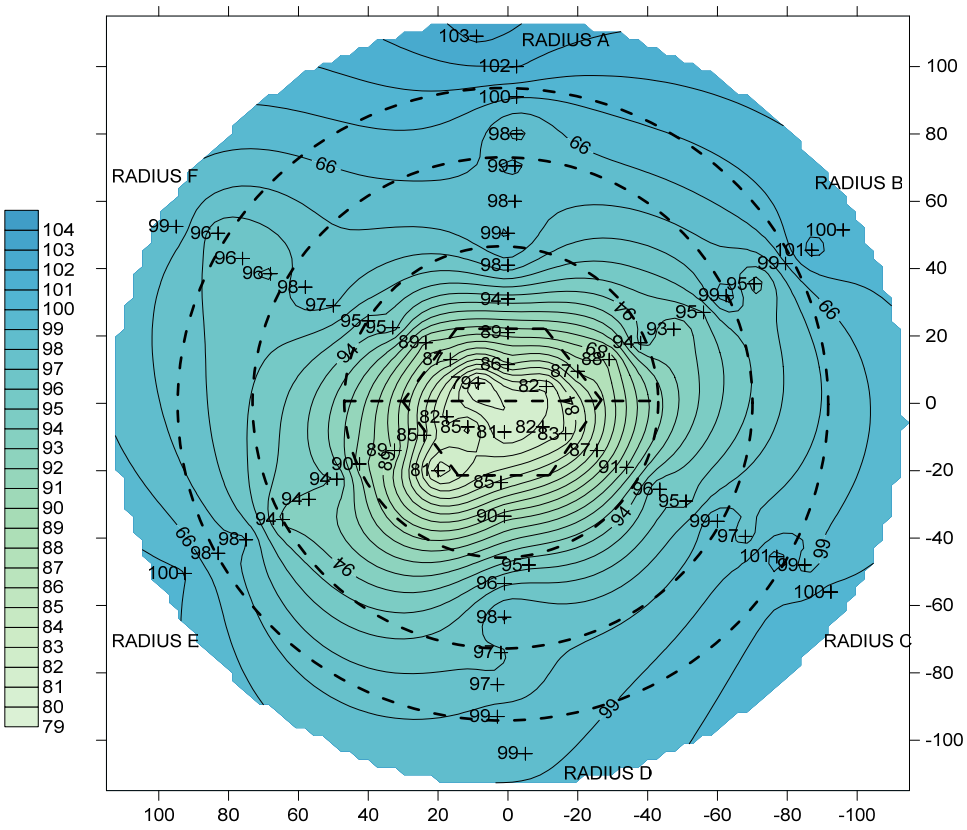

Fig. 81: Contour map for degree of saturation in Section 56 (inexact values because of solid specific weight and water density uncertainties).

Tab. 15: Summary Section 56.

Slice/Instrumented section	22	
Estimated *T* during operation	< 36 – 88 °C (estimated from instrumented Section D2, Slice 24)	
Sampling date/time since switching-off	July 20 – 21st 2015/87 – 88 days	
As built/final *x*-coordinate (m)	14.555/14.520	
Observations	Vein filled with minerals in the lower left side	
Initial/final thickness (mm)	125/130	
	Mean output grid values	Polynomial functions
w (%)	26.1	26.2
ρ_d (g/cm^3)	1.57	1.57
S_r (%)	98	98

3.9 Section 58, Slice 13

This section was between the back of the heater and the back of the gallery, approximately in the middle of this area. Hence, the impact of the heater on this section was very attenuated, and the temperatures during operation must have been between those measured in Section D2 (Slice 24), in which the temperatures were between 36 and 88 °C, and those measured in instrumented Section B2 (Slices 1 – 3), which were around 23 °C (AITEMIN 2014). In any case, the temperature in the section during dismantling, which was undertaken 94 days after switching off, dropped below 20 °C (AITEMIN 2016b). The bottom of the gallery was crossed at this area by a thick vein filled by different minerals (Fig. 2).

The dimensions measured on the surface of the blocks before dismantling are summarised in Tab. 16. Fig. 82 shows the final appearance of this slice. The lighter colour of the core of the section indicates the lower water content in this area. The location and reference of the core samples taken for on-site determinations are given in Fig. 83.

Tab. 16: Dimensions of the blocks along the radius in Slice 13, Section S58 (the kinds of blocks are indicated in Fig. 4, the original dimension for all was 216.7 mm).

Θ (°)	**BB-G-01** (mm)	**BB-G-02** (mm)	**BB-G-03** (mm)
0	226	220	218
60	220	215	213
120	215	220	213
240	213	210	212
300	215	218	220
Average	218	217	215

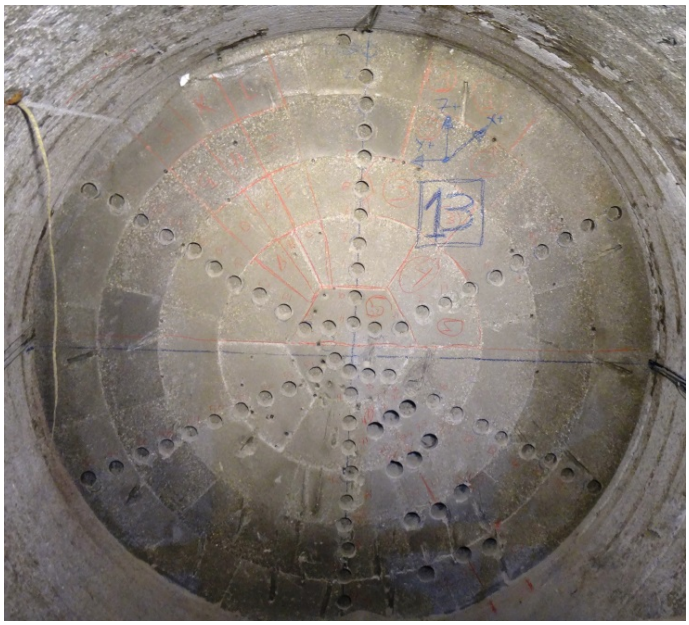

Fig. 82: Final appearance of Section 58 (Slice 13).

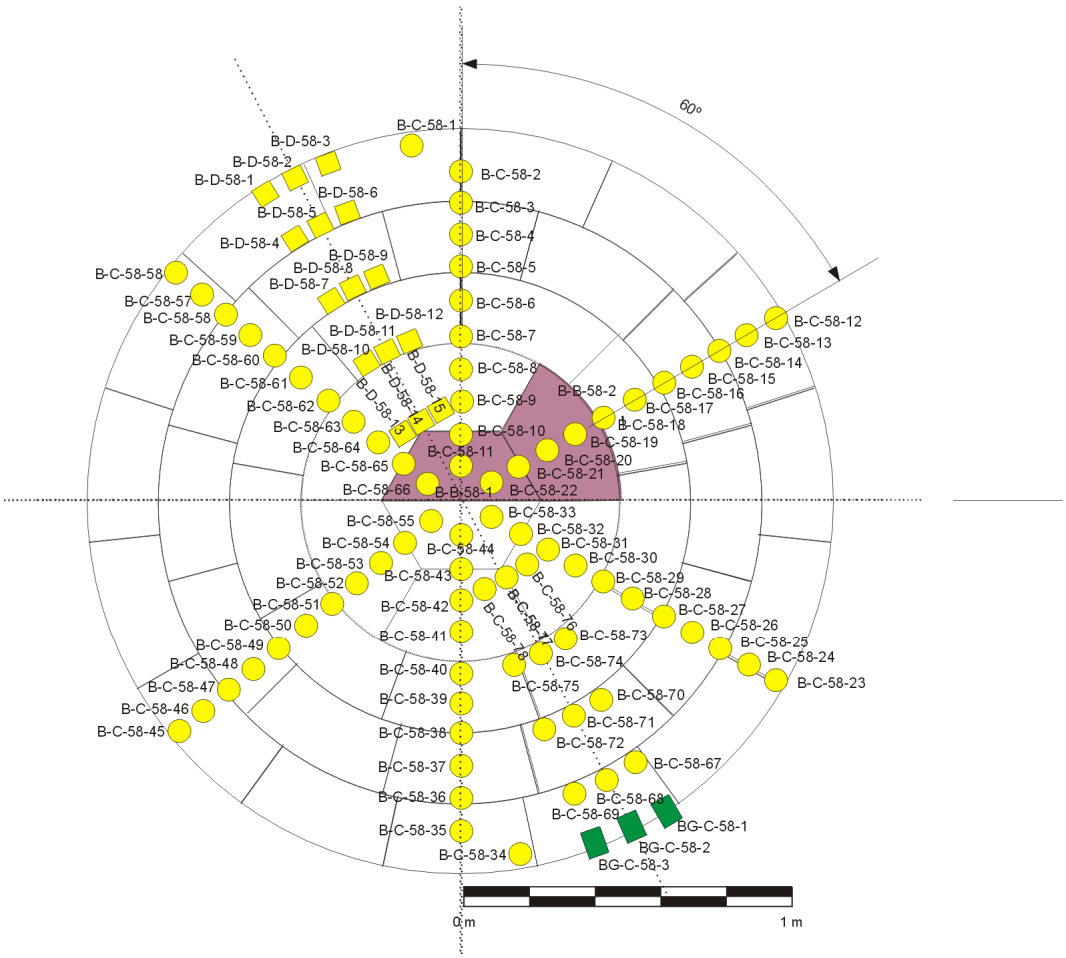

Fig. 83: Location of samples taken in Section 58.

The information about the section is summarised in Tab. 17; Fig. 84 through Fig. 89 show the results for water content, dry density and computed degree of saturation, first as a function of the distance to the gallery axis and then as contour maps. The water content decreased from values near the gallery wall of about 30 % to average values of 24 % (which is quite above the initial one) in a circular area around the axis of the barrier of radius 40 cm (Fig. 85). The dry density was on average 1.60 g/cm^3 in a circular area of radius 60 cm around the axis of the section, and then decreased towards the granite (Fig. 87). This pattern of density change is not clearly reflected on the radial dimensions of the blocks, because the radial dimension of the blocks in the external radius did not change much with respect to the initial ones (Tab. 16). This suggests that the expansion of the bentonite could have taken place mostly along the longitudinal direction, which is confirmed by the final higher thickness of this slice (Tab. 17). This would also explain the low average dry density of the section. The degree of saturation was between 102 and 92 %, decreasing towards the axis of the section (Fig. 89). The values measured were similar in all the radii, although the highest water contents were measured in the external part of Radius F, i.e. in the upper left of the barrier.

Tab. 17: Summary Section 58.

Slice/instrumented section	13	
Estimated *T* during operation	Intermediate between 36 – 88 °C (estimated from Section D2) and 23 °C (estimated from Section B2)	
Sampling date/time since switching-off	July 27th 2015/94 days	
As built/final *x*-coordinate (m)	16.695/15.711	
Observations		
Initial/final thickness (mm)	127/134	
	Mean output grid values	Polynomial functions
w (%)	27.2	26.9
ρ_d (g/cm^3)	1.55	1.55
S_r (%)	98	98

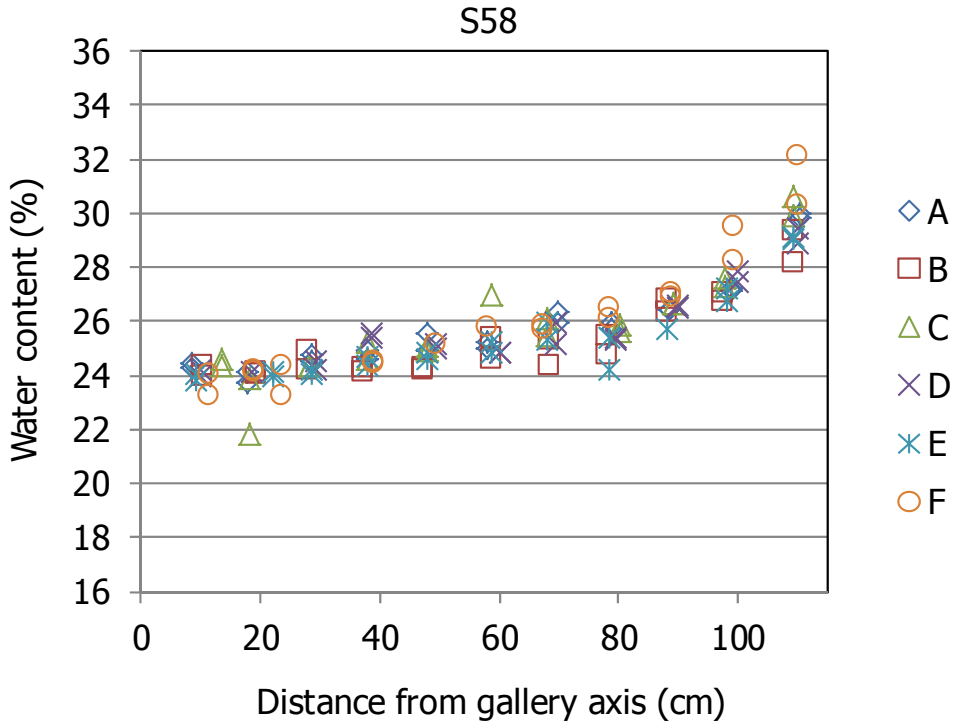

Fig. 84: Water content measured in subsamples along the six sampling radii in Section 58.

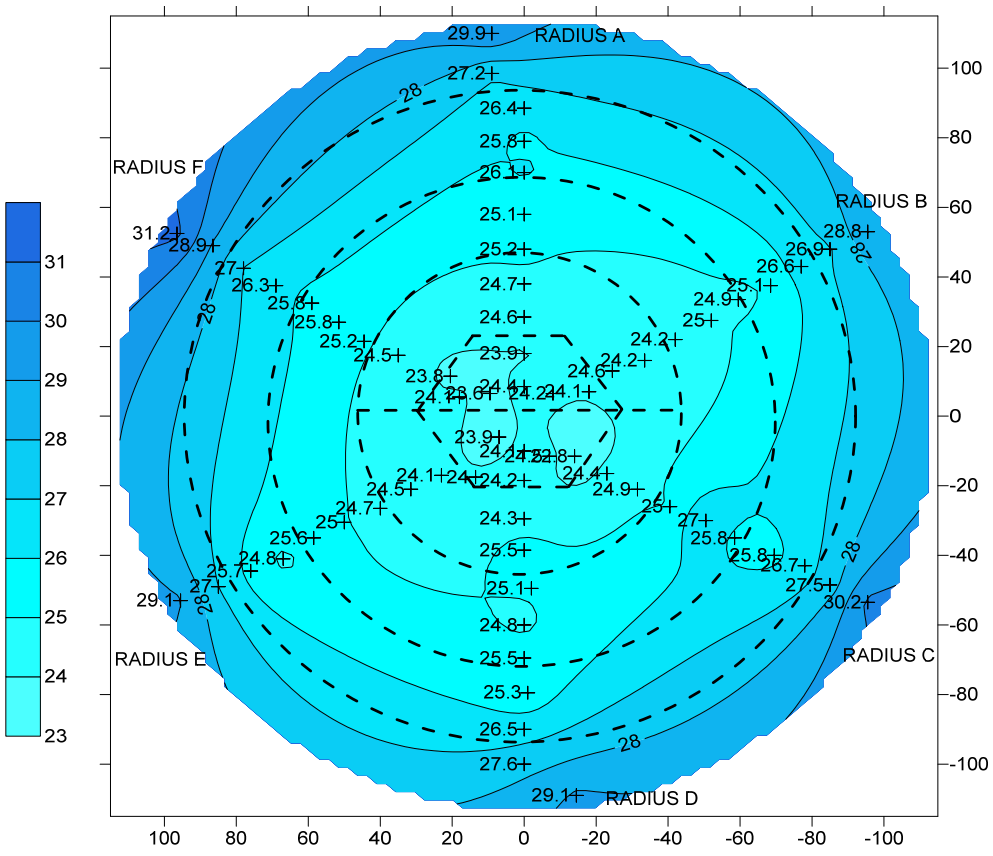

Fig. 85: Contour map for water content in Section 58.

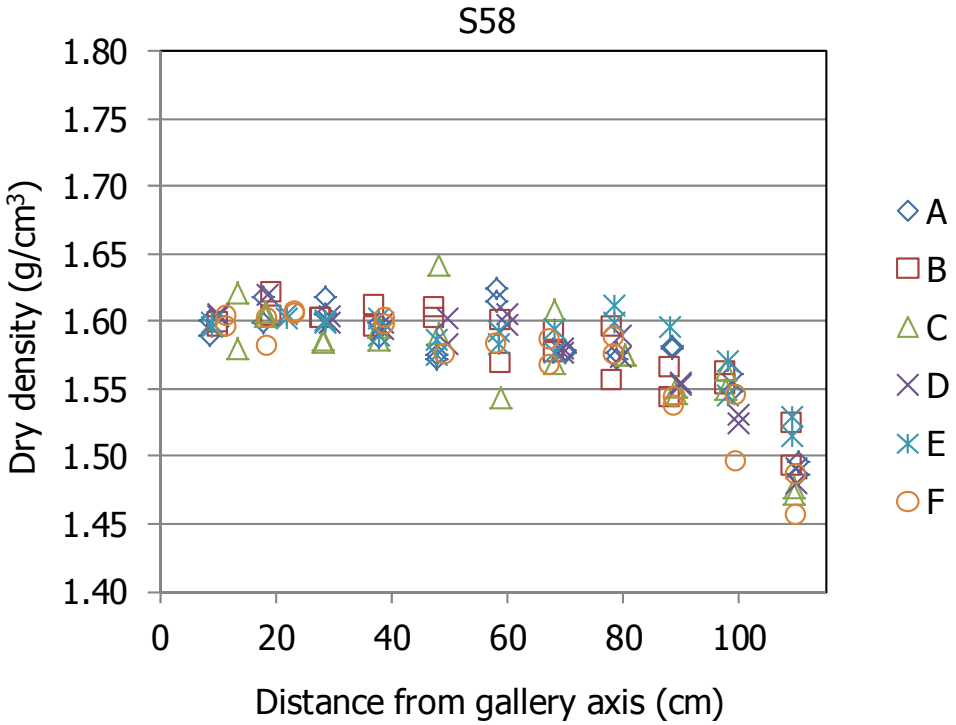

Fig. 86: Dry density measured in subsamples along the six sampling radii in Section 58.

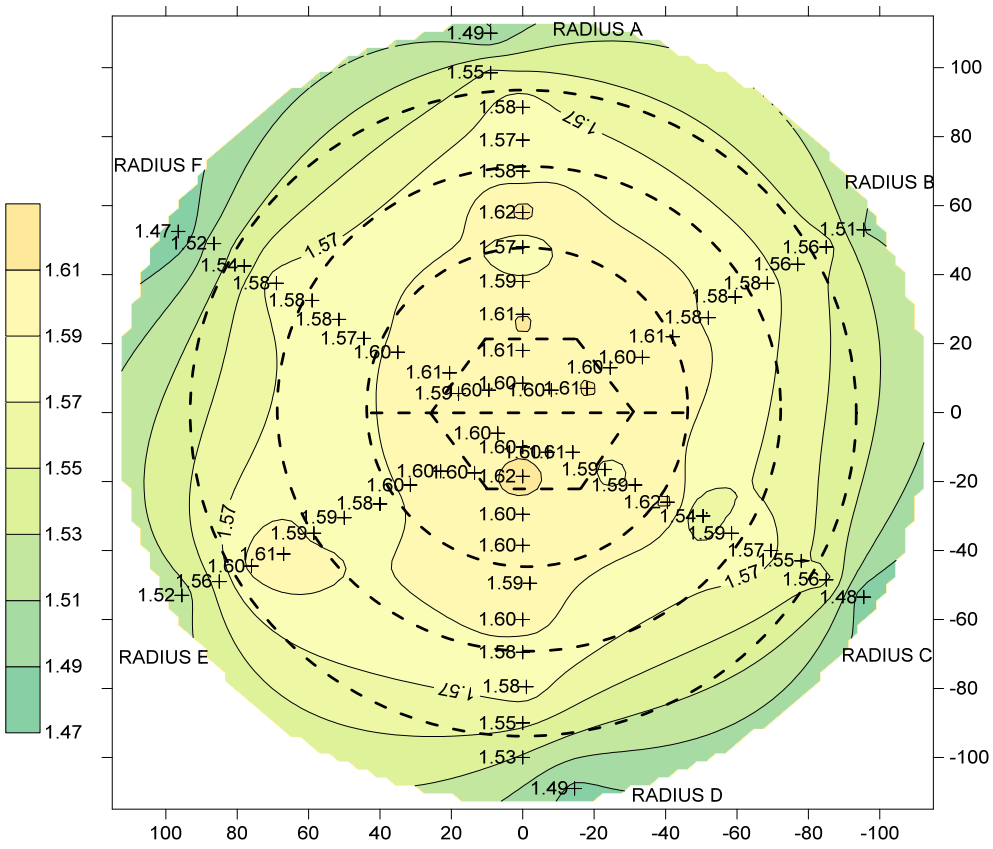

Fig. 87: Contour map for dry density in Section 58.

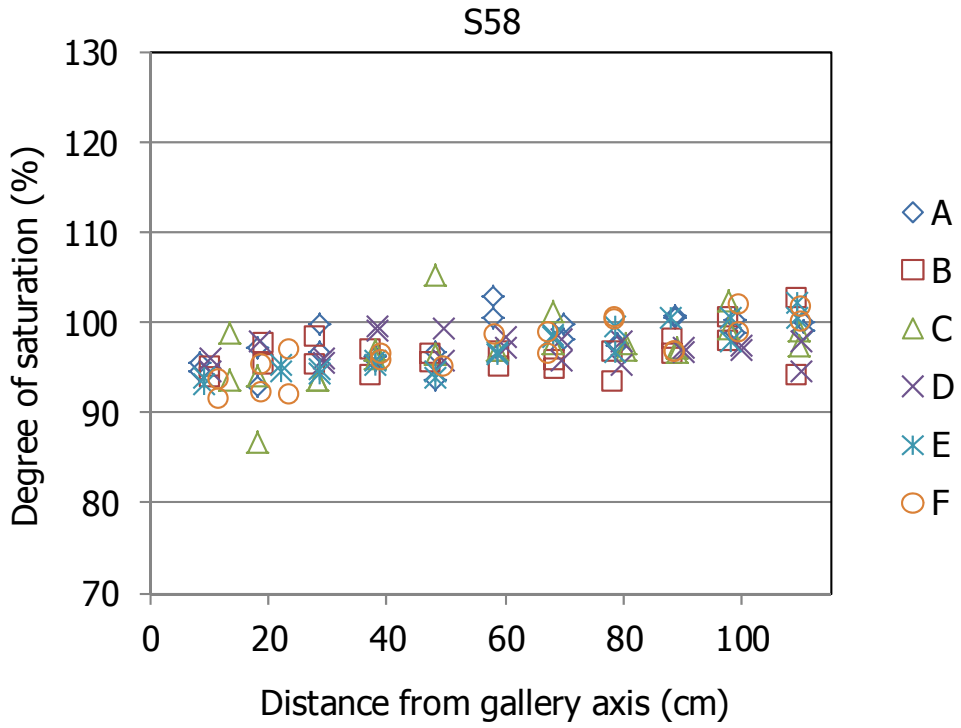

Fig. 88: Degree of saturation of subsamples along the six sampling radii in Section 58 (inexact values because of solid specific weight and water density uncertainties).

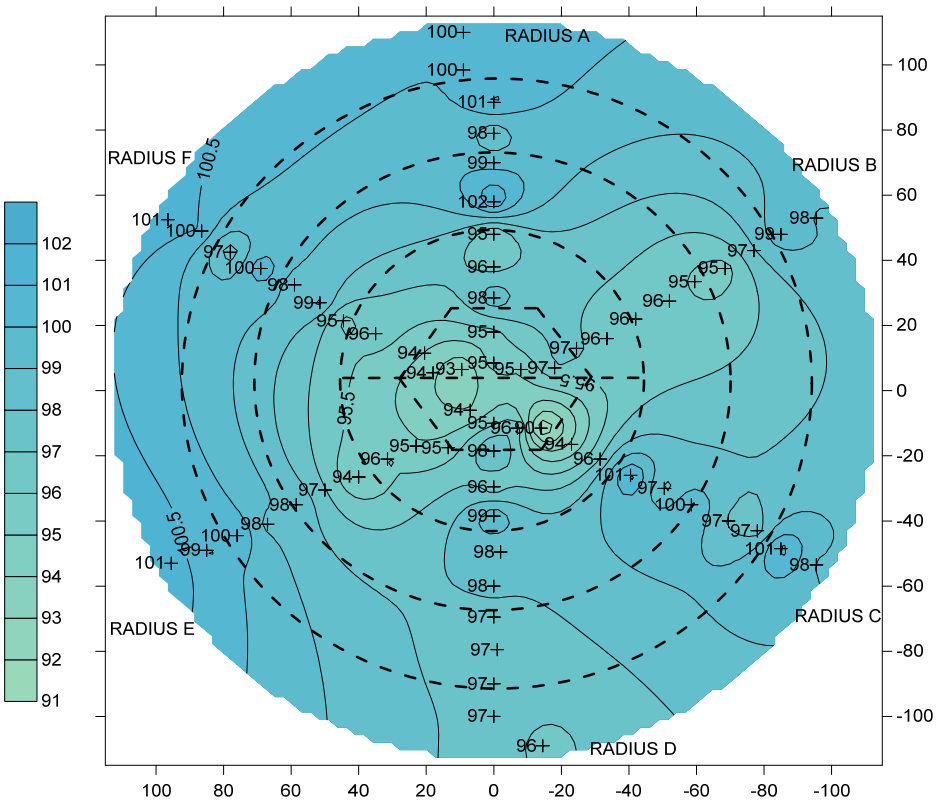

Fig. 89: Contour map for degree of saturation in Section 58 (inexact values because of solid specific weight and water density uncertainties).

3.10 Section 61, Slice 4

This section was very close to the back part of the gallery and had been a "cold" section during operation, with temperatures expected to have been similar to those measured in the nearby instrumented Section B2 (Slices 1 – 3), which were around 23 °C (AITEMIN 2014). When the section was dismantled, 97 days after switching off the heater, the temperature had decreased to 18 °C. The following Slices 1 – 3, had a void volume at the time of installation of 37.07 %, whereas the preceding Slice 5, had a percentage of gaps of 18.58 % (Fuentes-Cantillana & García-Siñeriz 1998). These two values are much higher than the average installation gap volume of the whole barrier, which was 5.51 %, and of the average of Slice 4, which was 5.76 %. Nevertheless, a total pressure sensor in section B2 placed between the second and the third rings of the barrier was recording pressure close to 6 MPa when it stopped working in 2013.

The right side of the gallery in this area was crossed by a thick vein filled by different minerals, whereas the left side presented numerous fractures (Fig. 2). In fact, during the hydrogeological characterisation of the gallery, it was determined that the last meter of the drift had the highest flow rate (Guimerà et al. 1998).

The section was sampled in two consecutive days (Fig. 90, Fig. 91). The first day radii A, B and F and the inner cores of the other radii were taken. The upper left part of the section presented a glassy appearance which could have been caused by the friction between sections upon expansion. The location and reference of the core samples taken are shown in Fig. 92. Tab. 18 shows the radial dimensions of some blocks as measured on their surface before dismantling.

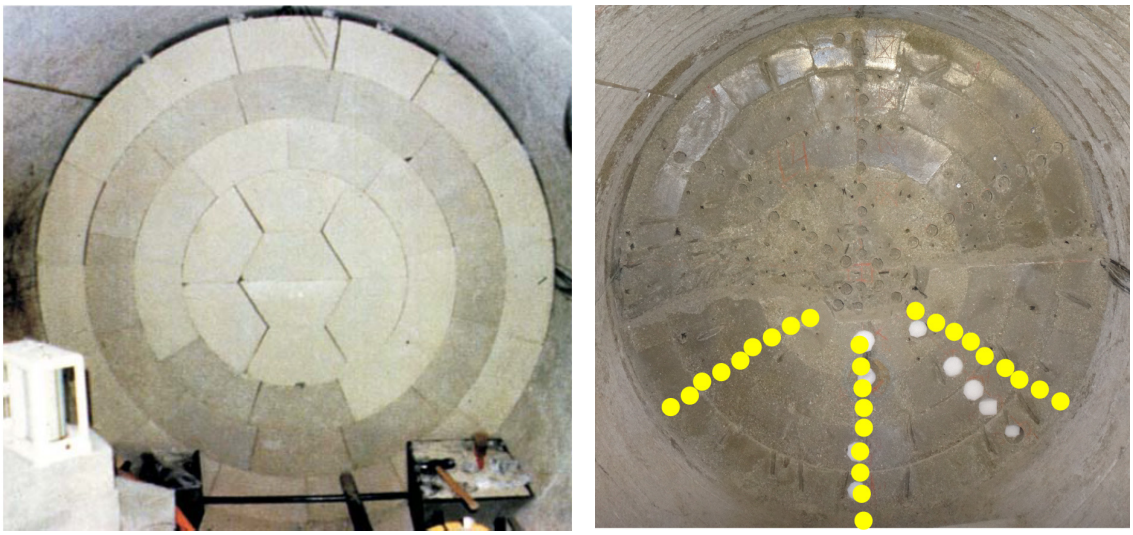

Fig. 90: Initial and final appearance of Section 61 (first sampling day July 30th, the highlighted cores were sampled on July 31st).

Fig. 91: Appearance of Section 61 (Slice 4) at the end of the second sampling day.

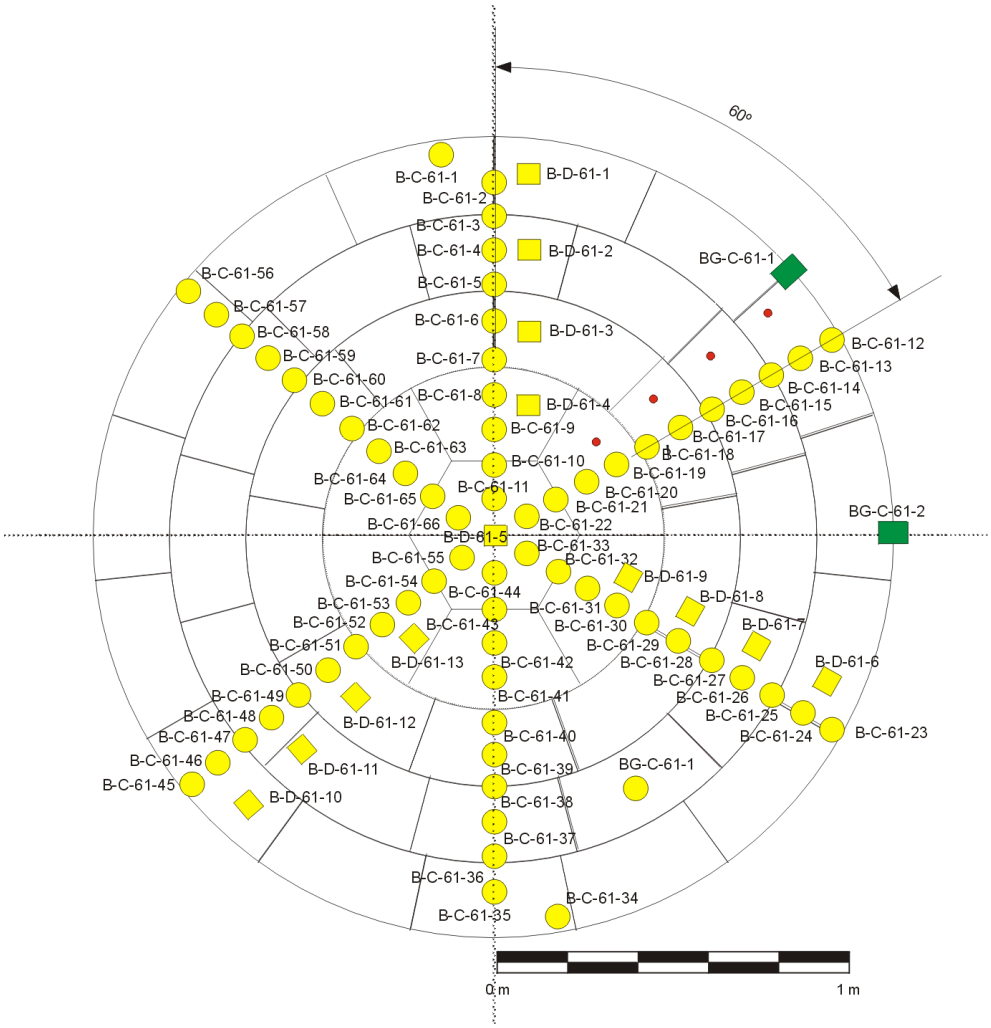

Fig. 92: Location of samples taken in Section 61 (sample B-C-61-34 was finally taken aligned with the others in Radius D).

Tab. 18: Dimensions of the blocks along the radius in Slice 4, Section S61 (the kinds of block are indicated in Fig. 4, the original dimension for all was 216.7 mm).

Θ (°)	**BB-G-01** (mm)	**BB-G-02** (mm)	**BB-G-03** (mm)
60	215	219	210
90	220	210	212
180	222	220	215
300	220	210	215
Average	219	215	213

Fig. 93 through Fig. 98 show the results for water content, dry density and computed degree of saturation, first as a function of the distance to the gallery axis and then as contour maps. The information about the section is summarised in Tab. 19. All along the different radii the water content and dry density were homogeneous, in the range 30 – 34 % and 1.42 – 1.51 g/cm^3, respectively. Only the 20 cm closest to the gallery wall showed a changing trend in all radii, the water content increasing towards the gallery wall (Fig. 93) and the dry density decreasing (Fig. 95). Radii E and F, on the left hand side of the gallery, had higher water content and lower dry density than the other radii: 33.2 *vs*. 31.4 % and 1.44 *vs*. 1.48 g/cm^3, respectively. This part of the gallery, the left hand side approximately 1.5 m apart from the back of the gallery, has a high fracture density with abundant veins filled by quartz, feldspar, biotite, muscovite, chlorite and calcite (Pardillo et al. 1997). Although they were not identified as supplying particularly high water flows (2×10^{-4} mL/min/m), their existence could provide an explanation to the higher water content on the left hand side of the barrier. The degree of saturation was homogeneous throughout this section (102 ± 2 %), with no significant differences related to the axial distance or the position of the radius (Fig. 97, Fig. 98).

The low densities measured, which were all below the nominal average dry density of the barrier, could be explained by the large construction gaps volume in the neighbouring slices, which would allow the expansion upon saturation of Slice 4 towards the back and the front of the gallery. The fact that the radial dimensions of the blocks did not increase significantly in any ring with respect to the initial ones (Tab. 18) is an indication that the radial expansion was not particularly important, and that the bentonite expansion that caused the significant density decrease of the section took place in the longitudinal direction of the gallery (towards the back).

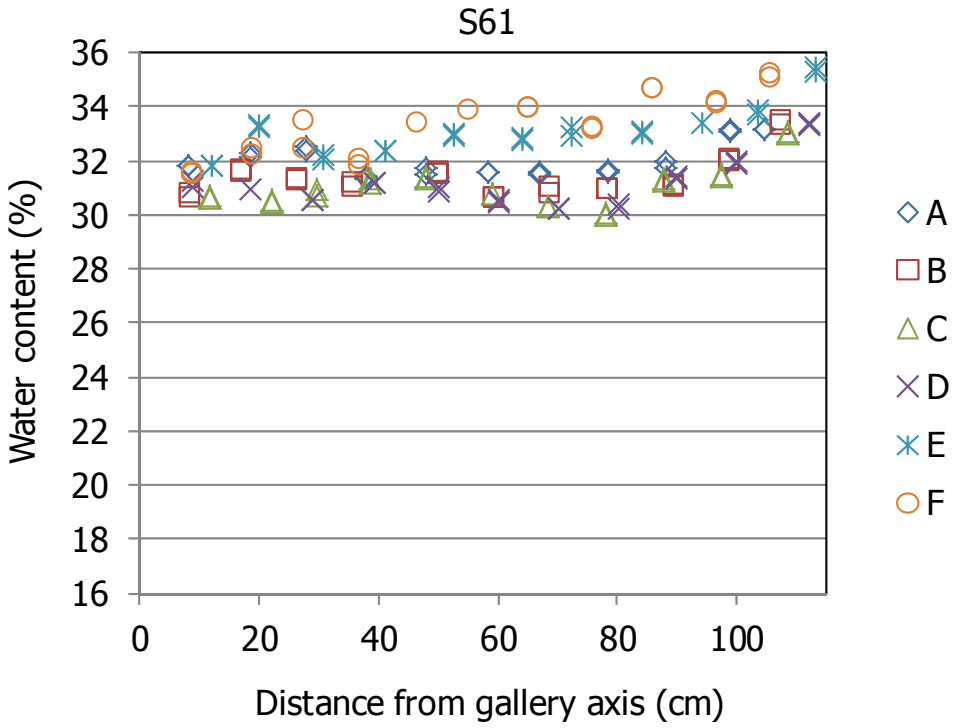

Fig. 93: Water content measured in subsamples along the six sampling radii in Section 61.

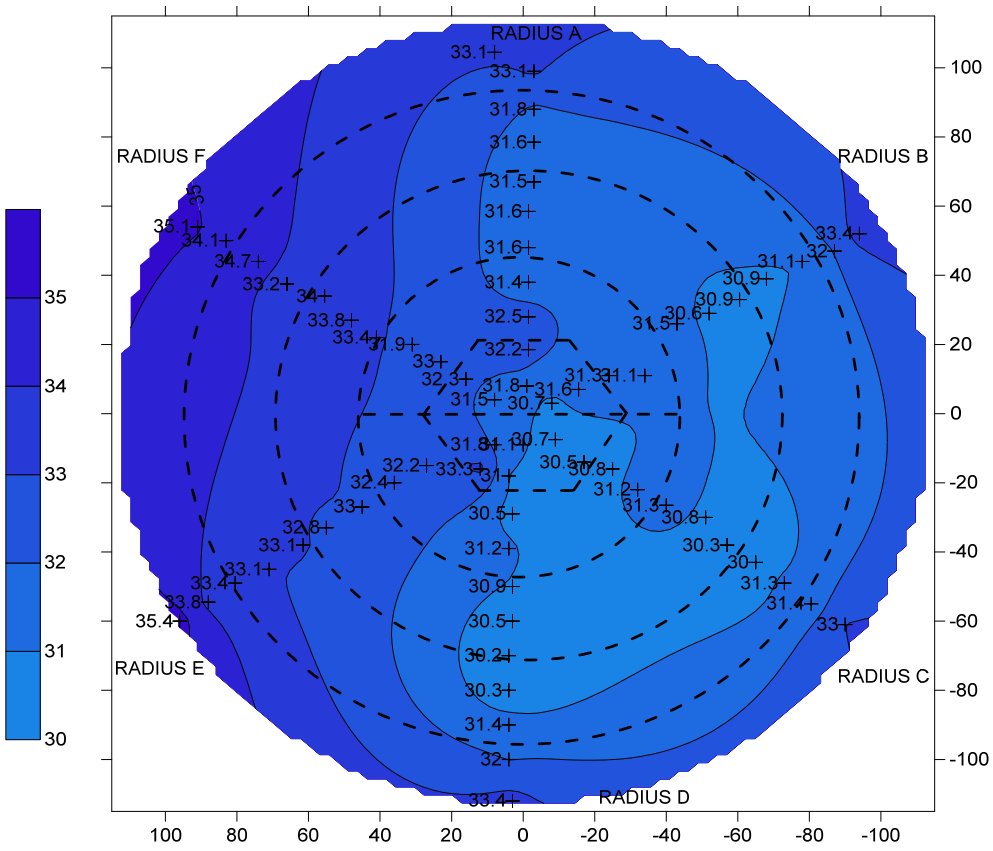

Fig. 94: Contour map for water content in Section 61.

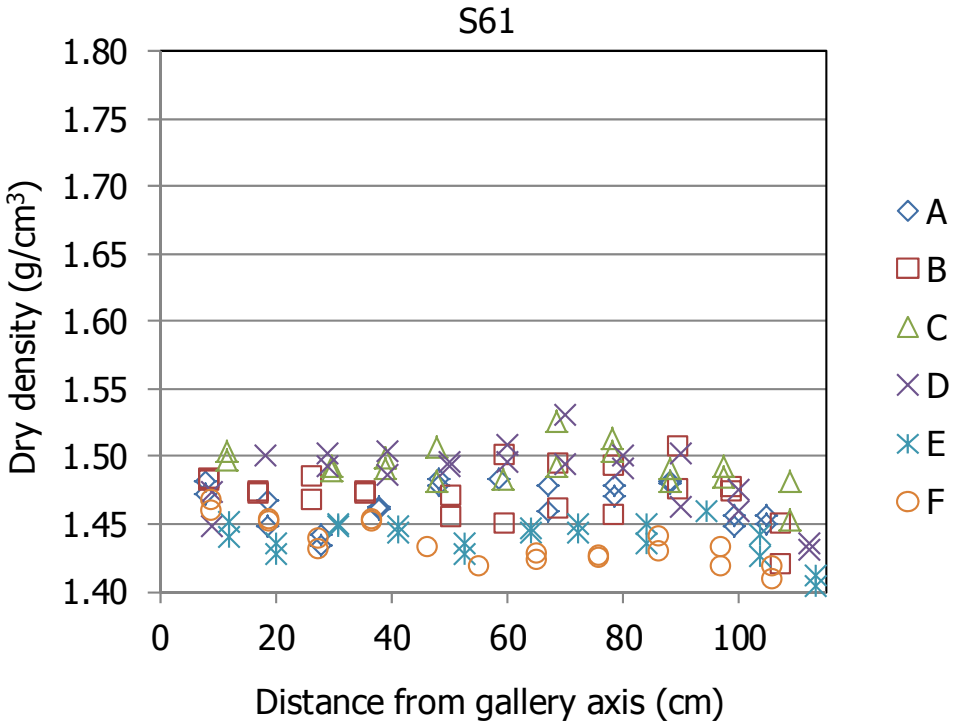

Fig. 95: Dry density measured in subsamples along the six sampling radii in Section 61 (inexact values because of solid specific weight and water density uncertainties).

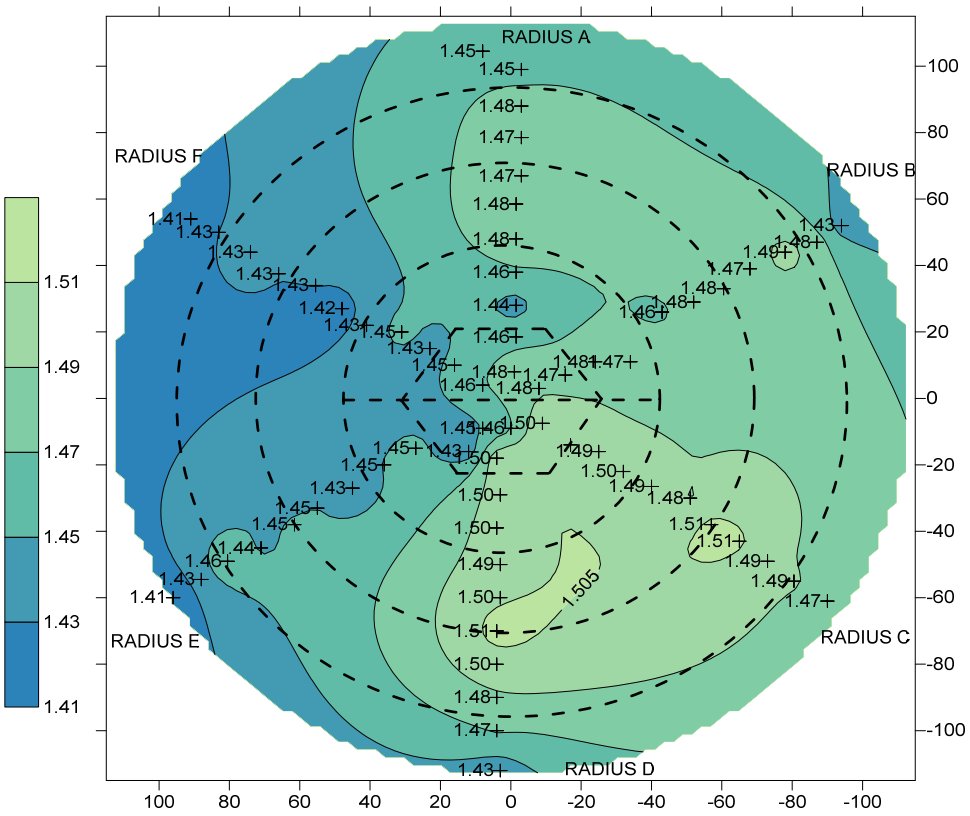

Fig. 96: Contour map for dry density in Section 61 (inexact values because of solid specific weight and water density uncertainties).

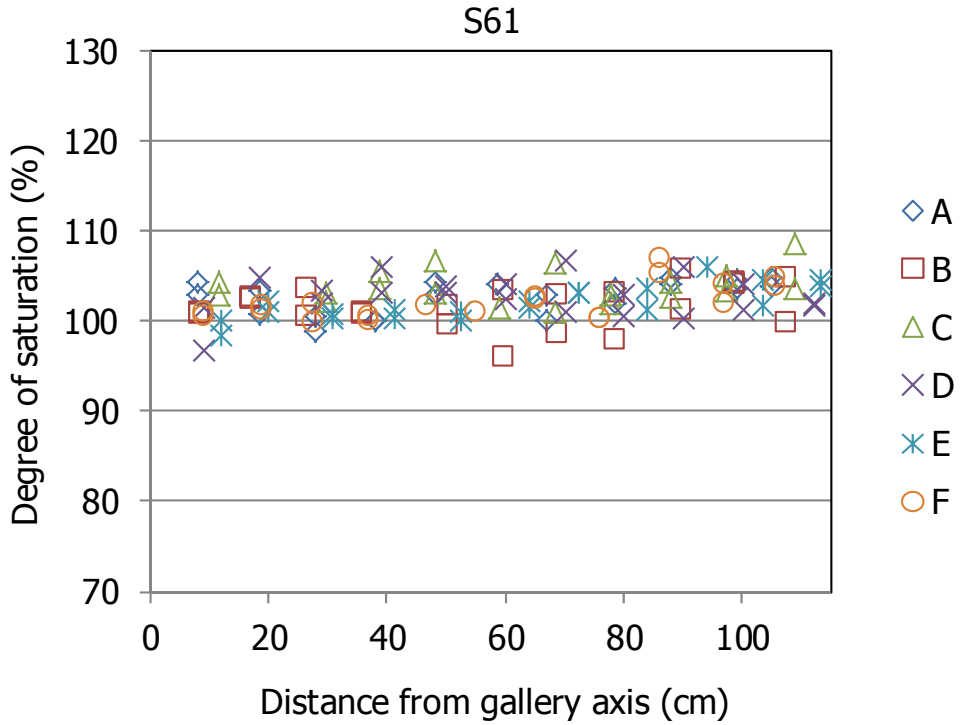

Fig. 97: Degree of saturation measured in subsamples along the six sampling radii in Section 61 (inexact values because of solid specific weight and water density uncertainties).

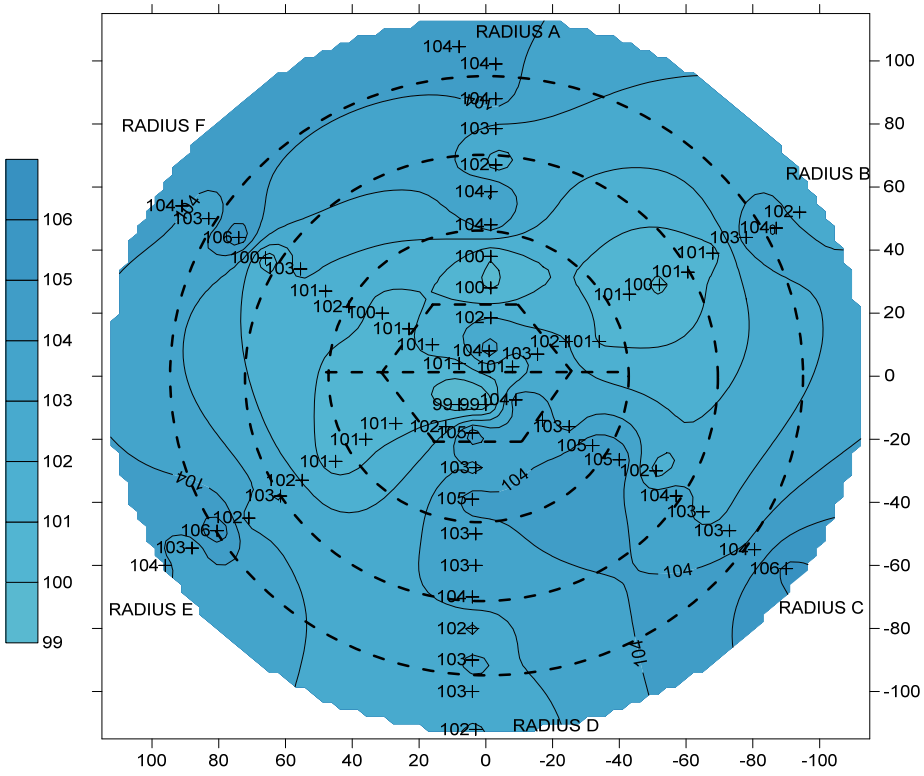

Fig. 98: Contour map for degree of saturation in Section 61 (inexact values because of solid specific weight and water density uncertainties).

Tab. 19: Summary Section 61.

Slice/instrumented section	4	
Estimated *T* during operation	23 °C (estimated from Section B2)	
Sampling date/time since switching-off	July 30 – 31st 2015/97 – 98 days	
As built/final *x*-coordinate (m)	16.870/16.944	
Observations	• Glassy appearance of external bentonite ring • High fracture density on left hand side of gallery • Slices 1 – 3 had an installation void volume of 37 %, Slice 5 was more separated because of installation issues	
	Mean output grid values	Polynomial functions
w (%)	32.7	32.4
ρ_d (g/cm^3)	1.46	1.46
S_r (%)	103	103

3.11 Intermediate sections

In addition to the sections presented above, two additional sections were sampled at just three different radial distances in order to provide a more complete view of the longitudinal changes. These were Sections S38 and S55 (Fig. 6), whose characteristics are shown in Tab. 20. Fig. 99 and Fig. 100 show their final appearance and the position of the samples taken for on-site measurements.

Tab. 20: Summary of intermediate sections.

Sampling section	**S38**	**S55**
Slice/instrumented section	67/G	23
Estimated T during operation	30 – 44 °C (2nd op. phase)	38 – 88 °C (instrumented Section D2, Slice 24)
Sampling date/time since switching-off	May 21st 2015/27 days	July 16th 2015/83 days
As built/final x-coordinate (m)	8.835/8.815	14.430/14.410
Initial/final thickness (mm)	129/not measured	125/110

Section S38 was located around the dummy canister near the start of installation and the values measured in it, along with those measured in the adjacent Sections S37 and S39 are shown in Fig. 101. The distinct feature of Section S37 of having higher water content and lower dry density in the internal ring than observed in those sections immediately adjacent to it, is

attributed to the extrusion of bentonite through the liner holes into the gap between the liner and the dummy. This extrusion of material was also found in Section S38. The contrast of the internal ring and the others is even more remarkable than in Section S37, despite the fact that in Slice 67 the liner was filled with compacted blocks and there should not be any significant gap between them and the liner. The blocks inside the liner had lower dry density than those in the three external rings (Fuentes-Cantillana & García-Siñeriz 1998), and this could have facilitated the extrusion of bentonite from the internal ring inside the liner. Section S39, which was located between the dummy and the heater, had a different distribution of water content and dry density. The degree of saturation along the radius sampled in Section S38 was around 100 % with no trend along it, like in the nearby sections.

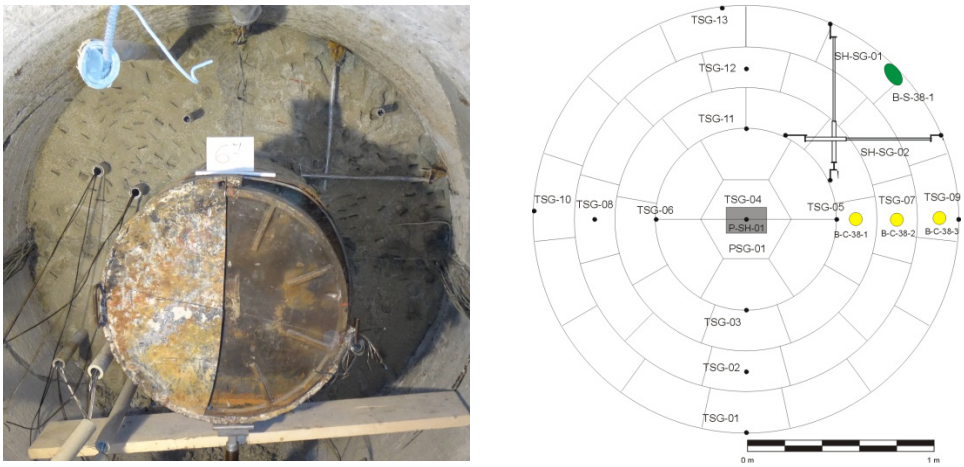

Fig. 99: Final appearance of Section S38 and location of the samples taken.

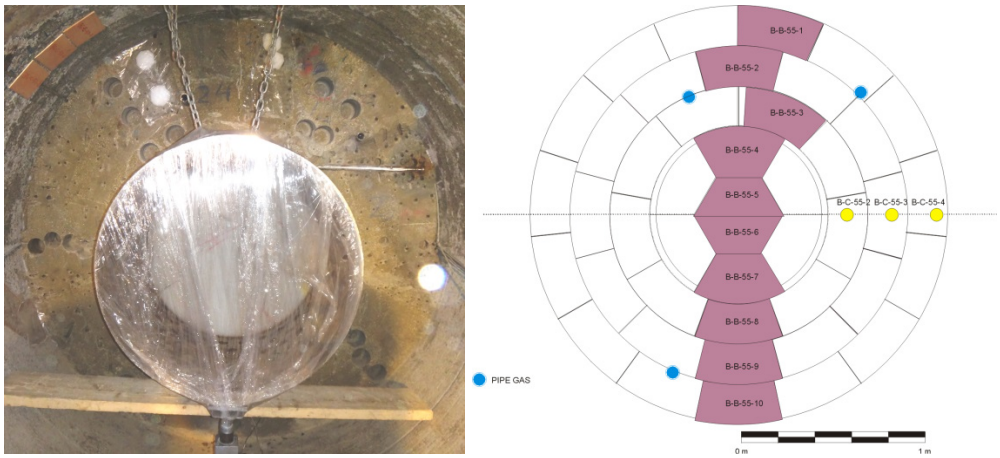

Fig. 100: Final appearance of Section S55 and location of the samples taken.

Fig. 102 shows the on-site results for Section S55 along with those for the nearby Sections S52 and S56. This section was placed at the back of the heater. The dry densities measured in Section S55 were slightly higher in the internal rings than those measured in Section S56, which was away from the heater and cooler. The water content in Section S55 was a little higher than in Section S52, which was hotter because it was placed closer to the middle part of the heater. Consequently, the degrees of saturation in Section S55 were somewhat higher than those in Sections S52 and S56, but with the same decreasing trend towards the axis.

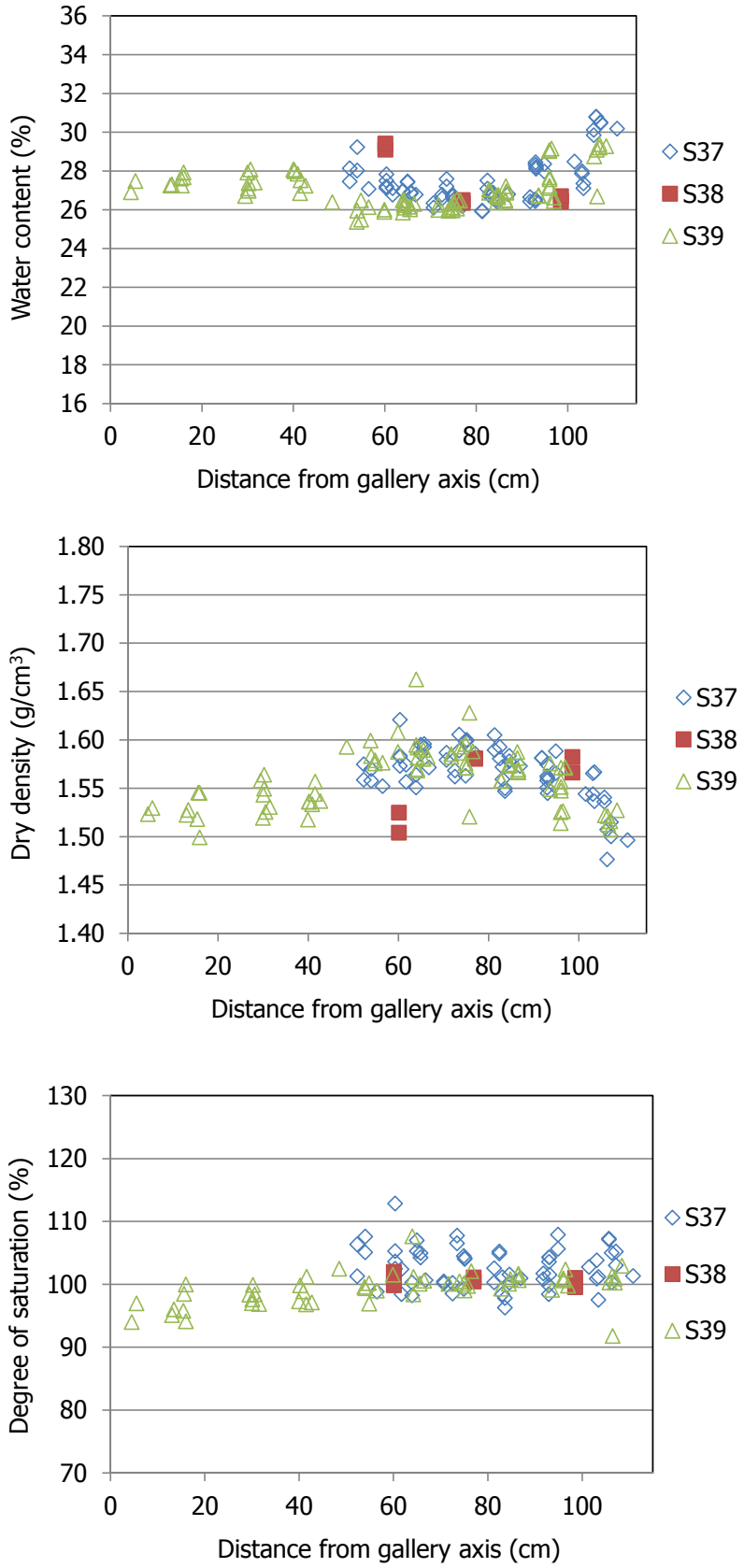

Fig. 101: Results of the on-site measurements in Section S38 and adjacent ones.

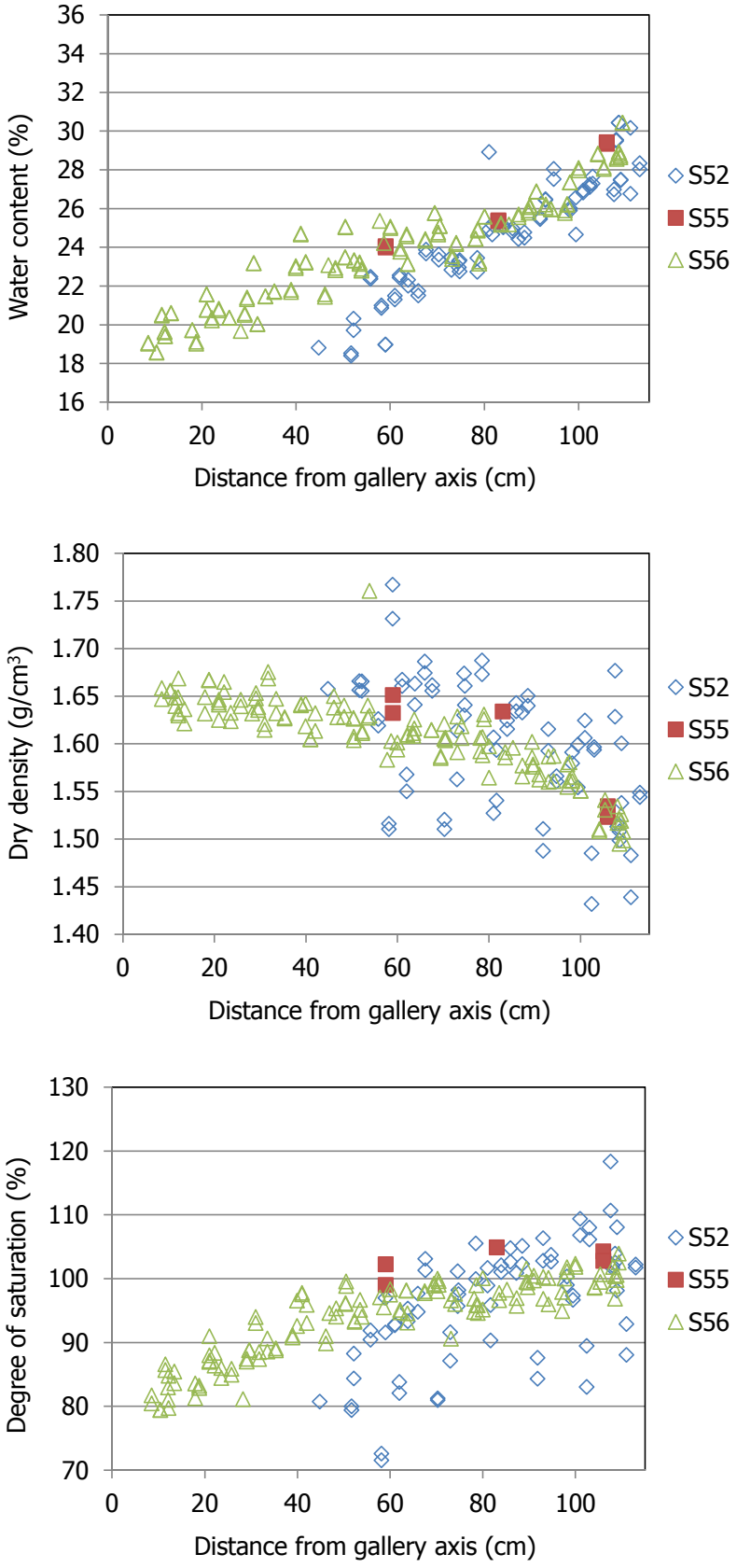

Fig. 102: Results of the on-site measurements in Section S55 and adjacent ones.

4 Discussion

4.1 Summary of patterns observed

The physical state of the barrier after 18 years of operation was very much affected by the processes, to which it had been subjected, namely hydration from the granite and/or thermal gradient-induced moisture redistribution. The observed conditions are discussed in detail in Sections 2.2 through 2.5. A brief summary of these observations and common/distinct patterns found is given here:

- All the construction gaps between blocks had sealed both those among blocks of the same section and the gaps between bentonite slices (Fig. 103). This became clear from the difficulties encountered when separating sampling sections. The effect of these vertical gaps on the water content distribution is analysed in Section 2.2. The granite/bentonite contact was also tight at all locations (Fig. 104) and the gaps hewn in the blocks to let the cables pass had been completely filled by the swelling of the bentonite. A detailed account of the closing of gaps between blocks is given in Extra Report No. 7 in Kober (2015).
- The water content and dry density in every section followed a radial distribution around the gallery axis, with the water content decreasing from the granite towards the axis of the gallery and the dry density following the inverse pattern. The water content at all points in the barrier, even those close to the heater, was higher than the initial one, i.e. greater than 14 %. The water content and density gradients were more noticeable in those sections affected by the heater. These effects were identifiable as lighter colours of the internal ring of the barrier, which were an indication of their lower water content.
- Consistently with the water content and dry density distributions, the radial dimensions measured on the surface of the blocks during dismantling usually indicated the expansion of the external and middle rings and the compression of the internal one. The values measured have been summarised in Tab. 21 and plotted in Fig. 105. The radial dimension of the blocks decreased from the external ring to the internal ring all along the gallery, but particularly around the heater, where the radial dimension of the external ring increased notably with respect to the initial one, whereas the inner ring suffered the strongest shrinkage. The reduction of the radial dimension of the internal ring could have been favoured by the intrusion of bentonite through the liner holes (Fig. 106).
- However, the degree of saturation tended to be homogeneous and very high in all the sections, with no clear spatial trend in most of them. This was particularly clear in Sections S37 to S43 and S58 to S61. Only the sections around the heater or very close to it (S56) had degrees of saturation that decreased towards the gallery axis, but at all points the degree of saturation was higher than 80 %. It is noticeable that in many samples the degree of saturation was higher than 100 %, particularly in the external ring of those sections around the heater (S45, S49 and S52). In Sections S37, S43 and S61 the average degree of saturation was higher than 100 %. This observation is discussed below.
- There were also significant changes in dry density and water content along the axis of the tunnel, which caused the average of these properties in different sections to be different along the gallery. This feature is analysed below in Section 2.3.

Fig. 103: Appearance of blocks from Slices 52 and 53 retrieved together showing that mechanical bonding occurred.

Fig. 104: Granite/bentonite contact in Slice 58.

Tab. 21: Radial dimension of blocks as measured on their surface upon dismantling (the kinds of blocks are indicated in Fig. 4, the original dimension for all was 216.7 mm).

Slice	**Sampling section**	***x*-coordinate** (mm)	**BB-G-01** (mm)	**BB-G-02** (mm)	**BB-G-03** (mm)
70	37	8'405	218	221	204
67	38	8'815	221	214	214
55		10'343	222	220	213
54		10'473	224	218	212
53	44	10'605	221	223	207
49	45	11'100	227	219	208
40	49	12'253	228	220	205
23		14'410	225	222	212
22	56	14'540	226	221	215
13	58	15'711	218	217	215
8		16'385	221	214	210
4	61	16'944	219	215	213

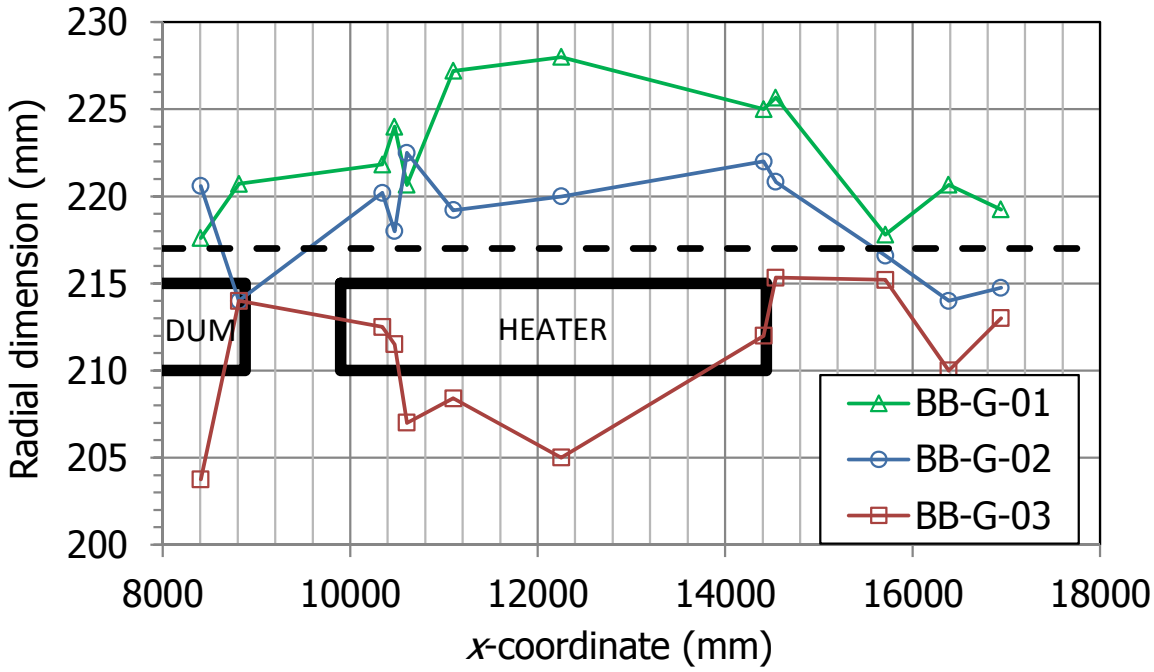

Fig. 105: Radial dimension of different kinds of blocks measured along the gallery upon dismantling (Tab. 21).

The dotted line shows the initial dimension.

Fig. 106: Bentonite intruded inside the liner.

Although common patterns have been observed along the barrier, the state of those sections around the heater (S43 – S56) was different from the state of the cold sections placed towards the back of the gallery (S58 – S61) and of those that were subjected to a thermal gradient during the 1st operational phase but were cool during the 2nd operational phase (S37 – S39). This is discussed below in Section 2.3. Concerning the axial symmetry of the water content and dry density distribution in the vertical slices, in most sections the differences among the six sampled radii were negligible, particularly in terms of water content, except in Sections 52 and 61. The higher water content and lower dry density of the external part of Radius D in Section S43, Radius F in Section 52 and radii E and F in Section 61 could be related to granite geological features (veins, fractures) that could have supplied more water, especially in the case of Section S61. No other reasons have been found to explain other differences among radii, such as the large dispersion of the measurements in Section S52.

The average water content (w), dry density (ρ_d) and degree of saturation (S_r) for each sampled section as determined from the contour plots shown above are given in Tab. 22. Besides, the average values for each section have been computed following the same procedure used for the first dismantling by Daucausse & Lloret (2003): taking advantage of the axial symmetry of the distributions, the average values of the variables in a vertical section have been obtained by fitting polynomial functions to represent their variation with the distance to the gallery axis. These values are also shown in Tab. 22. The two methods give similar values, with differences below the accuracy of the methods used to determine water content and dry density.

Tab. 22: Average properties for each section as computed from the contour plots and the fitting of polynomial functions.

***x*-coordinate** (cm)	**Slice**	**Sampling section**	**Contour plots**			**Polynomial functions**		
			W (%)	ρ_d (g/cm^3)	S_r (%)	W (%)	ρ_d (g/cm^3)	S_r (%)
8'455	70	S37	28.3	1.55	103	27.9	1.56	103
9'214	64	S39	27.7	1.54	100	27.3	1.56	100
10'107	57	S43	27.3	1.59	106	27.0	1.59	105
11'112	49	S45	25.0	1.59	97	24.9	1.60	97
12'265	40	S49	25.0	1.60	98	25.0	1.60	98
13'413	31	S52	24.8	1.59	95	25.0	1.59	97
14'555	22	S56	26.1	1.57	98	26.2	1.57	98
15'695	13	S58	27.2	1.55	98	26.9	1.55	98
16'870	4	S61	32.7	1.46	103	32.4	1.46	103

4.2 Contact between vertical slices

As it has been explained in Chapter 2 (Methodology), each core sample taken for on-site determinations was divided into two subsamples: one corresponding to the external part of the block and one towards the inner part of the block, i.e. towards the back of the gallery. The plots included in the previous sections showing the evolution of water content and dry density along the six sampling radii include for each core the two determinations, whereas the 2-D plots showing isolines were obtained using the average of the two subsamples for each core. The difference between the external and the internal subsamples has been analysed by computing the average water content and dry density in each radius of each sampling section taking into account separately the values for the external samples and for the internal samples. The values obtained are shown in Tab. 23, where the columns ‘avg-1' and ‘avg-2' show the average values for each section of the external and the internal subsample, respectively. The last column shows the difference between the external and internal averages, which is usually below 0.1 %. These values have been plotted in Fig. 107 and Fig. 108, where it can be observed that the average water content in the external and internal part of the blocks is the same in all the sections except in S43 and S49, where it is 0.2 and 0.3 % higher in the external part of the blocks. It has not been possible to relate distribution difference in S43 and S49 to any particular process or locally-unique condition. Although the dispersion is a bit higher for dry density, there is no clear difference between internal and external subsamples. Thus, it can be concluded that the vertical interfaces between slices did not affect the final distribution of water inside the barrier. The adjacent slices were perfectly sealed (Fig. 103).

Tab. 23: Average values of water content (w, %) and dry density (ρ_d, g/cm^3) for the different radii (A to F) of the sampling sections (S37 to S61), considering the subsamples taken in the external part of the block (1) or the internal part (2).

		A-1	A-2	B-1	B-2	C-1	C-2	D-1	D-2	E-1	E-2	F-1	F-2	avg-1	avg-2	
S37	w	28.2	28.4	27.6	27.6	27.1	27.1			27.3	27.3	27.9	27.8	27.6	27.6	-0.01
	ρ_d	1.57	1.56	1.58	1.58	1.56	1.55			1.57	1.56	1.55	1.54	1.57	1.56	0.01
S39	w	27.3	27.1	27.1	26.6	26.9	26.8			26.4	26.5	26.6	26.7	26.8	26.7	0.12
	ρ_d	1.56	1.59	1.56	1.58	1.56	1.57			1.56	1.58	1.56	1.58	1.56	1.58	-0.02
S43	w	26.5	26.9	26.1	26.2	25.3	25.5	27.6	27.8	26.7	26.7	26.8	27.3	26.5	26.7	-0.23
	ρ_d	1.59	1.58	1.62	1.60	1.62	1.62	1.61	1.61	1.60	1.61	1.60	1.58	1.61	1.60	0.00
S45	w	24.6	24.6	24.7	24.6	24.3	24.3	23.6	23.8	23.8	23.9	25.0	24.9	24.3	24.4	-0.03
	ρ_d	1.61	1.61	1.60	1.61	1.62	1.61	1.60	1.59	1.60	1.61	1.61	1.61	1.61	1.61	0.00
S49	w	25.2	25.3	25.4	26.3	24.2	25.0	22.9	23.0	24.1	24.1	25.2	25.3	24.5	24.8	-0.32
	ρ_d	1.60	1.59	1.59	1.58	1.58	1.55	1.66	1.67	1.67	1.64	1.60	1.59	1.62	1.60	0.01
S52	w	25.8	25.9	24.0	23.9	26.5	25.6	23.6	23.8	23.6	23.1	24.8	25.3	24.7	24.6	0.11
	ρ_d	1.58	1.57	1.62	1.63	1.58	1.59	1.66	1.68	1.61	1.63	1.50	1.51	1.59	1.60	-0.01
S56	w	25.1	25.1	23.7	23.7	23.6	23.6	23.7	23.6	22.7	22.8	23.7	23.6	23.7	23.7	0.01
	ρ_d	1.59	1.59	1.61	1.61	1.61	1.61	1.61	1.61	1.63	1.62	1.60	1.60	1.61	1.61	0.00
S58	w	25.7	25.8	25.2	25.4	25.7	25.8	25.9	25.7	25.3	25.3	26.3	26.0	25.7	25.7	0.01
	ρ_d	1.58	1.58	1.58	1.58	1.57	1.58	1.57	1.57	1.58	1.58	1.56	1.57	1.58	1.58	0.00
S61	w	32.0	32.0	31.4	31.4	31.1	31.1	31.1	31.2	33.1	33.1	33.4	33.2	32.0	32.0	0.04
	ρ_d	1.45	1.47	1.47	1.47	1.52	1.50	1.48	1.48	1.44	1.44	1.43	1.44	1.47	1.47	0.00

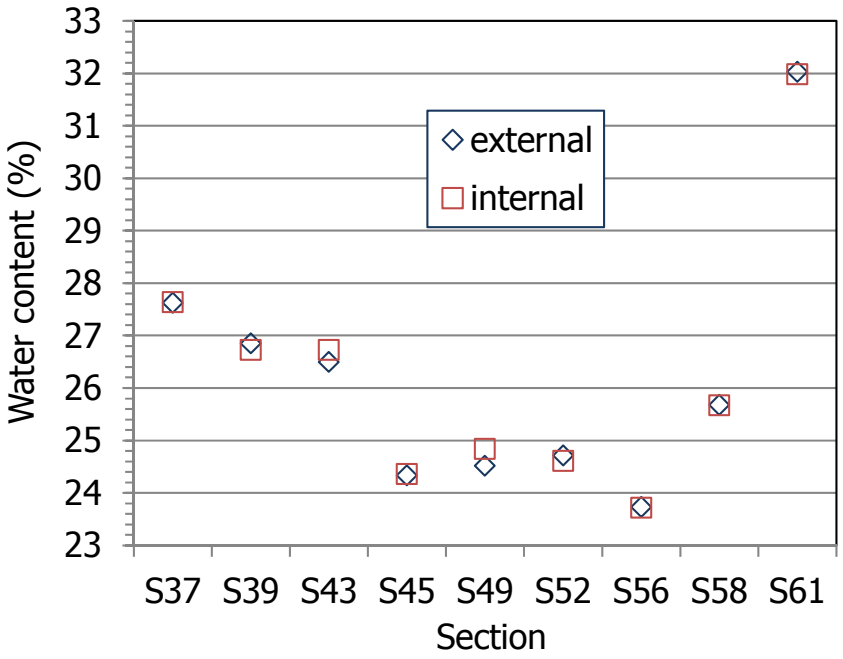

Fig. 107: Arithmetic mean of water content of all the external and internal subsamples for each section.

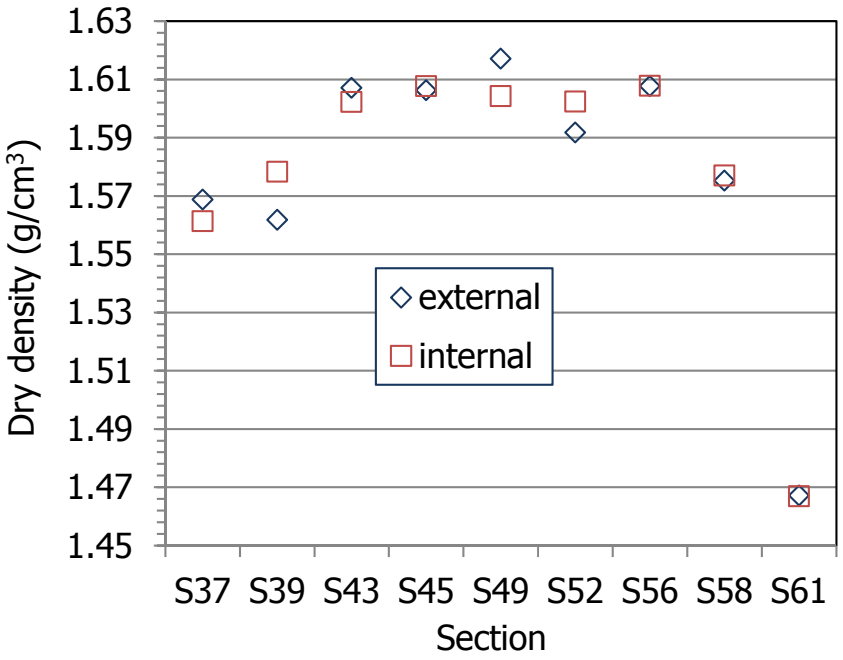

Fig. 108: Arithmetic mean of dry density of all the external and internal subsamples for each section.

4.3 Longitudinal changes

Fig. 107 and Fig. 108 showed that there was also a significant change in the average water content and dry density of the different sections along the axis of the gallery. This becomes clear in the contour maps for water content, dry density and degree of saturation of sections along the gallery shown in Fig. 109 to Fig. 117. They have been drawn with the measurements taken in radii A and D (Fig. 109 to Fig. 111), i.e. the vertical ones; taken in radii B and E (Fig. 112 to Fig. 114); and in radii C and F (Fig. 115 to Fig. 117). All these longitudinal profiles show that the back of the gallery had the highest water contents and the lowest dry densities. The highest dry densities were found around the rear half of the heater, whereas around the dummy canister dry densities below the average of the barrier were observed. From these contour plots the average values for each parameter can be computed and are shown in Tab. 24. According to these values, the final average water content, dry density and degree of saturation of the entire clay barrier would be 25.5 %, 1.59 g/cm^3 and 97 %, respectively.

Plots of the average water content and dry density as a function of the *x*-coordinate for each of the sections sampled on site show similar patterns and are provided in Fig. 118. These values have been computed by adjusting polynomial functions to the change of each parameter with the distance to the gallery axis (Tab. 22). As noted previously, the highest water content and lowest dry density were found at the back of the gallery, while the lowest water content and highest dry density were found around the heater. The fact that the gallery had a concave shape at the back made it difficult to fill this part with bentonite blocks during installation of the barrier and the percentage of construction voids in the area was very high, 37 % for Slices 1 – 3 *vs*. an average along the barrier of 5.5 % (Fig. 119, Fuentes-Cantillana & García-Siñeriz 1998). This would have contributed to the conditions observed in the rear of the test tunnel.

Fig. 120 compares the initial densities along the barrier estimated during installation and the average dry densities of the sections sampled on site. The average dry density of the bentonite that remained in place during the 2nd operational phase was of 1.61 g/cm^3, with values that typically varied between 1.56 and 1.65 g/cm^3. The exception to this density range was in the rearmost 50 cm of the gallery, where it decreased significantly. Obviously, the initial as-built difference in density between the main gallery and the innermost region had not entirely disappeared after 18 years. It should be noted that the hydration surface of the first bentonite slice (at the back of the gallery) was larger than for the slices installed further into the gallery, and this probably contributed to the higher water content observed at the gallery end. The other slices were hydrated just from the external circular surface. Towards the concrete plug the water content tended to be higher than in the regions further into the gallery, which could be because these sections were cooler after having been subjected to heating during the 1st operational phase. It is possible that due to hysteresis effects, the water retention capacity of a material previously submitted to drying is higher.

The average dry density along the barrier, as computed from the longitudinal contour maps shown above, was 1.59 g/cm^3 (Tab. 24), which is lower than the initial average value of 1.61 g/cm^3. The decrease of the dry density measured with respect to the value given during construction was also noted during the partial dismantling done in 2002, when a decrease from the initial as-built dry density value of 1.59 g/cm^3 to a final measured average value of 1.58 g/cm^3 was reported. This change was attributed to the slight decompression suffered by the barrier on dismantling and sampling (Villar et al. 2005). It is worth noting that the installation average dry density of the part of the barrier dismantled in 2002 was lower than that of the part of the barrier dismantled in 2015, 1.59 *vs*. 1.61 g/cm^3. The fact that the density reduction with respect to the installation dry density was more important in the final dismantling could be attributed to the higher expansion of the samples on retrieving and trimming, due to their higher water content. In the case of the final dismantling, the intrusion of bentonite inside the liner

(Fig. 106) could have contributed to the decrease in the average dry density of the barrier. Although it could be thought that the expansion of the barrier upon demolition of the concrete plug could be higher in the final dismantling, since the swelling pressure released was higher because of the higher water content. It has been verified, however, that the average expansion observed is not enough for causing a significant reduction in dry density (see below).

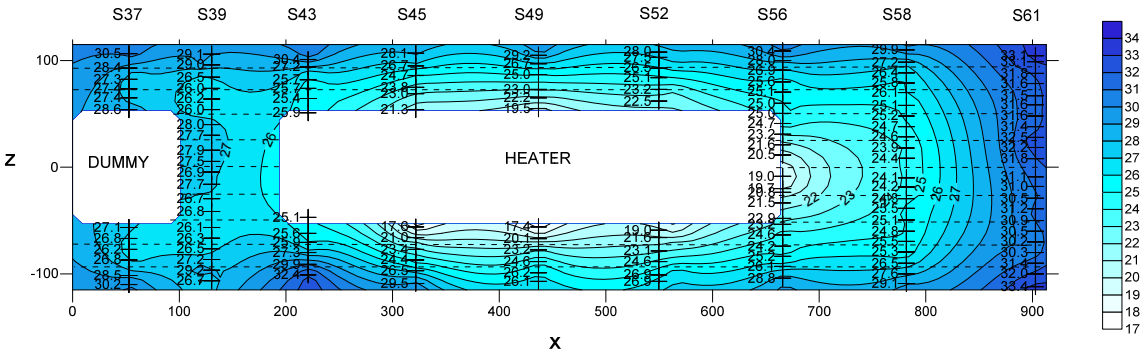

Fig. 109: Water content distribution in a vertical longitudinal section (radii A-D).

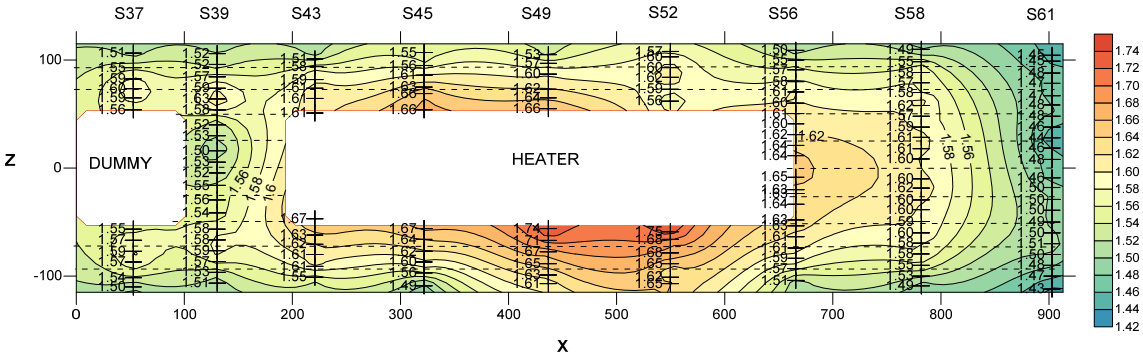

Fig. 110: Dry density distribution in a vertical longitudinal section (radii A-D).

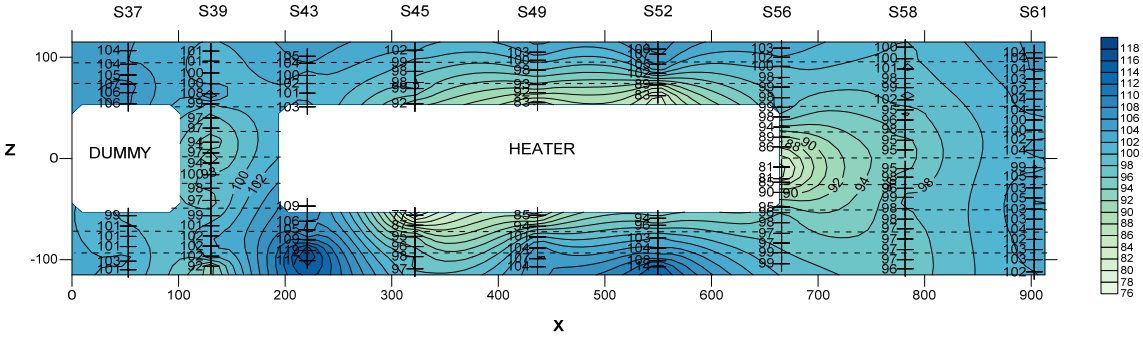

Fig. 111: Degree of saturation distribution in a vertical longitudinal section (radii A-D) (inexact values because of solid specific weight and water density uncertainties).

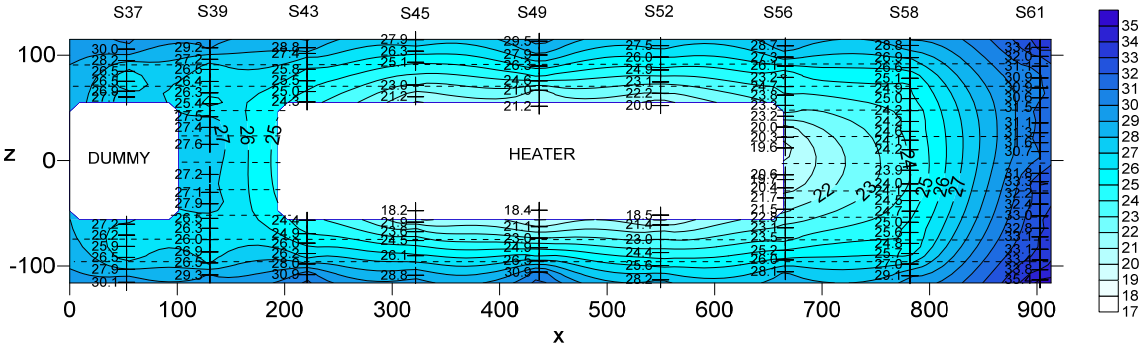

Fig. 112: Water content distribution in a longitudinal section across radii B-E.

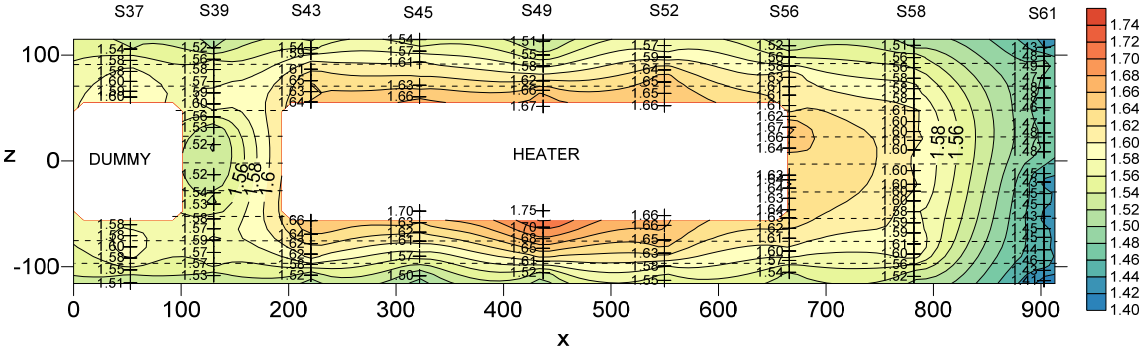

Fig. 113: Dry density distribution in a longitudinal section across radii B-E.

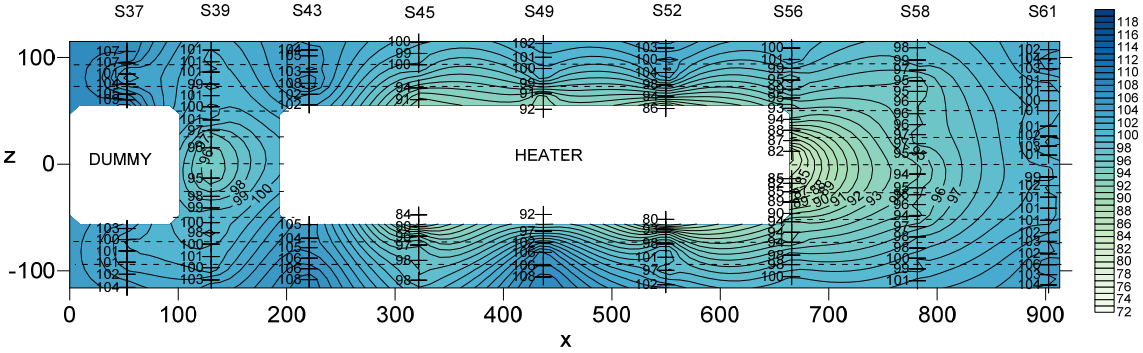

Fig. 114: Degree of saturation distribution in a longitudinal section across radii B-E (inexact values because of solid specific weight and water density uncertainties)

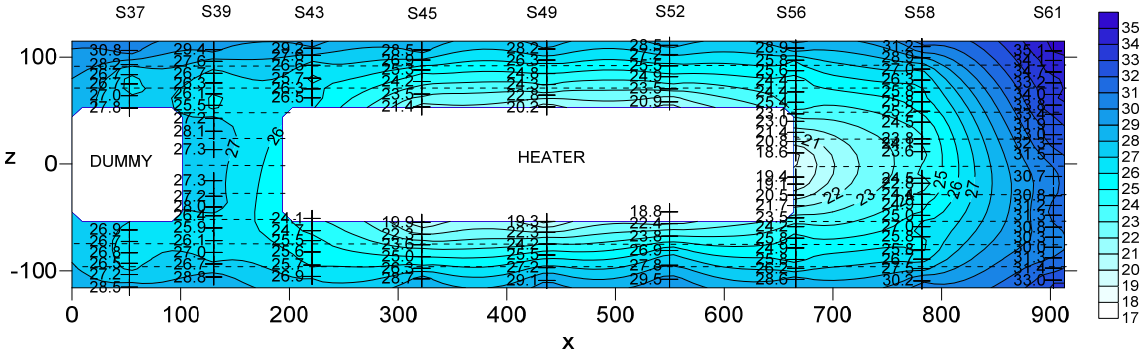

Fig. 115: Water content distribution in a longitudinal section across radii C-F.

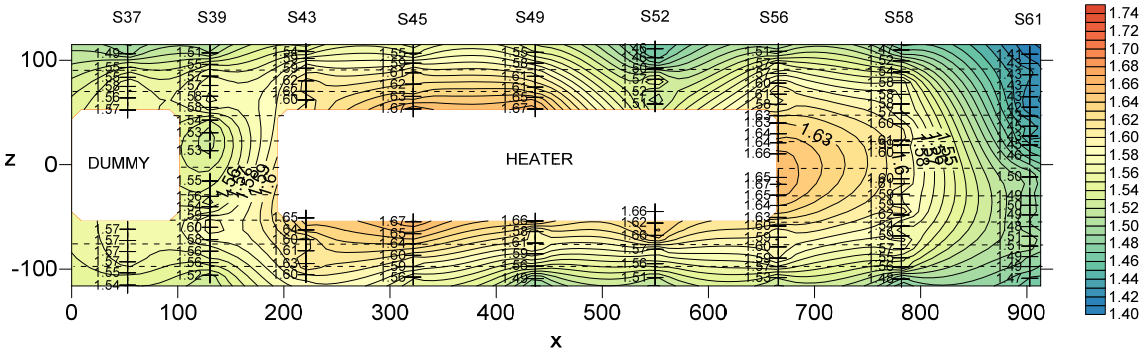

Fig. 116: Dry density distribution in a longitudinal section across radii C-F.

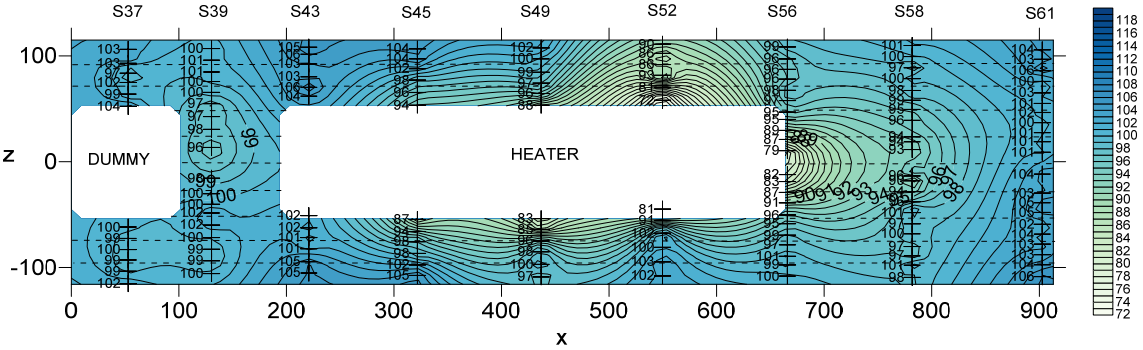

Fig. 117: Degree of saturation distribution in a longitudinal section across radii C-F (inexact values because of solid specific weight and water density uncertainties)

Tab. 24: Average values computed from the longitudinal profiles shown in Fig. 109 to Fig. 117.

Longitudinal profile	w (%)	ρ_d (g/cm^3)	S_r (%)
Radii A-D	26.0	1.59	97
Radii B-E	25.1	1.60	97
Radii C-F	25.4	1.58	96
Average	25.5	1.59	97

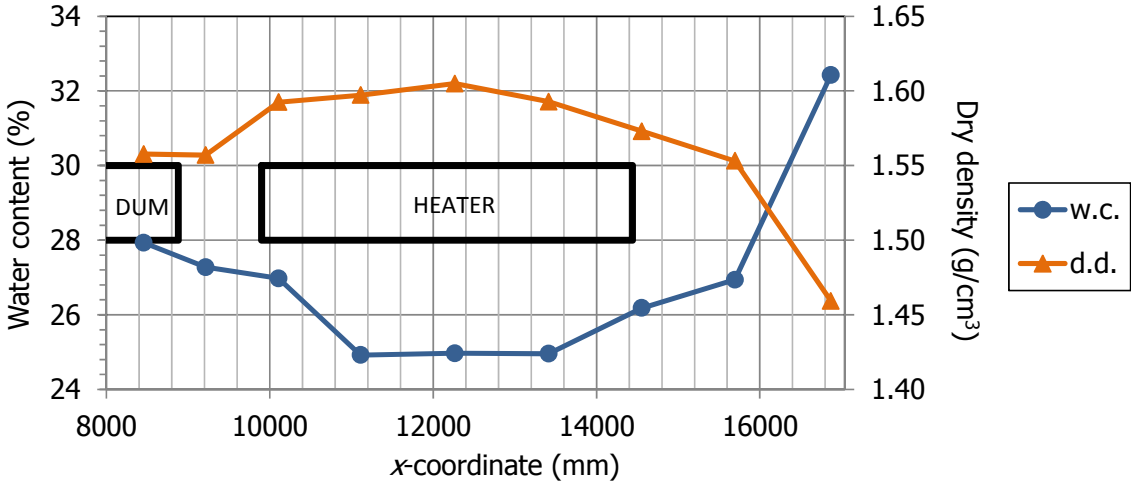

Fig. 118: Average water content (w.c.) and dry density (d.d.) for the sections sampled along the barrier as computed from the polynomial functions (Tab. 22).

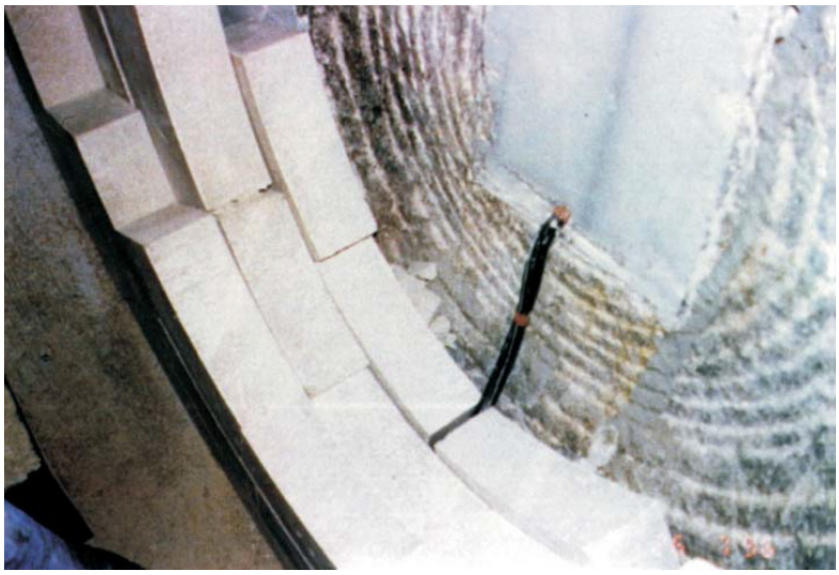

Fig. 119: Back of the gallery during installation (Slices 1 – 3).

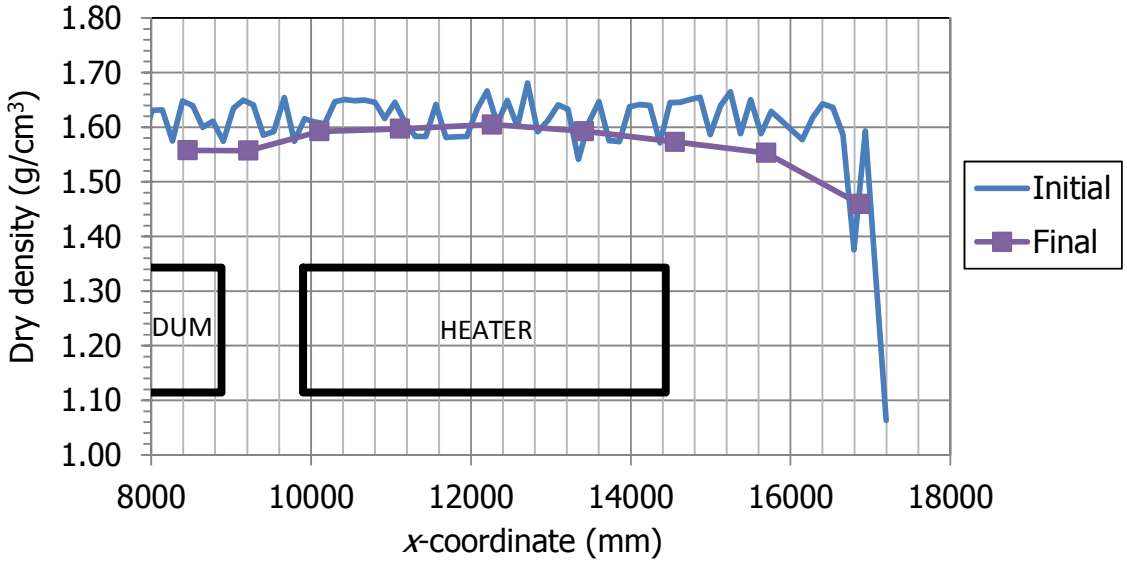

Fig. 120: Dry densities along the barrier as estimated during installation (Fuentes-Cantillana & García-Siñeriz 1998) and measured on-site during dismantling.

During dismantling the position of the slices with respect to the origin of coordinates (indicated in Fig. 1) was measured using a laser. At least two measurements were taken in every slice (at the two sides of the heater). A metric tape fixed during installation to the middle left side of the gallery was also used to check the position of the slices (Fig. 104). The values obtained were presented in AITEMIN (2016a). The difference between the installation coordinate of every section (as built) and the final coordinate has been plotted in Fig. 121 as a function of the initial coordinate. Positive values indicate that the barrier "moved" forward and negative values that it "moved" backwards. The measurements of the laser and the metric tape agree quite well. Two kinds of movement can be detected, one of them probably took place during operation and the other one during dismantling:

- Most slices moved towards the entrance of the gallery, particularly those closest to the concrete plug. Indeed, in the front part of the barrier the displacement was as high as 50 mm and decreased with distance into the gallery. This displacement towards the gallery entrance took probably place as the concrete plug was demolished and the swelling pressure released. The stresses measured on the concrete plug just before the start of the dismantling operations were 6 MPa (AITEMIN 2016b). Up to approximately the x-coordinate 14.8 m, the average displacement was of 20 mm.
- From that point to the back of the gallery, the slices had moved in the opposite direction, towards the rear of the gallery, more significantly as the slice was closest to the rearmost part of the gallery. This backward movement took place during operation, when the expansion of the bentonite was easier towards the rear of the gallery, where the void volume was higher.

The observations on-site confirmed this displacement: the external part of the blocks of the outer ring frequently showed grooves in the direction of the gallery axis, caused by the friction with the granite (Fig. 122, left), whereas the granite surface was covered by a film of bentonite showing striation parallel to the gallery axis (Fig. 122, right; Fig. 123).

The average of all the longitudinal movements measured gives a value of 7.2 mm, which would mean that the barrier experienced a net displacement of 7.2 mm (extension of barrier length from initial dimensions), which is too low to be reflected on the final average dry density of the overall barrier (a rough calculation indicates a decrease from 1.607 to 1.606 g/cm^3).

Fig. 121 also shows the average dry density of some slices (Tab. 22). It is clear that the dry density decreased towards both ends of the gallery, particularly towards the back of the gallery, where the volume of construction gaps was larger. The decrease observed at the front of the barrier is related to the displacement of the slices towards the gallery entrance that was also measured.

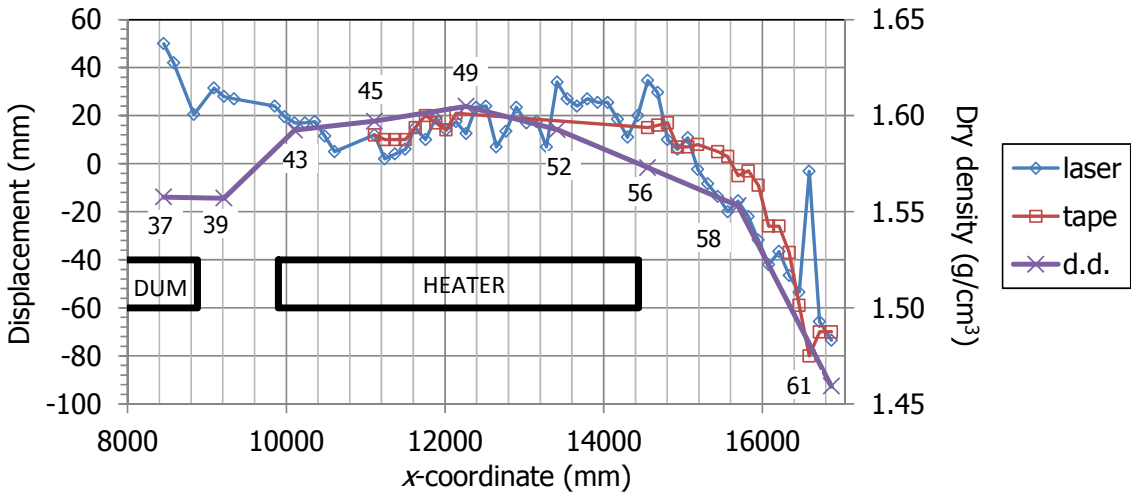

Fig. 121: Displacement of bentonite slices during operation and dismantling (positive values indicate movement towards the front of the gallery) and average dry density (d.d.) of sampling sections (Tab. 22).

Fig. 122: Displacement grooves in a bentonite block (left) and bentonite adhered to granite showing friction marks (see arrow).

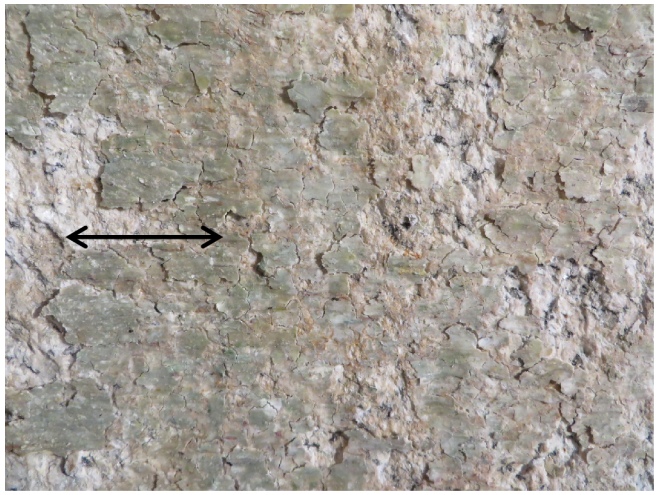

Fig. 123: Bentonite adhered to granite showing striation in the sense along the gallery axis.

4.4 Changes of the barrier during dismantling

The bentonite dismantling operations took three months and started after the heater had been switched off for 24 days. During this time changes took place in the bentonite, and the state observed upon dismantling did not exactly reflect the state of the barrier during operation. The different processes that could have affected the barrier since switching off the heater in particular on water content and dry density determinations need to be identified, assessed and taken into account in the final evaluation.

The changes concerning the barrier dry density have been discussed above: the demolition of the concrete plug implied a release of stresses and an expansion of the bentonite towards the front of the gallery that in the first sections sampled could have given lower density values (Sections S37 to S43) than those present during operation. This effect attenuated towards the back of the gallery and probably did not affect the rest of the sections (although some of them had moved towards the rear of the gallery during operation, this movement did not imply any change in the overall dry density of the barrier, since it filled the as-built void volume).

Core drilling and subsample trimming would introduce an additional decrease in dry density that would affect all the samples, but particularly those with higher water content.

When analysing the water distribution in the barrier it has to be taken into account that when the sections were dismantled the temperature in them was lower than the temperatures during operation, since the heater had been switched off between 25 and 97 days earlier, for Sections S37 and S61, respectively. The change in temperature during this time was of a few degrees (4 – 8 °C) for the sections farther away from the heater, and up to 80 °C in the bentonite closest to the liner in the central part of the heater. This temperature change definitely had an impact on the water distribution around the heater, where water in the vapour phase would condense because of cooling. Since the internal part of the barrier closest to the heater was not completely saturated, water movement from the external, saturated part of the barrier towards the drier central part would be feasible and driven by the suction potential. This was already observed during the first dismantling, when relative humidity sensors were still working near the heater and the increase in relative humidity in this area upon switching-off was recorded (Villar et al. 2005, 2006). Because no relative humidity or suction sensors were working in this area during the final dismantling, it is not possible to evaluate the extent of this water redistribution, but it is very likely that the water content around the heater was lower at the time of heater shutdown than what was measured during dismantling.

Relative humidity and temperature sensors were placed inside the liner once the heater was extracted (on June 4th 2015), one at the back of the liner and another one at the excavation front. The measurements taken showed that the relative humidity inside the liner was higher than 65 % during dismantling (Fig. 124), despite the fact that an Expanded Polystyrene (EPS) plug was placed at the front of the heater to avoid external influences (Fig. 125). The EPS plug was moved backwards as the dismantling operations proceeded. This RH was very likely much higher than the one around the heater during operation. Although water transfer in the vapour phase is very slow in bentonite, the possibility of water vapour getting into the bentonite of the internal ring through the liner holes after the extraction of the heater cannot be ruled out. In any case this would have been a small contribution that is not reflected clearly in the water content distribution measured along the radii.

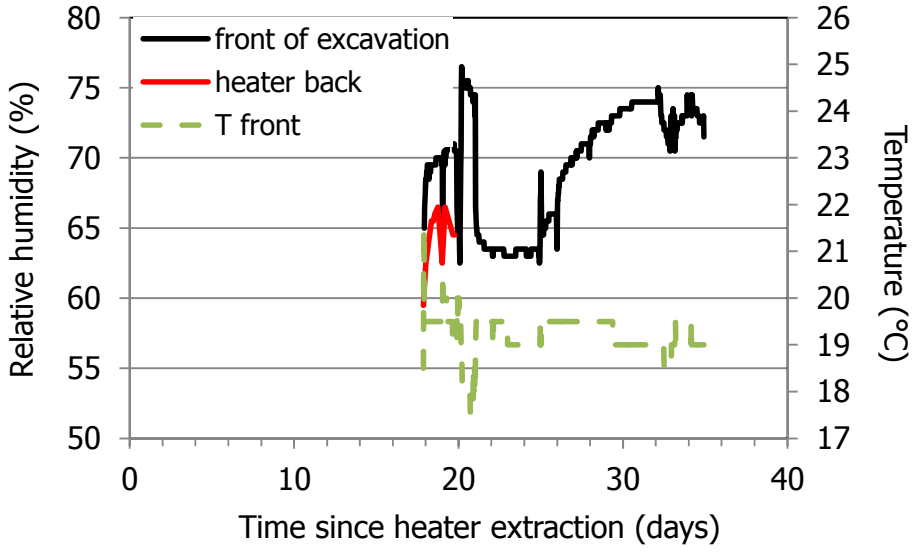

Fig. 124: Relative humidity and temperature measured at two positions inside the liner after heater extraction.

Fig. 125: EPS plug placed at the front of the liner once the heater was extracted.

In some sections the cores of some of the radii were taken over a period of several days (between one and four days between recovering first cores and completion of sampling). This happened in Sections S43 (radii C to F), S49 (radii D and E), S52 (radii F, D and E), S56 (radii C to E and some samples of radii B and F) and S61 (radii C to D). In those cases, the surface of the section that was not sampled the same day was left covered, the slice (or slices) in front of it remaining in place. This was done to avoid desiccation, which could take place very quickly because of the high water content of the bentonite and the circulation of drier air within the gallery (Fig. 126). The water content of the radii sampled later did not differ significantly from those of the other radii in any case. However, the dry density of radii D and E in Section S49, which were sampled four days later than the others, was considerably higher than that of the rest of the radii in the same section. This was not observed in any of the other sections, in which the differences among radii, if any, could not be related to the sampling date.

Only in Section S52 significant differences among the six radii were observed. Of the two radii sampled four days later than the others (D and E), only the samples in Radius D had higher dry density and displayed considerable scatter in values. In contrast, Radius F, sampled one day later, had much lower dry densities than the others. It could be concluded that the water content of the bentonite was well preserved during dismantling for as long as four days by leaving the clay slice in front of it in place, and that the sampling date (in an interval of four days) did not affect the dry density measurements clearly.

Fig. 126: Desiccation cracks upon exposure of Slice 43 (June 29th 2015)

Taking into account the different processes that could have taken place since switching off the heater, it is likely that the actual state of the barrier during operation differed with respect to what was measured as follows:

- The water content of the bentonite in contact with the liner was probably lower during heater operation than the values measured during dismantling, because of the water transfer caused by cooling. Conversely, the water content of the middle barrier ring in these areas could have been higher than that measured.
- Sampling and trimming reduced the density of the samples and consequently their degree of saturation. Hence, the overall as-built dry density of the barrier was higher than the one measured.
- The dry density and degree of saturation of the front sections (S37 and S39) were likely slightly higher during FEBEX operation than those measured during dismantling, because of the decompression and expansion experienced upon plug demolition.

4.5 Degree of saturation

In many samples the degree of saturation computed from the dry density and water content measured on site was higher than 100 %, which makes no physical sense. As it was explained in Subchapter 0, the degree of saturation was computed taking a value of 2.70 g/cm^3 for the density of solid particles and 1 g/cm^3 for water density. A degree of saturation higher than 100 % was usually found in tests in which the FEBEX bentonite was saturated under constant volume, particularly if the dry density of the bentonite was higher than 1.4 g/cm^3. This was already observed by Villar (2002) and explained as a consequence of taking an incorrect value for the water density, since the density adsorbed in clay particles can be higher than 1 g/cm^3 (Lloret & Villar 2007). It must be said that, since there is no certainty about the proportion of adsorbed water in the bentonite (which would depend on dry density and water content, among others) and of its density, the usual value of 1 g/cm^3 was used to compute the degree of saturation. The fact of using an average value for the specific weight –whereas there is a relatively large range of values determined in FEBEX bentonite for this parameter, with a

standard deviation of 0.04 g/cm^3– could have also contributed to the inaccuracy of the degree of saturation computed.

Since the samples retrieved during FEBEX-DP were close to full saturation in many areas of the barrier, this observation has been very significant, particularly in those samples with higher water content and dry density, such as the samples from Sections S37 and S39, which were cool and highly saturated sections. The degree of saturation computed in these sections are plotted in Fig. 127 as a function of the dry density of the samples. It can be observed that the calculated degree of saturation was mostly above 100 % in Section S37 and that they increased as the dry density was higher, which was also observed in Section S39. In contrast, in the sections around the heater, in which the inner ring was far from saturation, the relationship between degree of saturation and dry density was inverse, since the higher density samples were those close to the heater, which in turn were less saturated (Fig. 128). Concerning the cool sections at the back of the heater (S58 and S61), it is remarkable that Section S58 had degrees of saturation mostly below 100 %, whereas Section S61, with much lower dry density, had degrees of saturation that tended to increase with the dry density and that were higher on average than 100 % (Fig. 129).

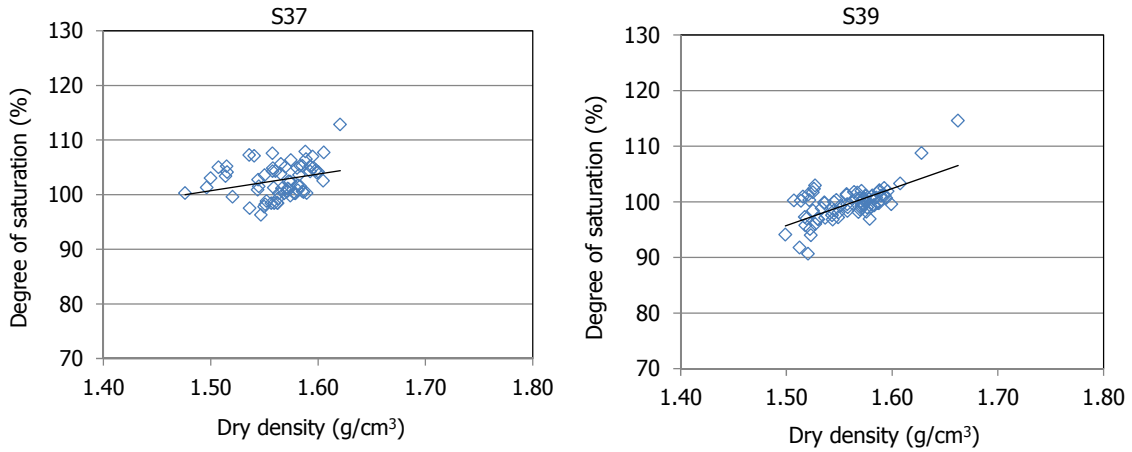

Fig. 127: Relationship between degree of saturation (inexact values because of solid specific weight and water density uncertainties) and dry density for cool sections at the heater front

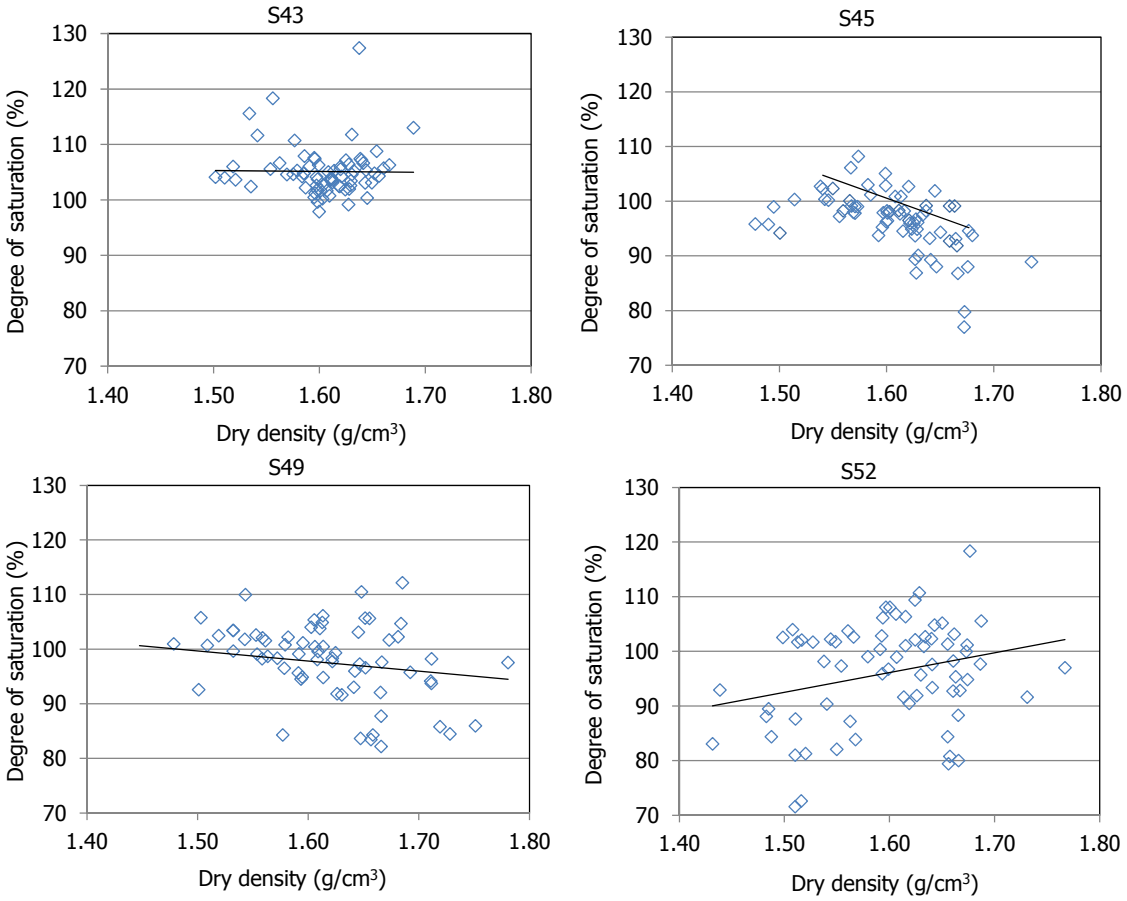

Fig. 128: Relationship between degree of saturation (inexact values because of solid specific weight and water density uncertainties) and dry density in sections around the heater.

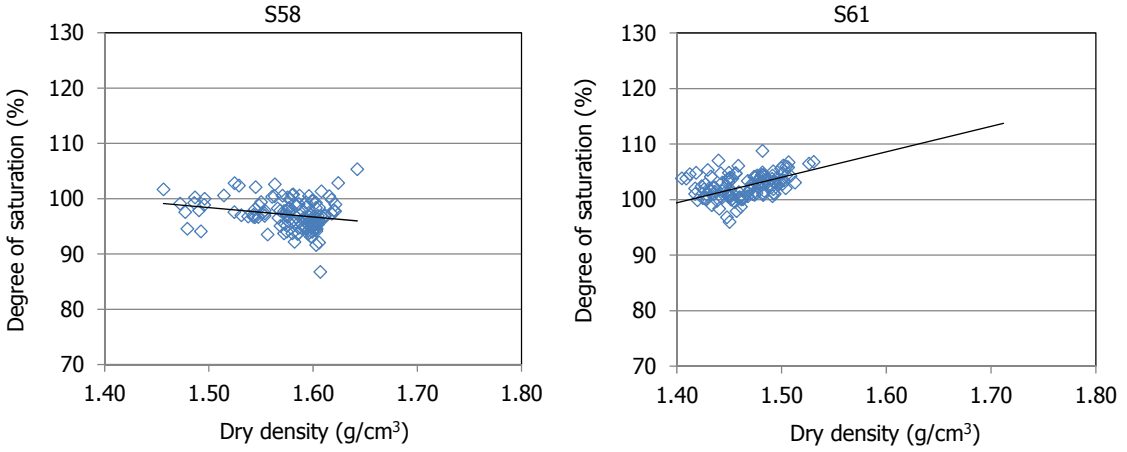

Fig. 129: Relationship between degree of saturation and dry density for sections at the back of the heater (inexact values because of solid specific weight and water density uncertainties).

5 Summary and conclusions

The FEBEX "in-situ" experiment was a full-scale test performed under natural water inflow conditions at the Grimsel Test Site (GTS, Switzerland), an underground laboratory managed by Nagra. The aim of the test was to reproduce the conditions of the engineered barrier system in an underground repository of nuclear waste. The barrier was composed of FEBEX bentonite blocks. The thermal effect of the heat-generating canisters was simulated by means of two heaters whose surface temperatures were set to100 °C, whereas hydration was natural. The heating stage of the *in-situ* test began in 1997.

After five years of operation, the heater closer to the gallery entrance (Heater #1) was switched off and extracted, along with all the bentonite and instruments preceding and surrounding it. This is known as the "partial dismantling". In place of the heater a dummy canister with the same dimensions was installed, the remaining part of the experiment was then sealed with a new sprayed concrete plug and a second operational phase started. The test continued running until April 2015, when Heater #2 was switched off. The final complete dismantling of the experiment was undertaken, and in particular the buffer removal and sampling took place between May and August 2015. Numerous samples of bentonite were taken in selected sections evenly distributed along the gallery for the on-site determination of dry density and water content. Additionally, the blocks' dimensions were measured, as well as the x-coordinate changes for the block sections. The results of the on-site measurements and other field observations concerning the state of the bentonite barrier have been reported and analysed.

At the moment the barrier was dismantled many sensors were still providing information and continued doing so during the dismantling operations (AITEMIN 2016b). The temperatures in the barrier during operation were between 100 °C and 36 °C in the sections around the heater and around 22 °C at the back of the gallery. Upon switching off the heater, the temperatures dropped to values below 30 °C at all points in the barrier. The operational relative humidity measurements, which are related to the degree of water saturation of the clay, mostly indicated full saturation conditions (100 %) at the time of dismantling. The total pressure recordings, which are also related to the degree of saturation –since swelling pressure is assumed to increase with increasing degree of saturation–mostly showed an increasing trend, with values at locations further away from the heater of between 5 and 6 MPa (and even higher at the contact bentonite/rock). These values would correspond to a swelling pressure of saturated bentonite with a density of 1.58 – 1.61 g/cm^3 (Villar 2002). However, the sensors located in the intermediate ring of sections around the heater recorded pressure values just slightly above 2 MPa, far from the equilibrium pressure expected for the average dry density of the barrier. This would indicate that full saturation was not reached.

The on-site measurements showed that the physical state of the barrier after 18 years of operation was very much affected by the processes to which it had been subjected, namely hydration from the granite and/or the imposed thermal gradient. The patterns observed are summarised below:

- All the gaps between blocks had sealed, both those among blocks of the same section and the gaps between bentonite slices. There was no effect of the vertical gaps between bentonite slices on the water content and dry density distribution. The granite/bentonite contact was tight at all locations and the gaps carved in the blocks for letting the cables pass had been completely filled by the swelling of the bentonite.
- The water content and dry density in every section followed a radial distribution around the axis of the gallery, with the water content decreasing from the granite towards the axis of

the gallery and the dry density following the inverse pattern. The water content and density gradients were more noticeable in those sections affected by the heater. Natural features (lamprophyre, fractures) or artefacts (plastic film, filter paper) that could potentially modify the water input to the bentonite did not systematically affect the water content distribution in the barrier, were localised and few in number.

- Consistently with the water content and dry density distributions, the radial dimensions measured on the surface of the blocks during dismantling indicated the expansion of the external and middle bentonite rings and the compression of the internal one.
- The degree of saturation tended to be homogeneous and very high in all the sections, with no clear spatial trend, except in those sections around or close to the heater, in which the degree of saturation decreased towards the heater. It is noticeable that in many samples the degree of saturation was higher than 100 %, which is attributed to using a water density value of 1 g/cm^3 (corresponding to free water, whereas most of the water in compacted bentonite is adsorbed water with different properties and probably a higher density).
- The measurements of the *x*-coordinate of the bentonite slices showed that the slices closest to the concrete plug moved towards the entrance of the gallery, which is assumed to have happened as the concrete plug was demolished and the swelling pressure (about 6 MPa at the concrete/bentonite interface) released. The net forward displacement of the slices decreased towards the back of the gallery. The innermost sections of blocks, located beyond the heater, moved in the opposite direction, probably during the operation phases and in response to the less densely installed buffer and construction gaps at the back of the gallery. As a consequence of this longitudinal displacement, the external part of the blocks of the outer ring frequently showed grooves in the direction of the gallery axis, caused by the friction with the granite, whereas the granite surface was covered by a film of bentonite showing striation parallel to the gallery axis. This had an appearance similar to slickensides observed in geological formations.
- There were also significant changes in dry density and water content along the axis of the tunnel:
  - The materials in the rear-most portion of the gallery contained the highest water contents and the lowest dry densities. This was most probably caused by a larger volume of construction gaps, which resulted in a lower installation density, a condition that remained to some extend to the end of operation.
  - The highest dry densities were found around the rear half of the heater, where the temperatures were higher and the end-of-test water content lowest.
  - Around the dummy canister dry densities below the average of the barrier were found. This density decrease was related to the displacement of the slices towards the gallery entrance upon plug demolition and pressure release. The bentonite around the dummy canister had also been subjected to high thermal gradient during the 1st operational phase but it was cool during the 2nd operational phase, which may have also affected its condition.
- The best estimates of the final average water content, dry density and degree of saturation of the whole bentonite barrier are 25.5 %, 1.59 g/cm^3 and 97 %, respectively.
- The final average dry density along the barrier was lower than the previously measured initial average value of 1.61 g/cm^3 (average value for half of the experiment remaining in place during the 2nd operational phase). This is attributed to the slight decompression suffered by the barrier on dismantling and to the sampling procedures. The intrusion of bentonite into the liner void could also have contributed to the decrease in the average dry

density of the barrier. Studies on formation and transport of colloids show that the rate of this process, if it exists, would be very low (Missana et al. 2015) and so colloid transport is not considered to be a mechanism that could have contributed to the average density decrease observed.

When analysing the state of the barrier observed at the time of dismantling, the processes that could have taken place between switching off the heater and doing the on-site measurements need to be considered. The actual state of the barrier during operation could differ from the state when dismantled with respect to the following measurements:

- The water content of the bentonite in contact with the liner was probably lower during operation than the values measured during dismantling, because of water transfer caused by cooling. Conversely, the water content of the middle barrier ring in these areas could have been higher than that measured.
- The average dry density of the barrier was actually higher than the measurements indicated, because of density decrease induced by sampling and trimming. If this were occurring, the degree of saturation would also be higher than indicated by the measurements.
- The dry density and degree of saturation of the front sections may have been higher during FEBEX operation than those measured, because of the decompression and expansion of the bentonite experienced upon plug demolition.

A comparison of the results reported here and those obtained during the partial dismantling performed after 5 years of operation (Villar et al. 2006) shows that the main changes during the 2nd Phase took place in the internal part of the barrier. After 5 years of operation the cold and hot sections had distinctly different features that were observed in the final dismantling. In particular:

- The water content in the 10 cm closest to the granite of the cold sections was the same after 18 years operation as after 5 years, whereas the additional operation time allowed for the saturated region to extend further towards the interior of the barrier.
- In the regions closest to the heater the water content near the granite, i.e. in the external ring of the barrier, decreased between that observed at 5 years and what was present after 13 additional years of operation. In contrast, the water content had increased in the medium and internal rings of the barrier.
- The dry density distribution along the radii around the heaters did not seem to have changed over time.
- The swelling and sealing capacity of the bentonite was observed after 5 years of operation, since all the construction gaps in the barrier were completely filled.

A thorough comparison of the results obtained in the partial and final dismantling would allow to draw conclusions concerning the saturation rate and the reversibility of the bentonite deformations coupled to hydration and drying.

6 References[1]

AITEMIN (2009): Sensors Data Report (In Situ Experiment) #2. Full report. Madrid, 118 pp.

AITEMIN (2014): FEBEX-e. Sensors Data Report (In Situ Experiment) #8. Full report. Madrid, 119 pp.

AITEMIN (2015): FEBEX-DP (GTS) Full Dismantling Sampling Plan (in situ Experiment). Nagra Arbeitsbericht NAB 15-14. 103 pp.

AITEMIN (2016b): FEBEX-e/FEBEX-DP. Final Sensor Data Report (FEBEX In Situ Experiment) Report #9. Full final report. Madrid, 230 pp. Nagra Arbeitsbericht NAB 16-19.

ASTM D2216–10 (2010): Standard Test Methods for Laboratory Determination of Water (Moisture) Content of Soil and Rock by Mass.

Bárcena, I., Fuentes-Cantillana, J.L., García-Siñeriz, J.L. (2003): Dismantling of the Heater 1 at the FEBEX "in situ" test. Description of operations. Publicación Técnica ENRESA 09/2003, Madrid, 134 pp.

Bárcena, I., García-Siñeriz, J.L., Huertas, F. (2006): FEBEX Project Final Report. Addendum sensors data report. In situ experiment. Publicación Técnica ENRESA 05-5/2006. Madrid, 157 pp.

Chávez-Páez, M., Van Workum, K., de Pablo, L., de Pablo, J.J. (2001): Monte Carlo simulations of Wyoming sodium montmorillonite hydrates. Journal of Chemical Physics 114 (3) 1405–1413.

Daucausse, D. & Lloret, A. (2003): Results of "in situ" measurements of water content and dry density. FEBEX report 70-UPC-L-5-012. 85 pp. Barcelona.

Dixon, D. & Kober, F. (2015): FEBEX material characterization summary. Nagra Aktennotiz AN 15-126. 28 pp.

ENRESA (1995): Almacenamiento geológico profundo de residuos radiactivos de alta actividad (AGP). Diseños conceptuales genéricos. Publicación Técnica ENRESA 11/95. 105 pp. Madrid.

ENRESA (2000): FEBEX Project. Full-scale engineered barriers experiment for a deep geological repository for high level radioactive waste in crystalline host rock. Final Report. Publicación Técnica ENRESA 1/2000, Madrid, 354 pp.

ENRESA (2006): FEBEX Full-scale Engineered Barriers Experiment, Updated Final Report 1994 – 2004. Publicación Técnica ENRESA 05-0/2006, Madrid, 590 pp.

Ferrage, E., Kirk, C.A., Cressey, G. & Cuadros, J. (2007): Dehydration of Ca-montmorillonite at the crystal scale. Part I: Structure evolution. Amer. Miner. 92(7): 994-1006.

[1] ANs cited in the document are available on request with Nagra.

Fuentes-Cantillana, J.L. & García-Siñeriz, J.L. (1998): FEBEX. Final design and installation of the "in situ" test at Grimsel. Publicación Técnica ENRESA 12/98. Madrid, 184 pp.

García-Siñeriz J.L., Abós H., Martínez V. & De la Rosa C. (AITEMIN) (2016): FEBEX-DP Dismantling of the Heater 2 at the FEBEX "in situ" test. Nagra Working Report NAB 16-11.

Guimerà, J., Carrera, J., Martínez, L., Vázquez, E., Ortuño, F., Fierz, T., Bühler, C., Vives, L., Meier, P., Medina, A., Saaltink, M., Ruiz, B. & Pardillo, J. (1998): Hydrogeological characterization and modeling. FEBEX Report 70-UPC-M-1-1001. 106 pp.

Huang, W.-L., Bassett, W.A. & Wu, T.C. (1994): Dehydration and hydration of montmorillonite at elevated temperatures and pressures monitored using synchrotron radiation. American Mineralogist 79: 683 – 691.

Jacinto, A., Villar, M.V. & Ledesma, A. (2012): Influence of water density on the water-retention curve of expansive clays. Géotechnique 62 (8), 657 – 667

Kober, F. (2015): FEBEX-DP Summary of Extra Reports (1 – 13). Nagra Aktennotiz AN 15-619.

Lloret, A. & Villar, M.V. (2007): Advances on the knowledge of the thermo-hydro-mechanical behaviour of heavily compacted FEBEX bentonite. Physics and Chemistry of the Earth Parts A/B/C 32 (8 – 14), 701 – 715.

Marcial, D. (2003): Comportement hydromécanique et microstructural des matériaux de barrière ouvragée. Ph.D. Thesis. École Nationale des Ponts et Chausées, Paris, 316 pp.

Missana, T., Alonso, U., García-Gutiérrez, M. & López, T. (2015): Analysis of bentonite colloid generation in-situ at the FEBEX gallery (GTS) global evaluation of experimental data obtained. BELBAR Deliverable 2.10. 70 pp.

Monsalvo, R., De Pablo, L. & Chávez, M.L. (2006): Hydration of Ca-Montmorillonite at basin conditions: a Monte Carlo molecular simulation. Revista Mexicana De Ciencias Geológicas 23(1): 84 – 95.

Pardillo, J., Campos, R. & Guimerà, J. (1997): Caracterización geológica de la zona de ensayo FEBEX (Grimsel, Suiza). Informe FEBEX 70-IMA-M-2-01, CIEMAT/UPC, Madrid/Barcelona, 45pp.

Skipper, N.T., Refson, K. & McConnell, J.D.C. (1991): Computer simulation of interlayer water in 2:1 clays. J. Chem. Phys. 94 (11): 7434 – 7445.

Tambach, T.J., Hensen, E.J.M. & Smit, B. (2004): Molecular Simulations Of Swelling Clay Minerals. J. Phys. Chem. B 108: 7586 – 7596.

Villar, M.V. (Ed.) (2006): FEBEX Project Final report. Post-mortem bentonite analysis. Publicación Técnica ENRESA 05-1/2006, Madrid, 183 pp.

Villar, M.V. (2002): Thermo-hydro-mechanical characterisation of a bentonite from Cabo de Gata. A study applied to the use of bentonite as sealing material in high level radioactive waste repositories. Publicación Técnica ENRESA 01/2002, Madrid, 258 pp.

Villar, M.V., García-Siñeriz, J.L., Bárcena, I. & Lloret, A. (2005): State of the bentonite barrier after five years operation of an in situ test simulating a high level radioactive waste repository. Engineering Geology 80(3-4): 175 – 198.